

c. /

THE SYNTHESIS AND SPECTRAL AND MAGNETIC PROPERTIES OF
SOME IRON SULFONATE COMPOUNDS

by

JOHN STEPHEN HAYNES

Graduate of the Royal Institute of Chemistry, 1976

A THESIS SUBMITTED IN PARTIAL FULFILLMENT OF THE
REQUIREMENTS FOR THE DEGREE OF
MASTER OF SCIENCE

in

THE FACULTY OF GRADUATE STUDIES
(Chemistry)

We accept this thesis as conforming
to the required standard

THE UNIVERSITY OF BRITISH COLUMBIA

August 1980

© John Stephen Haynes, 1980

In presenting this thesis in partial fulfilment of the requirements for an advanced degree at the University of British Columbia, I agree that the Library shall make it freely available for reference and study. I further agree that permission for extensive copying of this thesis for scholarly purposes may be granted by the Head of my Department or by his representatives. It is understood that copying or publication of this thesis for financial gain shall not be allowed without my written permission.

Department of

Chemistry

The University of British Columbia
2075 Wesbrook Place
Vancouver, Canada
V6T 1W5

Date

Sept. 2 1980

ABSTRACT

The work described in this thesis involved the synthesis and characterisation of a number of iron sulfonate compounds, $\text{Fe}(\text{XSO}_3)_n$, where X is CF_3 , CH_3 and $p\text{-CH}_3\text{C}_6\text{H}_4$, and n is 2 or 3. The work is an attempt to probe the coordinating ability of the XSO_3^- anion and extends previous studies in this laboratory on other divalent metal sulfonates.

The physical methods of characterisation included infrared, electronic and Mössbauer spectroscopy and magnetic susceptibility measurements. These techniques have enabled a detailed picture of the structure of the iron(II) sulfonates to be envisaged. The general structure proposed involves terdentate bridging anions, each anion bridging to three different metal centres resulting in FeO_6 octahedra; the distortions from perfect octahedral geometry have also been analysed.

Iron(II) methanesulfonate was found to exist in two closely related structural forms, the α -isomer containing trigonally compressed FeO_6 octahedra and the β -isomer containing trigonally elongated FeO_6 octahedra. No evidence for structural isomerism was found for $\text{Fe}(\text{CF}_3\text{SO}_3)_2$ or $\text{Fe}(p\text{-CH}_3\text{C}_6\text{H}_4\text{SO}_3)_2$ but vibrational spectroscopy revealed structural isomerism in other $\text{M}(\text{CH}_3\text{SO}_3)_2$ compounds, where M is Co and Zn. Both α - and β - $\text{Fe}(\text{CH}_3\text{SO}_3)_2$ showed unusual magnetic properties and Mössbauer spectroscopy enabled an antiferromagnetic phase transition to be observed in the case of the β -isomer. Preliminary results for

the iron(III) sulfonates, $\text{Fe}(\text{CF}_3\text{SO}_3)_3$, $\text{Fe}(\text{CH}_3\text{SO}_3)_3$ and $\text{Fe}(\text{p-CH}_3\text{C}_6\text{H}_4\text{SO}_3)_3$ indicate antiferromagnetic exchange in these compounds.

TABLE OF CONTENTS

	<u>PAGE</u>
ABSTRACT	ii
TABLE OF CONTENTS	iv
LIST OF TABLES	ix
LIST OF FIGURES	xi
ACKNOWLEDGEMENT	xiv
CHAPTER 1 INTRODUCTION.	1
1.1 Previous Work.	1
1.2 Purpose and Outline of the Present Work.	3
CHAPTER 2 EXPERIMENTAL METHODS.	7
2.1 Introduction.	7
2.2 Materials.	8
2.3 The Dry Box.	9
2.4 Synthesis of Compounds.	9
2.4.1 Iron(II) Trifluoromethanesulfonate, $\text{Fe}(\text{CF}_3\text{SO}_3)_2$.	9
2.4.2 Iron(II) Paratoluenesulfonate, $\text{Fe}(\text{p-CH}_3\text{C}_6\text{H}_4\text{SO}_3)_2$.	10
2.4.3 Iron(II) Methanesulfonate, $\text{Fe}(\text{CH}_3\text{SO}_3)_2$.	10
2.4.4 Preparation of other Methanesulfonates, $\text{M}(\text{CH}_3\text{SO}_3)_2$ where M is Co, Ni, Cu, Zn and Ca.	12
2.4.5 Iron(III) Trifluoromethanesulfonate, $\text{Fe}(\text{CF}_3\text{SO}_3)_3$.	12
2.4.6 Iron(III) Paratoluenesulfonate, $\text{Fe}(\text{p-CH}_3\text{C}_6\text{H}_4\text{SO}_3)_3$.	12

	<u>PAGE</u>
2.4.7 Iron(III) Methanesulfonate, $\text{Fe}(\text{CH}_3\text{SO}_3)_3$.	13
2.5 Analytical Data.	13
2.6 Physical Experimental Techniques.	13
2.6.1 Infrared Spectroscopy.	13
2.6.2 Electronic Spectroscopy.	15
2.6.3 Magnetic Susceptibility Measurements.	15
2.6.4 Mossbauer Spectroscopy.	16
2.6.5 Analysis of Mossbauer Spectra.	21
CHAPTER 3 VIBRATIONAL SPECTROSCOPY.	23
3.1 Introduction.	23
3.2 Theory of Vibrational Spectra and Structure.	24
3.3 Infrared Spectrum of $\text{Fe}(\text{CF}_3\text{SO}_3)_2$.	31
3.4 Infrared Spectrum of $\text{Fe}(\text{p-CH}_3\text{C}_6\text{H}_4\text{SO}_3)_2$.	33
3.5 Infrared Spectra of $\text{Fe}(\text{CH}_3\text{SO}_3)_2$.	35
3.5.1 Infrared Spectrum of α -Iron(II) Methanesulfonate.	35
3.5.2 Infrared Spectrum of β -Iron(II) Methanesulfonate.	39
3.5.3 Infrared Spectrum of a Mixture of α - and β - $\text{Fe}(\text{CH}_3\text{SO}_3)_2$.	41
3.5.4 Infrared Spectrum of $\text{Fe}(\text{CH}_3\text{SO}_3)_2 \cdot \text{CH}_3\text{SO}_3\text{H}$.	41
3.6 Structural Isomerism in FeO_6 Octahedra.	43
3.7 The Search for Structural Isomerism in $\text{Fe}(\text{CF}_3\text{SO}_3)_2$ and $\text{Fe}(\text{p-CH}_3\text{C}_6\text{H}_4\text{SO}_3)_2$ using Infrared Spectroscopy.	44

	<u>PAGE</u>
3.8 The Search for Structural Isomerism in $M(\text{CH}_3\text{SO}_3)_2$ Compounds using Infrared Spectroscopy.	45
3.8.1 Infrared Spectrum of $\text{Co}(\text{CH}_3\text{SO}_3)_2$.	45
3.8.2 Infrared Spectrum of $\text{Ni}(\text{CH}_3\text{SO}_3)_2$.	47
3.8.3 Infrared Spectrum of $\text{Cu}(\text{CH}_3\text{SO}_3)_2$.	47
3.8.4 Infrared Spectrum of $\text{Zn}(\text{CH}_3\text{SO}_3)_2$.	47
3.8.5 Infrared Spectrum of $\text{Ca}(\text{CH}_3\text{SO}_3)_2$.	50
3.9 Summary of Results and Conclusions.	51
CHAPTER 4 ELECTRONIC SPECTRA OF $\text{Fe}(\text{XSO}_3)_2$ COMPOUNDS.	54
4.1. Introduction.	54
4.2 Results and Discussion.	54
CHAPTER 5 MAGNETIC SUSCEPTIBILITIES OF $\text{Fe}(\text{XSO}_3)_2$ COMPOUNDS.	63
5.1 Introduction.	63
5.2 Origins of the Magnetic Effects.	64
5.3 Diamagnetism.	64
5.4 Paramagnetism.	65
5.5 Theory of Paramagnetic Susceptibility, the Van Vleck Equation and its Application to High-Spin Iron(II) Systems.	66
5.6 The Figgis and Lewis Model.	71
5.7 Results and Discussion.	73
5.7.1 Magnetic Moment Data for $\text{Fe}(\text{CF}_3\text{SO}_3)_2$ and $\text{Fe}(\text{p-CH}_3\text{C}_6\text{H}_4\text{SO}_3)_2$.	79
5.7.2 Magnetic Moment Data for α - and β - $\text{Fe}(\text{CH}_3\text{SO}_3)_2$.	84

	<u>PAGE</u>
5.8 Summary of Results and Conclusions.	89
CHAPTER 6 ⁵⁹ MOSSBAUER SPECTROSCOPY.	90
6.1 Introduction.	90
6.2 Theory of ⁵⁹ Mossbauer Spectroscopy.	91
6.2.1 Electric Monopole Interaction, the Isomer Shift.	91
6.2.2 Second-Order Doppler Effect.	93
6.2.3 Electric Quadrupole Interaction, The Quadrupole Splitting.	94
6.3. Isomer Shift and Quadrupole Splittings for Iron(II) Sulfonates.	103
6.3.1 Isomer Shift Values.	103
6.3.2 Quadrupole Splitting Values.	109
6.4 Crystal-Field, Spin-Orbit and Spin-Spin Splitting Parameters for Iron(II) Sulfonates.	114
CHAPTER 7 ⁵⁹ MAGNETICALLY-PERTURBED MOSSBAUER SPECTRA.	120
7.1 Introduction.	120
7.2 Magnetically-Perturbed ⁵⁹ Mossbauer Spectra of Fe(p-CH ₃ C ₆ H ₄ SO ₃) ₂ .	121
7.2.1 Determination of the Sign of e ² qQ.	124
7.2.2 The Spin Hamiltonian Model.	125
7.3 Magnetically-Perturbed ⁵⁹ Mossbauer Spectra of Fe(CF ₃ SO ₃) ₂ .	134
7.4 Magnetically-Perturbed ⁵⁹ Mossbauer Spectra of α-Fe(CH ₃ SO ₃) ₂ .	141
7.5 ⁵⁹ Mossbauer Spectra of β-Fe(CH ₃ SO ₃) ₂ Below 25K.	146

	<u>PAGE</u>
CHAPTER 8 STUDIES ON IRON(III) SULFONATES.	151
8.1 Introduction.	151
8.2 Infrared Spectra of Iron(II) Sulfonates.	151
8.3 Magnetic Susceptibilities of Iron(III) Sulfonates.	153
8.4 " Mossbauer Spectroscopy of Iron(III) Sulfonates.	159
8.4.1 Isomer Shift Values.	161
8.4.2 Quadrupole Splitting Values.	163
8.5 Conclusions.	164
CHAPTER 9 CONCLUSIONS AND SUGGESTIONS FOR FURTHER STUDY.	165
9.1 Conclusions.	165
9.2 Suggestions for Further Study.	167
REFERENCES.	171
APPENDIX.	177

LIST OF TABLES

<u>TABLE</u>		<u>PAGE</u>
2.1	Analytical Data.	14
3.1	Correlation Table for C_{3v} and C_s Point Groups.	25
3.2	Infrared Spectral Data (cm^{-1}) for $\text{Fe}(\text{XSO}_3)_2$ Compounds.	29
3.3	Infrared Spectral Data (cm^{-1}) for $\text{M}(\text{CF}_3\text{SO}_3)_2$ Compounds.	32
3.4	Infrared Spectral Data (cm^{-1}) for $\text{M}(\text{p-CH}_3\text{C}_6\text{H}_4\text{SO}_3)_2$ Compounds.	34
3.5	Infrared Spectral Data (cm^{-1}) for $\text{Fe}(\text{CH}_3\text{SO}_3)_2$ in the CH_3 Stretching and Bending Regions.	40
3.6	Infrared Spectral Data (cm^{-1}) for $\text{Fe}(\text{CH}_3\text{SO}_3)_2$. $\text{CH}_3\text{SO}_3\text{H}$ and a Comparison with $\alpha\text{-Fe}(\text{CH}_3\text{SO}_3)_2$ and $\text{CH}_3\text{SO}_3\text{H}$.	42
3.7	Infrared Spectral Data (cm^{-1}) for $\text{Co}(\text{CH}_3\text{SO}_3)_2$ Before and After Treatment with 2,2-Dimethoxypropane.	46
3.8	Infrared Spectral Data (cm^{-1}) for $\text{Zn}(\text{CH}_3\text{SO}_3)_2$ Before and After Treatment with 2,2-Dimethoxypropane.	48
3.9	Infrared Spectral Data (cm^{-1}) for $\text{Ca}(\text{CH}_3\text{SO}_3)_2$.	52
3.10	Summary of Results Concerning Isomerism in $\text{M}(\text{CH}_3\text{SO}_3)_2$ Compounds.	53
4.1	Electronic Spectra of $\text{Fe}(\text{XSO}_3)_2$ Compounds.	56
4.2	Dq Values (cm^{-1}) for $\text{M}(\text{XSO}_3)_2$ Compounds.	61
5.1	Magnetic Susceptibility Data for $\text{Fe}(\text{CF}_3\text{SO}_3)_2$.	75
5.2	Magnetic Susceptibility Data for $\alpha\text{-Fe}(\text{CH}_3\text{SO}_3)_2$.	76
5.3	Magnetic Susceptibility Data for $\beta\text{-Fe}(\text{CH}_3\text{SO}_3)_2$.	77
5.4	Magnetic Susceptibility Data for $\text{Fe}(\text{p-CH}_3\text{C}_6\text{H}_4\text{SO}_3)_2$.	78

LIST OF TABLES

<u>TABLE</u>		<u>PAGE</u>
5.5	Crystal-Field Splitting Parameters for Iron(II) Sulfonate Compounds.	82
6.1	Values of q_{VAL} for the 3d Orbitals.	99
6.2	^{57}Fe Mossbauer Effect Data for Iron(II) Sulfonates.	104
6.3	Isomer Shift Values of $Fe(XSO_3)_2$ Compounds at 80K.	108
6.4	Crystal-Field Splitting Parameters Derived from Quadrupole Splitting Data.	118
7.1	Magnetically-Perturbed ^{57}Fe Mossbauer Spectral Parameters for $Fe(p-CH_3C_6H_4SO_3)_2$.	128
7.2	Magnetically-Perturbed ^{57}Fe Mossbauer Spectral Parameters for $\alpha-Fe(CH_3SO_3)_2$ and $Fe(H_2O)_6 SiF_6$.	145
8.1	Infrared Spectral Data (cm^{-1}) for Iron(III) Sulfonate Compounds.	152
8.2	Magnetic Susceptibility Data for $Fe(CF_3SO_3)_3$.	154
8.3	Magnetic Susceptibility Data for $Fe(CH_3SO_3)_3$.	155
8.4	Magnetic Susceptibility Data for $Fe(p-CH_3C_6H_4SO_3)_3$.	156
8.5	^{57}Fe Mossbauer Effect Data for Iron(III) Sulfonates.	160

LIST OF FIGURES

<u>FIGURE</u>		<u>PAGE</u>
1.1	Proposed Structure of $\text{Fe}(\text{XSO}_3)_2$ Compounds.	2
2.1	Schematic Diagram of a Mössbauer Spectrometer.	17
2.2	Schematic Diagram of Apparatus used for Obtaining Variable Temperature Mössbauer Spectra.	19
2.3	Schematic Diagram of Apparatus used for Obtaining Magnetically-Perturbed Mössbauer Spectra.	20
3.1	Normal Modes of Vibration of the XSO_3^- Anion.	25
3.2	Bonding and Symmetry Properties of the XSO_3^- Anion.	27
3.3	Infrared Spectra ($1500\text{-}250\text{cm}^{-1}$) of $\text{Fe}(\text{CF}_3\text{SO}_3)_2$ and $\text{Fe}(\text{p-CH}_3\text{C}_6\text{H}_4\text{SO}_3)_2$.	30
3.4	Infrared Spectra ($1500\text{-}250\text{cm}^{-1}$) of $\text{Fe}(\text{CH}_3\text{SO}_3)_2$.	36
3.5	The Cadmium Iodide Layer Structure .	38
3.6	Infrared Spectra ($1500\text{-}250\text{cm}^{-1}$) of $\text{Zn}(\text{CH}_3\text{SO}_3)_2$.	49
4.1	Splitting of the Free-Ion ^5D Ground Term in an Octahedral Crystal Field.	55
4.2	Electronic Spectrum of $\text{Fe}(\text{CF}_3\text{SO}_3)_2$.	57
4.3	Splitting Diagram for High-Spin Iron(II) in Crystal Fields of O_h , D_{4h} and D_{3d} Symmetry.	59
5.1	The Effect of Spin-Orbit Coupling on the $^5\text{T}_{2g}$ Ground Term.	69
5.2	Temperature Dependence of the Magnetic Moment for $\text{Fe}(\text{XSO}_3)_2$ Compounds.	74
5.3	Plots of Reciprocal Susceptibility Against Temperature for $\text{Fe}(\text{CF}_3\text{SO}_3)_2$ and $\text{Fe}(\text{p-CH}_3\text{C}_6\text{H}_4\text{SO}_3)_2$.	80
5.4	Plots of Reciprocal Susceptibility Against Temperature for α - and β - $\text{Fe}(\text{CH}_3\text{SO}_3)_2$.	85

LIST OF FIGURES

<u>FIGURE</u>		<u>PAGE</u>
5.5	Temperature Dependence of the Magnetic Moment for α - and β -Fe(CH ₃ SO ₃) ₂ .	87
6.1	(i) Source and Absorber Nuclear Energy Levels.	92
	(ii) Resultant Mossbauer Spectrum.	92
6.2	(i) Energy Level Scheme Including Quadrupole Hyperfine Interaction.	96
	(ii) Resultant Mossbauer Spectrum.	96
6.3	3d Orbital Splittings in Octahedral, Axial and Rhombic Fields.	98
6.4	C ₄ Quantisation Axis and d Orbitals.	101
6.5	C ₃ Quantisation Axis and d Orbitals.	102
6.6	Temperature Dependence of the Quadrupole Splitting for Fe(XSO ₃) ₂ Compounds.	110
6.7	Mossbauer Spectra of Fe(p-CH ₃ C ₆ H ₄ SO ₃) ₂ at Various Temperatures.	111
6.8	Mossbauer Spectra of Fe(CH ₃ SO ₃) ₂ at 78K.	112
7.1	Magnetically-Perturbed Mossbauer Spectra of Fe(p-CH ₃ C ₆ H ₄ SO ₃) ₂ at 2.4K.	122
7.2	Magnetically-Perturbed Mossbauer Spectra of Fe(p-CH ₃ C ₆ H ₄ SO ₃) ₂ at 4.2K.	123
7.3	Comparison of Computed and Experimental Spectra for Fe(p-CH ₃ C ₆ H ₄ SO ₃) ₂ at 2.4 and 4.2K in an Applied Magnetic Field of 5.63T.	129
7.4	Comparison of Computed and Experimental Spectra for Fe(p-CH ₃ C ₆ H ₄ SO ₃) ₂ at 2.4 and 4.2K in an Applied Magnetic Field of 4.50T.	130
7.5	Comparison of Computed and Experimental Spectra for Fe(p-CH ₃ C ₆ H ₄ SO ₃) ₂ at 4.2K in an Applied Magnetic Field of 3.38T.	131

LIST OF FIGURES

<u>FIGURE</u>		<u>PAGE</u>
7.6	Comparison of Computed and Experimental Spectra for $\text{Fe}(\text{p-CH}_3\text{C}_6\text{H}_4\text{SO}_3)_2$ at 4.2K in an Applied Magnetic Field of 1.13T.	133
7.7	Magnetically-Perturbed ^{57}Fe Mossbauer Spectra of $\text{Fe}(\text{CF}_3\text{SO}_3)_2$ at 4.2K.	135
7.8	Comparison of ^{57}Fe Mossbauer Spectra of $\text{Fe}(\text{CF}_3\text{SO}_3)_2$ and $\text{Fe}(\text{p-CH}_3\text{C}_6\text{H}_4\text{SO}_3)_2$ at 4.2K in Applied Magnetic Fields of 1.13 and 5.63T.	140
7.9	Comparison of Computed and Experimental Spectra for $\alpha\text{-Fe}(\text{CH}_3\text{SO}_3)_2$. Recorded at 4.50T.	142
7.10	^{57}Fe Mossbauer Spectra of $\alpha\text{-Fe}(\text{CH}_3\text{SO}_3)_2$ at 4.2K in Applied Magnetic Fields of 4.50 and 5.63T.	143
7.11	^{57}Fe Mossbauer Spectra of $\beta\text{-Fe}(\text{CH}_3\text{SO}_3)_2$ in the Proximity of the Phase Transition Temperature.	147
7.12	^{57}Fe Mossbauer Spectra of $\beta\text{-Fe}(\text{CH}_3\text{SO}_3)_2$ below 21.15K.	149
8.1	Temperature Dependence of the Magnetic Moment for $\text{Fe}(\text{XSO}_3)_3$ Compounds.	157
8.2	^{57}Fe Mossbauer Spectrum of $\text{Fe}(\text{CH}_3\text{SO}_3)_3$ at 80K.	162

ACKNOWLEDGEMENTS

I would like to express my gratitude to my two research supervisors, Drs. J.R. Sams and R.C. Thompson, for their help and guidance throughout this work.

The informal discussions with colleagues in this laboratory and the department were stimulating and very much appreciated.

Most sincere thanks are due to Mrs. Lia Sallos for processing the Mossbauer data; Dr. A.R. Hulme for use of computer programmes he developed and to Mrs. Celine Gunawardene for typing this thesis.

CHAPTER I

INTRODUCTION

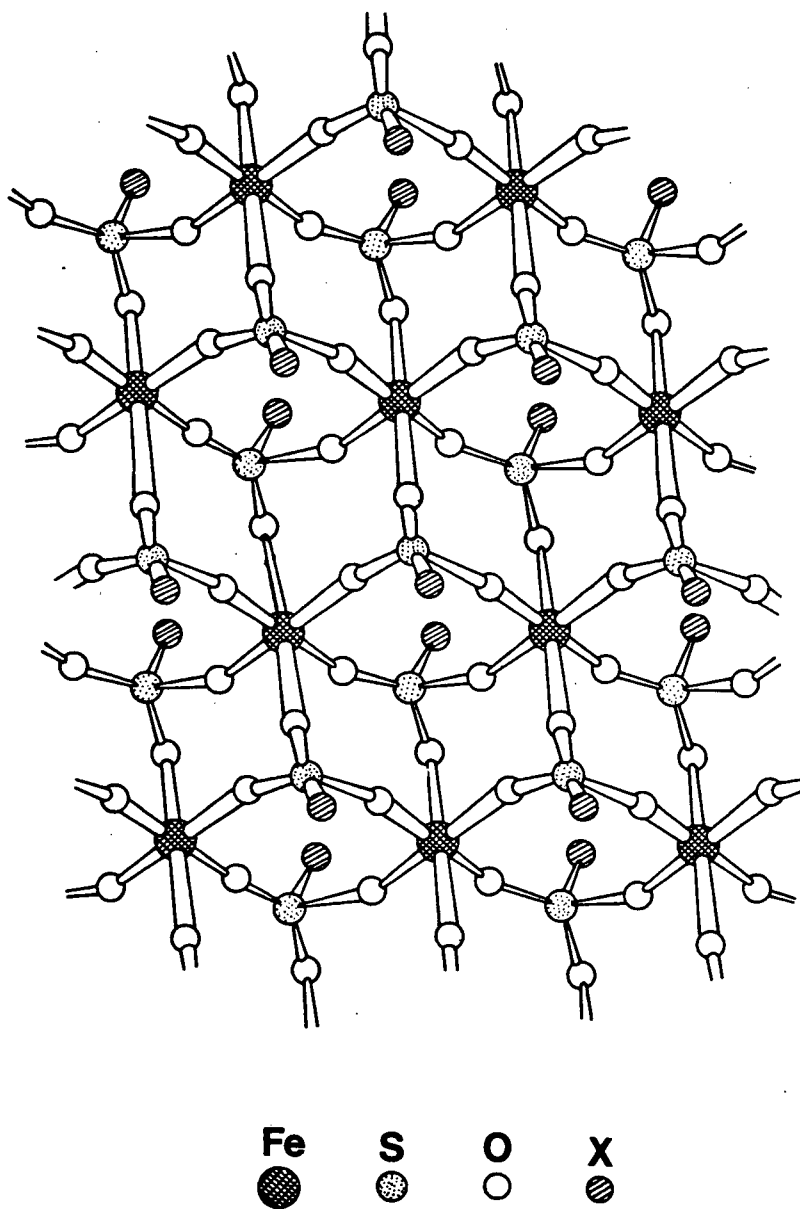
1.1. PREVIOUS WORK

Previous work on the coordinating properties of weakly basic anions has included studies on perchlorates (ClO_4^-), tetrafluoroborates (BF_4^-), perrhenates (ReO_4^-), hexafluorophosphates (PF_6^-) and hexafluoroarsenates (AsF_6^-), as well as sulfonates (XSO_3^- , where X is F, CF_3 , CH_3 , $p\text{-CH}_3\text{C}_6\text{H}_4$), (1-13). The anions are often regarded as non-coordinating or very weakly coordinating and the EF_6^- anions, where E is P or As, in particular have been widely used as counterions in the isolation of cationic species.

Transition - metal sulfonates of the type $\text{M}(\text{XSO}_3)_2$ have been studied previously in this laboratory and are particularly relevant to the present work. Sulfonates studied include those in which X is F, CF_3 , CH_3 and $p\text{-CH}_3\text{C}_6\text{H}_4$ and M is Co and Cu (14); and that where X is F and M is Fe (15).

The cobalt(II) and copper(II) analogues were investigated by infrared and electronic spectral techniques and magnetic susceptibility measurements. The studies indicated that all the salts have layer lattice structures with six-coordinate metal ions and terdentate bridging anions, each anion bridging to three different metal ions through oxygen. The general structure proposed for $\text{M}(\text{XSO}_3)_2$ compounds is shown in Fig. 1.1. Significant distortions of the MO_6 chromophores from regular octahedral geometry were

FIG. 1.1.

PROPOSED STRUCTURE OF $\text{Fe}(\text{XSO}_3)_2$ COMPOUNDS

indicated for all the cobalt and copper compounds with the possible exceptions of $\text{Co}(\text{FSO}_3)_2$ and $\text{Co}(\text{p-CH}_3\text{C}_6\text{H}_4\text{SO}_3)_2$.

Iron(II) fluorosulfonate was prepared and its infrared spectrum reported (16). Further studies (15) included Mössbauer and electronic spectroscopy and magnetic susceptibility measurements. These studies showed the compound to consist of FeO_6 octahedra distorted by a trigonal elongation and that the electronic ground state is an orbital doublet.

Crystallographic studies on sulfonate compounds are somewhat limited but single crystal X-ray studies have been reported on $\text{Ca}(\text{CH}_3\text{SO}_3)_2$ and $\text{Ag}(\text{CH}_3\text{SO}_3)$ (17,18). The calcium salt is a highly polymeric lattice containing terdentate bridging anions, each anion bridging to a different metal centre resulting in octahedral coordination around calcium. The structure is similar to that proposed in Fig. 1.1. In silver(I) methanesulfonate the silver ion is in a very distorted trigonal bipyramidal environment. Various hydrated species have also been studied by Charbonnier et al. and include $\text{Cu}(\text{CH}_3\text{SO}_3)_2 \cdot 4\text{H}_2\text{O}$ and $\text{Cd}(\text{CH}_3\text{SO}_3)_2 \cdot 2\text{H}_2\text{O}$ (19,20). The hydrated copper and cadmium salts contain mono- and bidentate CH_3SO_3^- anions and consist of monomeric units and infinite parallel chains respectively.

1.2. PURPOSE AND OUTLINE OF THE PRESENT WORK

This work concerns iron(II) sulfonates and is part of a general study of inorganic coordination polymers - specifically transition metal complexes having structures in which metal ions are

bridged in chains, planes and three dimensions by polyatomic anionic ligands.

The research described here involves the synthesis and characterisation of $\text{Fe}(\text{CF}_3\text{SO}_3)_2$, $\text{Fe}(\text{CH}_3\text{SO}_3)_2$ and $\text{Fe}(\text{p-CH}_3\text{C}_6\text{H}_4\text{SO}_3)_2$ and represents an extension of previous studies in this laboratory on related cobalt(II), copper(II) and iron(II) compounds.

The materials were prepared and studied with several objectives in mind :

- (i) To develop techniques and criteria for identifying modes of coordination and for molecular structure determination in sulfonate compounds.
- (ii) To understand factors determining the mode and strength of coordination of sulfonate ligands.
- (iii) To examine the phenomenon of structural isomerism in coordination polymers, understanding why it occurs and what effects it has on polymer properties.
- (iv) To obtain coordination polymers which show strong magnetic interactions and to study these to help in our understanding of magnetic exchange phenomena between paramagnetic centres.

The techniques used in the present work to characterise these sulfonate polymers will be discussed briefly.

The experimental techniques used in the synthesis and characterisation of the compounds studied will be presented in

Chapter 2.

Vibrational spectroscopy (Chapter 3) probes the nature of the anion and provides insight into anion-anion as well as anion-cation interactions.

Electronic spectroscopy (visible - u.v.) enables d-d transitions to be observed and provides a measure of the separation of ground and excited electronic states. These may be related to the ligand-field effects provided by the sulfonate anions and are discussed in Chapter 4.

Further information regarding the nature of the ground electronic state in these iron(II) sulfonate polymers may be obtained from magnetic susceptibility measurements and these are the topic of Chapter 5.

The presence of the ^{57}Fe nucleus in the compounds prepared has enabled the powerful tool of Mössbauer spectroscopy to be used to probe the electronic and structural environment of the iron cation. This technique is discussed in Chapter 6.

Magnetically-perturbed Mössbauer spectra in which the sample is perturbed by an applied magnetic field, provide even more detailed information and this is the topic of Chapter 7.

In view of the polymeric nature of these compounds the possibility exists for magnetic exchange between neighbouring iron ions through bridging anions. Previous work on the "parent"

compound FeSO_4 indicates that it becomes magnetically ordered below 23K (21). In the present work there is evidence for magnetic exchange in $\text{Fe}(\text{CH}_3\text{SO}_3)_2$ from both magnetic susceptibility measurements and Mossbauer spectroscopy.

In $\text{Fe}(\text{FSO}_3)_3$, previously studied by Goubeau and Milne (22), it was observed that the magnetic moment is significantly less than 5.92 B.M. expected for a high-spin d^5 electron configuration and is temperature and field dependent. Goubeau and Milne proposed that both ferro- and antiferromagnetic exchange mechanisms are operating in this material.

The possibility that such magnetic exchange may be present in the other iron(III) sulfonates led to the preparations of $\text{Fe}(\text{CF}_3\text{SO}_3)_3$, $\text{Fe}(\text{CH}_3\text{SO}_3)_3$ and $\text{Fe}(\text{p-CH}_3\text{C}_6\text{H}_4\text{SO}_3)_3$. Chapter 8 describes the preliminary studies on these compounds. Again in comparison with FeSO_4 the parent compound of these iron(III) sulfonates, $\text{Fe}_2(\text{SO}_4)_3$, spontaneously orders magnetically at temperatures below 28.7K (23).

CHAPTER 2

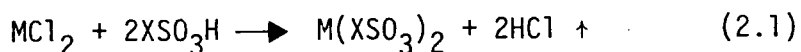
EXPERIMENTAL METHODS

2.1. INTRODUCTION

Experimental details of the work involved in this study are outlined in this chapter; included are sources of materials, synthesis of the compounds studied and information regarding the physical techniques of investigation.

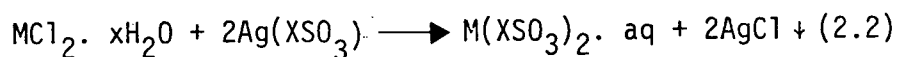
Two general methods of preparation have been utilised previously for sulfonate compounds of the type $M(XSO_3)_2$, (where M is a first-row transition metal cation and X is F, CF_3 , CH_3 , $p-CH_3C_6H_4$). These are:

- (i) A reaction between the anhydrous metal chloride and the acid (14,16).



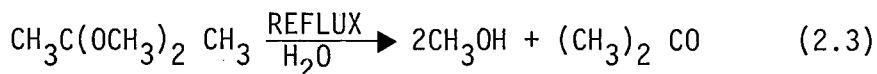
Where X is F or CF_3 .

- (ii) A stoichiometric reaction between aqueous solutions of the silver salt of the acid and the hydrated metal chloride (14).



Where X is CH_3 or $p-CH_3C_6H_4$.

Dehydration of the hydrated species $M(XSO_3)_2 \cdot aq$ was achieved either by heating under vacuum or by using the ether solvent 2,2-dimethoxypropane (D.M.P.) which proved to be a good dehydrating agent (24).



Boiling under reflux with D.M.P. led to some interesting structural modifications for iron(II) methanesulfonate and enabled two distinct isomers of this compound to be isolated.

Both methods of preparation have been used in this study; the resulting anhydrous compounds were found to be very susceptible to atmospheric moisture and when isolated were handled either in an inert atmosphere or under vacuum. To prevent oxidation of iron(II) to iron(III) all solvents were degassed prior to use by several freeze-pump-thaw cycles.

Both methods of preparation gave "nearly" quantitative yields of product.

Analytical data for the compounds prepared are given in Table 2.1.

2.2. MATERIALS

All chemicals and solvents were Reagent or Analytical grade and were used without further purification unless otherwise stated. The commercial sources of the materials used were: $\text{CF}_3\text{SO}_3\text{H}$, 3M Company; $\text{Ag}(\text{CH}_3\text{SO}_3)$, $\text{Ag}(\text{p-CH}_3\text{C}_6\text{H}_4\text{SO}_3)$ and $\text{CH}_3\text{SO}_3\text{H}$, Eastman Kodak Company Ltd. ; ZnCl_2 Analar and $\text{FeCl}_2 \cdot 4\text{H}_2\text{O}$ Analar, Mallinckrodt Inc. ; FeCl_2 and 2,2-dimethoxypropane, Aldrich Chemical Company Inc. ; FeCl_3 , Matheson, Coleman and Bell Ltd.; $\text{CoCl}_2 \cdot 6\text{H}_2\text{O}$ Analar, $\text{NiCl}_2 \cdot 6\text{H}_2\text{O}$ Analar, $\text{CuCl}_2 \cdot 2\text{H}_2\text{O}$ Analar and

$\text{CaCl}_2 \cdot 2\text{H}_2\text{O}$ Analar, British Drug Houses Ltd. ; $\text{FeCl}_3 \cdot 6\text{H}_2\text{O}$, Fisher Scientific Company Ltd.

2.3. THE DRY BOX

Inert atmospheres were obtained with a D.L. Herring Corporation Dri-Lab (Model HE-43), equipped with a Dry-train (Model HE-93). Purified K-grade nitrogen (Canadian Liquid Air Ltd.) was circulated through the box via Linde 4A Molecular Sieves. An oven incorporated into the system enabled the sieves to be regenerated periodically to maintain a dry atmosphere.

2.4. SYNTHESIS OF COMPOUNDS

2.4.1. Iron(II) Trifluoromethanesulfonate, $\text{Fe}(\text{CF}_3\text{SO}_3)_2$

Trifluoromethanesulfonic acid (20 mL) was freshly distilled at a pressure of 20 mm Hg at 70°C onto anhydrous iron(II) chloride (12 mmol). The iron(II) chloride was prepared by a literature method (25).

Indicative of its polymeric nature the product was found to be insoluble in the acid. During the course of the reaction, noted by the evolution of hydrogen chloride gas, an insoluble layer of product developed around the reactant inhibiting further reaction. To ensure complete reaction the mixture was stirred and boiled under reflux for approximately 40h. The product was vacuum filtered and washed with freshly distilled trifluoromethanesulfonic acid. Traces

of excess acid were removed from the white product by heating under vacuum at 50°C.

2.4.2 Iron(II) Paratoluenesulfonate, $\text{Fe}(\text{p-CH}_3\text{C}_6\text{H}_4\text{SO}_3)_2$

This salt was prepared by the reaction of aqueous solutions of silver(I) paratoluenesulfonate (17 mmol in 50 mL H_2O) with iron(II) chloride tetrahydrate (8.5 mmol in 10 mL H_2O). The resulting mixture was stirred under a flow of nitrogen gas and precipitated silver(I) chloride was removed by filtration. The solution of iron(II) paratoluenesulfonate was evaporated to dryness under vacuum and complete dehydration was accomplished by heating under vacuum at 120°C. The anhydrous compound is a pale green solid.

2.4.3. Iron(II) Methanesulfonate, $\text{Fe}(\text{CH}_3\text{SO}_3)_2$.

In a modification of the method used to prepare $\text{Fe}(\text{p-CH}_3\text{C}_6\text{H}_4\text{SO}_3)_2$, the stoichiometric reaction between silver(I) methanesulfonate (9.2 mmol in 30 mL H_2O) and iron(II) chloride tetrahydrate (4.6 mmol in 10 mL H_2O) resulted in a mixture of silver(I) chloride and an aqueous solution of the desired product. After removal of silver(I) chloride by filtration the solution was evaporated to dryness under vacuum, and further heating under vacuum at 130°C for 12h gave the anhydrous product, $\alpha\text{-Fe}(\text{CH}_3\text{SO}_3)_2$.

Initially dehydration by boiling under reflux in D.M.P. had resulted in a product which gave complex infrared and Mossbauer spectra. However, prolonged refluxing, three days under an inert

atmosphere, gave a structurally modified isomer, $\beta\text{-Fe}(\text{CH}_3\text{SO}_3)_2$.

To check the isomeric purity of each species Mössbauer spectroscopy could be used because of large differences in quadrupole splitting values for the two isomers at all temperatures. Anything less than approximately 98% conversion of the α -isomer into the β -form could be easily detected by the presence of more than one pair of quadrupole-split Mössbauer absorptions. Infrared spectroscopy was found to be a less sensitive test in this regard. It was estimated that infrared spectroscopy was incapable of detecting the α -isomer when it was present at less than approximately 10% in the mixture.

Because of the different structural modifications shown by iron(II) methanesulfonate, an attempt was made to prepare the compound under anhydrous conditions.

Methanesulfonic acid (20 mL) was distilled at a pressure of 8.5 mm Hg onto anhydrous iron(II) chloride (15 mmol). A vigorous reaction occurred as noted by the evolution of hydrogen chloride gas. The reaction mixture was heated at approximately 100°C for 8 h and then filtered under vacuum. The white product was washed with several portions of freshly distilled acid. However, even after drying under vacuum for 48 h at 150°C methanesulfonic acid still remained as a solvate as evidenced by the infrared spectrum and analytical data, see Tables 3.6 and 2.1 respectively.

Solvate formation of this type was observed previously when cobalt(II) chloride was reacted with methanesulfonic acid (26).

2.4.4. Preparation of other Methanesulfonates, $M(\text{CH}_3\text{SO}_3)_2$;

where M is Co, Ni, Cu, Zn and Ca.

The cobalt(II) and copper(II) analogues were prepared as described in Ref. 14; the remaining compounds were prepared by stoichiometric reactions between aqueous solutions of $\text{MCl}_2 \cdot x\text{H}_2\text{O}$ and $\text{Ag}(\text{CH}_3\text{SO}_3)$. Silver(I) chloride was removed by filtration and the product dried by heating under vacuum at approximately 100°C . The anhydrous products were then treated with D.M.P. to observe whether any structural modifications took place.

2.4.5. Iron(III) Trifluoromethanesulfonate, $\text{Fe}(\text{CF}_3\text{SO}_3)_3$.

Trifluoromethanesulfonic acid (20 mL) was freshly distilled at a pressure of 20 mm Hg onto anhydrous iron(III) chloride (10 mmol). Complete reaction was obtained by boiling the mixture under reflux for approximately 40h. The white product was filtered, washed with freshly distilled acid and dried under vacuum at 150°C .

2.4.6. Iron(III) Paratoluenesulfonate, $\text{Fe}(\text{p-CH}_3\text{C}_6\text{H}_4\text{SO}_3)_3$

Silver(I) paratoluenesulfonate (11.2 mmol in 20 mL H_2O) was reacted with an aqueous solution of iron(III) chloride hexahydrate (3.6 mmol in 15 mL H_2O). After removal of precipitated silver(I) chloride the aqueous solution was reduced in volume and dehydration was achieved by heating under vacuum at 70°C to yield the orange product.

2.4.7. Iron(III) Methanesulfonate, $\text{Fe}(\text{CH}_3\text{SO}_3)_3$

This salt was prepared by the reaction of stoichiometric quantities of silver(I) methanesulfonate (17.0 mmol in 20 mL H_2O) and iron(III) chloride hexahydrate (5.8 mmol in 15 mL H_2O). The pale yellow product was obtained by the usual technique of evaporation of excess solvent and heating under vacuum at 110°C .

2.5. ANALYTICAL DATA

Elemental analyses were performed in the microanalytical laboratory of this department by P. Borda. Iron analyses were done by a Redox titration with potassium dichromate using sodium diphenylamine sulfonate as indicator (27).

All analytical data are given in Table 2.1.

2.6. PHYSICAL EXPERIMENTAL TECHNIQUES

2.6.1. Infrared spectroscopy

Infrared spectra were recorded over the frequency range $4,000\text{--}250\text{cm}^{-1}$ using a Perkin Elmer 457 grating spectrophotometer. Mulling agents used were Nujol and hexachloro-1, 3-butadiene. Mulls were placed between KRS-5 plates (58% TlI , 42% TlBr), supplied from the Harshaw Chemical Company.

All mulls were prepared in the dry box and the windows sealed with adhesive tape to prevent hydration of samples. All spectra were calibrated at 1601 and 907cm^{-1} using a polystyrene

TABLE 2.1

ANALYTICAL DATA

COMPOUND	THEORY %			FOUND %		
	Fe	C	H	Fe	C	H
$\text{Fe}(\text{CF}_3\text{SO}_3)_2$	15.8	6.78	0.00	15.9	6.75	0.00
$\alpha\text{-Fe}(\text{CH}_3\text{SO}_3)_2$	22.7	9.76	2.46	22.5	9.93	2.48
$\beta\text{-Fe}(\text{CH}_3\text{SO}_3)_2$	22.7	9.76	2.46	22.5	9.59	2.60
$\text{Fe}(\text{p-CH}_3\text{C}_6\text{H}_4\text{SO}_3)_2$	14.0	42.22	3.55	13.9	42.50	3.60
$\text{Fe}(\text{CH}_3\text{SO}_3)_2 \cdot \text{CH}_3\text{SO}_3\text{H}$		10.53	2.95		10.37	2.86
$\text{Co}(\text{CH}_3\text{SO}_3)_2$		9.63	2.43		9.51	2.39
$\text{Ni}(\text{CH}_3\text{SO}_3)_2$		9.65	2.43		9.49	2.41
$\text{Cu}(\text{CH}_3\text{SO}_3)_2$		9.46	2.38		9.30	2.48
$\text{Zn}(\text{CH}_3\text{SO}_3)_2$		9.40	2.37		9.75	2.64
$\text{Ca}(\text{CH}_3\text{SO}_3)_2$		10.43	2.63		10.52	2.71
$\text{Fe}(\text{CF}_3\text{SO}_3)_3$	11.1	7.16	0.00	11.3	7.04	0.00
$\text{Fe}(\text{CH}_3\text{SO}_3)_3$	16.4	10.56	2.66	16.1	10.50	2.80
$\text{Fe}(\text{p-CH}_3\text{C}_6\text{H}_4\text{SO}_3)_3$	9.8	44.29	3.72	9.7	44.16	3.85

film, and tabulated infrared frequencies are considered accurate to $\pm 5\text{cm}^{-1}$ for broad bands and $\pm 2\text{cm}^{-1}$ for sharp bands.

2.6.2. Electronic spectroscopy

A Cary Model 14 recording spectrophotometer was used to record electronic spectra over the frequency range 4,000 - 30,000 cm^{-1} .

Solid state spectra were recorded on Nujol or hexachlorobuta-1,3-diene mulls contained between silica glass windows. Light scattering from the sample was compensated for by placing neutral density filters in the reference beam.

2.6.3. Magnetic susceptibility measurements

Magnetic susceptibility measurements were recorded over the temperature range 80-320K using a Gouy balance previously described (28). A magnetic field strength of 0.45T was employed and the sample was uniformly packed in a Pyrex tube which had been previously calibrated to compensate for its diamagnetism. All measurements were made in a nitrogen atmosphere and calibration of the apparatus was achieved using mercury(II) tetrathiocyanatocobaltate(II) as a standard (29).

Errors due to inhomogeneous packing of the sample were minimised by performing at least three separate determinations, each involving repacking of the Gouy tube.

All samples were tested for field dependence of the magnetic susceptibility using a Faraday magnetic balance, described now. An

Alpha Model 9500 6" water-cooled electromagnet with Heyding pole design was used to provide constant field gradients of $253,526,869 \text{ T}^2\text{cm}^{-1}$. The sample was placed in a quartz bucket suspended from a Cahn Rg electrobalance and measurements were made in a nitrogen atmosphere.

Minimal packing errors are involved in the Faraday method and room temperature susceptibilities obtained in this way were used to correct the variable temperature measurements from the Gouy balance.

The effective magnetic moment of the metal ion was calculated from the relationship

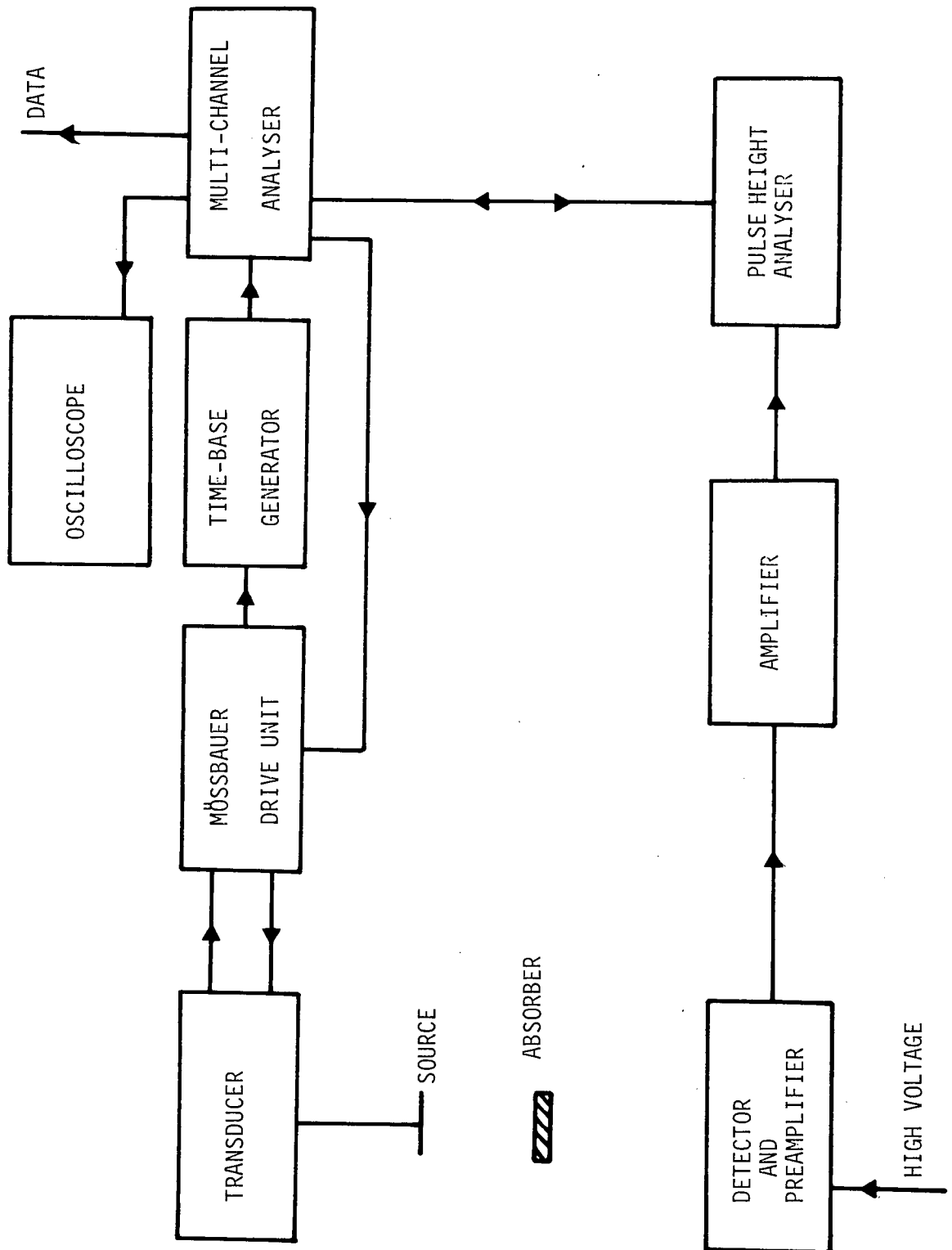
$$\mu_{\text{EFF}} = 2.828 (\chi_a \cdot T)^{\frac{1}{2}} \quad (2.4)$$

where T is the Kelvin temperature and χ_A the molar susceptibility corrected for the diamagnetism of the atoms and ions present. The diamagnetic corrections used in the present study were $\text{Fe}^{2+} = 13$, $\text{Fe}^{3+} = 10$, $\text{CF}_3\text{SO}_3^- = 46$, $\text{CH}_3\text{SO}_3^- = 35$, $\text{p-CH}_3\text{C}_6\text{H}_4\text{SO}_3^- = 89$. All are given in 10^{-6} c.g.s. units ($10^{-6} \text{ cm}^3 \text{ mol}^{-1}$) and were obtained from Pascal's constants (30-32).

2.6.4. Mössbauer spectroscopy

Fig. 2.1 shows a schematic diagram of a typical Mössbauer spectrometer. The velocity modulation of the gamma radiation is achieved using a Technical Measurements Corporation Model 306 drive unit powered by a K3-K linear motor. The transmitted gamma radiation was detected using a Reuter-Stokes RSG-61 proportional counter containing Xe with CO_2 at a pressure of two atmospheres and

FIG. 2.1. SCHEMATIC DIAGRAM OF A MÖSSBAUER SPECTROMETER



a Nuclear - Chicago Model 24-2 400-word multichannel analyser operating in the multiscalar mode. Also included (Nuclear - Chicago modules) were a Model 40-9B high-voltage power supply, a Model 238105 preamplifier, a Model 33-15 amplifier - single channel analyser, a Model 23-4 analog-to-digital converter, and a Model 021308 time-base generator.

Shown in Fig. 2.2 is a schematic diagram of the apparatus used to obtain variable temperature (8-300K) Mössbauer spectra in the absence of an applied magnetic field. Nylon sample holders which could be sealed with epoxy resin were designed to alleviate problems of sample hydration experienced with more conventional copper cells. The cell containing the finely powdered sample was mounted on a copper annulus to ensure good thermal contact between the sample and the coolant, which in the Janis Model DT-6 cryostat was helium exchange gas. The temperature was set and maintained to within $\pm 0.02^{\circ}\text{C}$ with a Cryogenic Research Model TC-101 temperature controller whilst a spectrum was recorded. Temperatures were measured with calibrated Ge and Pt resistance thermometers.

All spectra were recorded in a transmission geometry, the radiation source (^{57}Co in a Cu or Rh matrix) being maintained at room temperature. The Doppler velocity scale was calibrated using a metallic iron foil absorber and isomer shifts are quoted relative to the centroid of the iron foil spectrum.

The cryostat used in this work to record magnetically-perturbed Mössbauer spectra (magbauer spectra) is shown in Fig. 2.3.

FIG. 2.2 SCHEMATIC DIAGRAM OF APPARATUS USED FOR
OBTAINING VARIABLE TEMPERATURE MÖSSBAUER SPECTRA

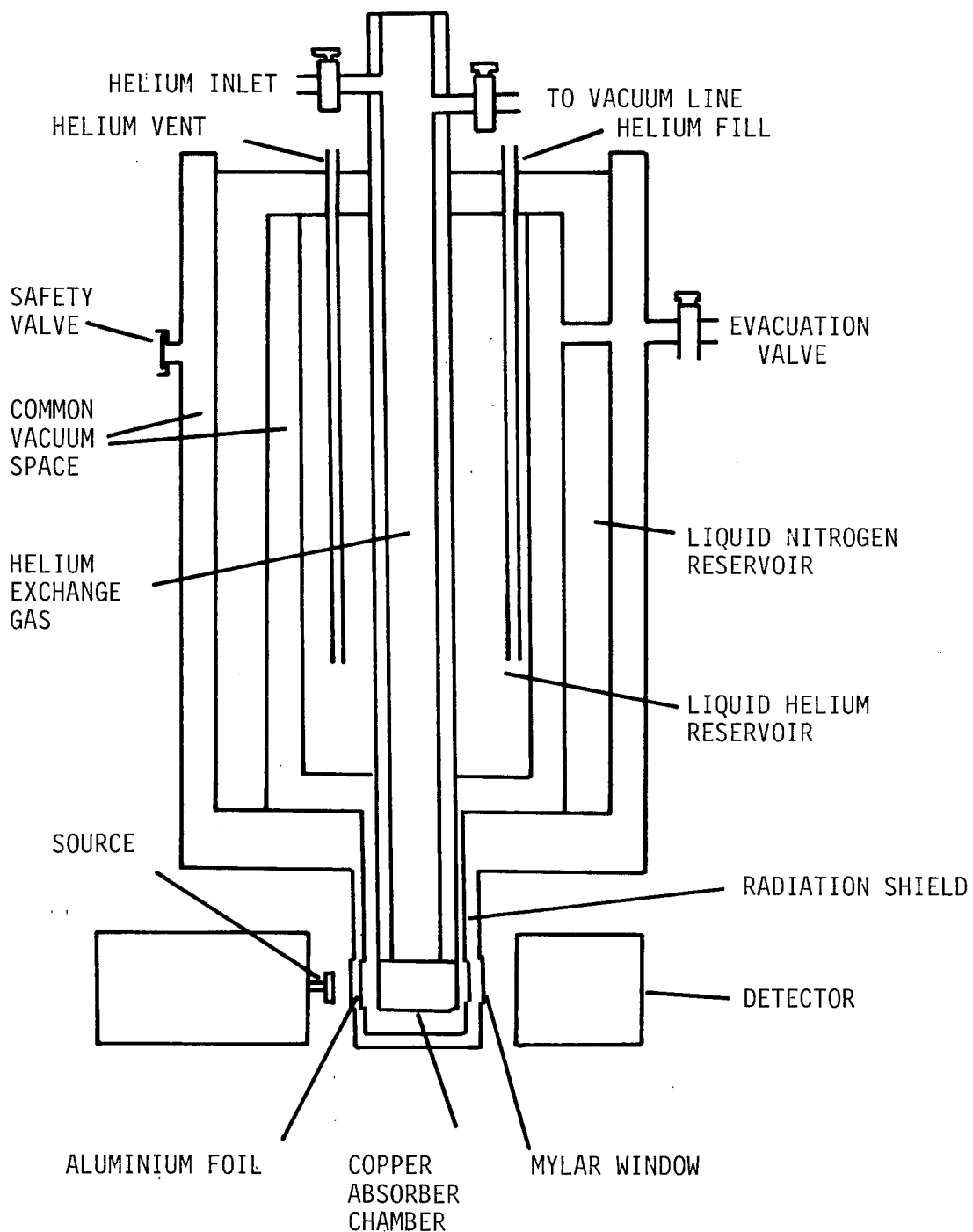
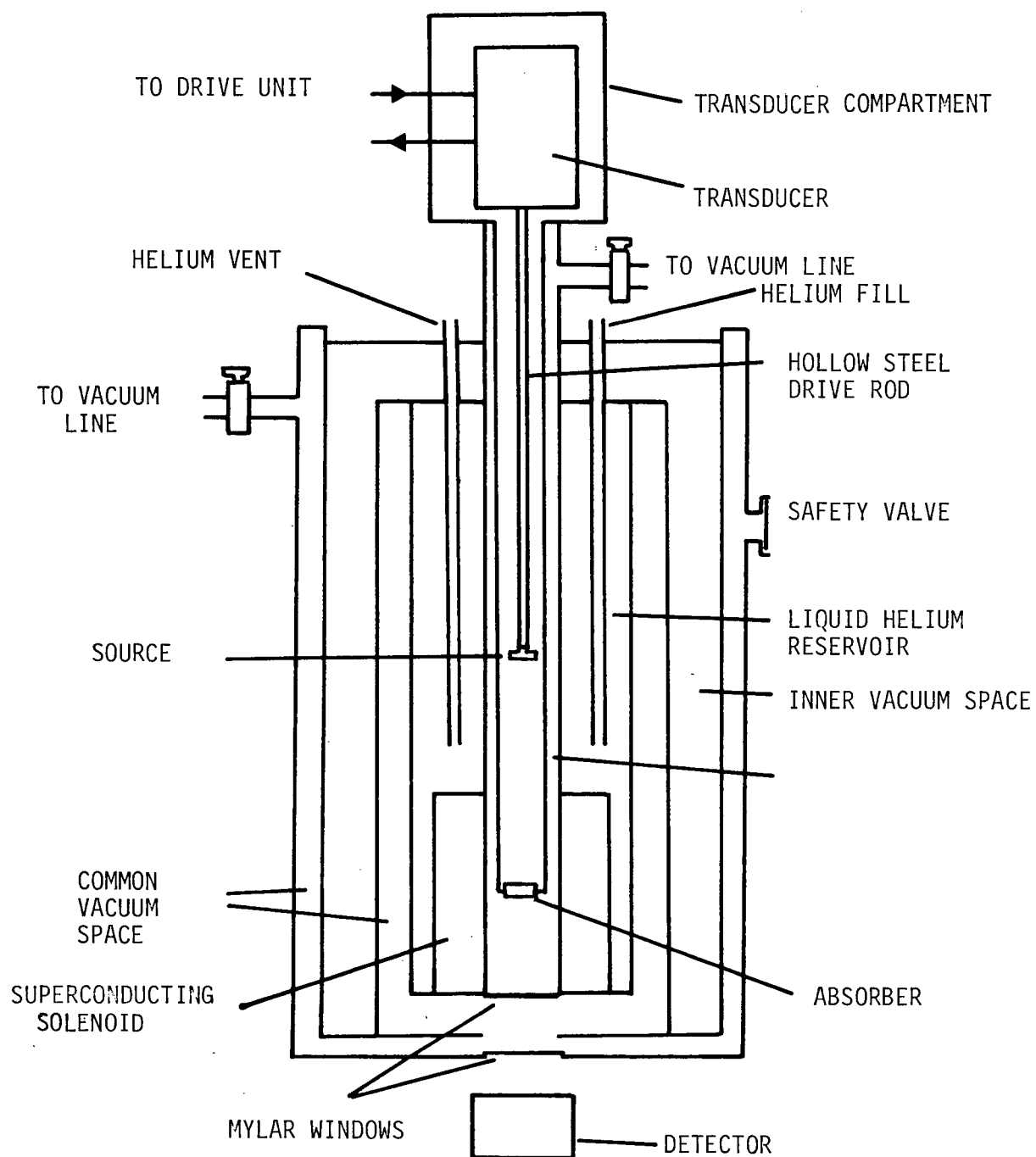


FIG. 2.3 SCHEMATIC DIAGRAM OF APPARATUS USED FOR OBTAINING
MAGNETICALLY-PERTURBED MÖSSBAUER SPECTRA



A transmission geometry was employed; however, the source, absorber and detector are aligned vertically in this cryostat as opposed to the horizontal arrangement in Fig. 2.2. The cryostat here is fitted with a Westinghouse superconducting solenoid capable of generating magnetic fields of up to 5.63T parallel to the direction of the γ -ray beam. The sample is located at the centre of the applied field. The vertically mounted source is outside the influence of the magnetic field and is driven, via a long thin-walled stainless steel drive shaft, by an Austin Science Associates K-3 linear motor.

The cryostat used for obtaining the magnetically perturbed Mössbauer spectra could be operated between 2.3K and room temperature. For magbauers above 80K the temperature was measured with a copper-constantan thermocouple; temperatures below 80K were measured with a germanium diode. The magbauer apparatus can be operated between 4.2K and room temperature by controlling the exchange gas pressure and the heater current, and between 2.3 and 4.2K by controlling the pumping speed, via a valve arrangement, and hence the helium vapour pressure. A high-capacity vacuum pump was used to enable the pumping of the vapour space above the liquid helium reservoir.

2.6.5. Analysis of Mössbauer spectra

Spectra obtained in the absence of an applied magnetic field were fitted to Lorentzian curves by a least squares fitting treatment of the data points. The programme treated the positions, line widths and intensities as unconstrained fitting parameters.

Magnetically - perturbed Mössbauer spectra were compared with theoretical spectra generated by programmes written by Dr. A. Hulme and based on one by Lang (33) or one derived from a phenomenological model first used by Varret (34). Details of fitting procedures for magnetically-perturbed Mössbauer spectra and the programme used for deriving the crystal-field splitting parameters will be given in the appropriate sections.

CHAPTER 3

VIBRATIONAL SPECTROSCOPY

3.1. INTRODUCTION

Vibrational spectroscopy has proven to be an invaluable tool for inorganic coordination chemists. Infrared and Raman spectroscopy have been found to be useful in structure elucidation, particularly where the result of single crystal X-ray diffraction studies are not available. On the basis of vibrational spectroscopy the basic structure of $(\text{CH}_3)_2\text{Sn}(\text{FSO}_3)_2$ was proposed (35), before being confirmed by a single crystal X-ray diffraction study (36).

In previous studies of $\text{M}(\text{XSO}_3)_2$ compounds very little structure determination by X-ray diffraction has been possible because of the difficulties of obtaining these compounds in a suitable crystalline form. Calcium(II) methanesulfonate (17) and silver(I) methanesulfonate (18) appear to be the only anhydrous methanesulfonate species to have been studied by X-ray diffraction methods. Various hydrated species have been studied (e.g. $\text{Cu}(\text{CH}_3\text{SO}_3)_2 \cdot 4\text{H}_2\text{O}$, (19) and $\text{Cd}(\text{CH}_3\text{SO}_3)_2 \cdot 2\text{H}_2\text{O}$, (20)). These contain mono- and bidentate CH_3SO_3^- anions and consist of monomeric units and infinite parallel chains respectively. In contrast $\text{Ca}(\text{CH}_3\text{SO}_3)_2$ is highly polymeric with anions acting as terdentate bridging ligands forming a layer lattice type structure, similar to that shown in Fig. 1.1.

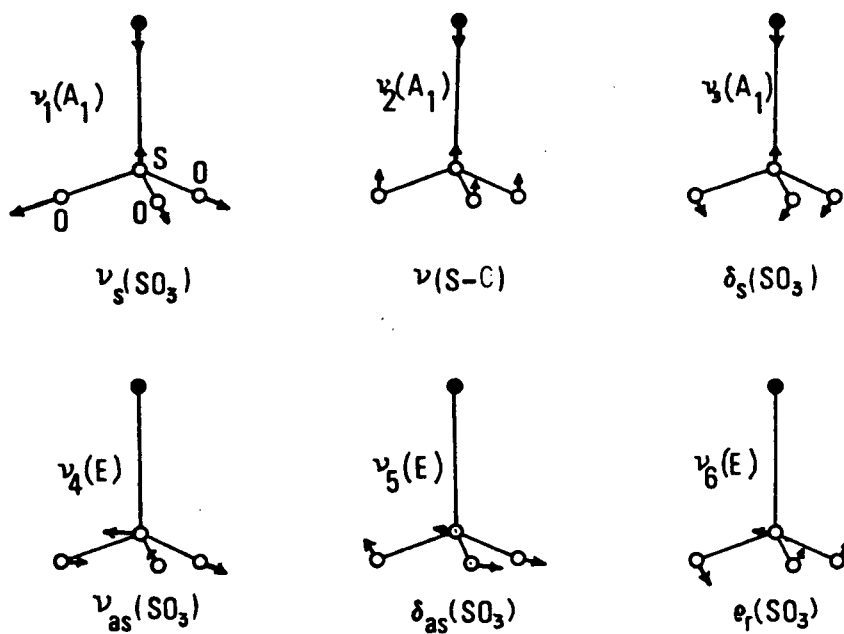
Structure determination using vibrational spectroscopy was particularly important in the present work as the compounds could not be isolated as single crystals and hence could not be studied by X-ray diffraction methods.

The frequency and number of vibrational bands provide information on the anion symmetry, which in turn may be used, with caution, to deduce the geometry around the cation. As well as investigating these anion-cation interactions this study has also probed the nature of anion-anion interactions.

This work represents an extension of previous studies of the relative coordination strengths of anions derived from strong protonic acids (14).

3.2. THEORY OF VIBRATIONAL SPECTRA AND STRUCTURE

The local symmetry around the sulfur atom in free uncoordinated XSO_3^- anions is C_{3v} . Group theory predicts six normal modes of vibration; three of symmetry species A_1 and three doubly degenerate vibrations of symmetry species E. All six vibrations are active in both infrared and Raman and may be qualitatively described as shown in Fig. 3.1. If the symmetry of the anion is lowered from C_{3v} to C_s the doubly degenerate E modes will split, giving rise to nine normal modes of vibration. Again they are all infrared and Raman active (see Table 3.1).

FIG. 3.1. NORMAL MODES OF VIBRATION OF THE XSO_3^- ANIONTABLE 3.1 CORRELATION TABLE FOR C_{3v} AND C_s POINT GROUPS

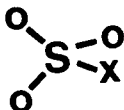
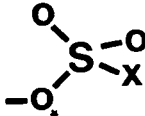
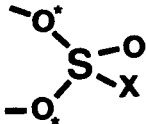
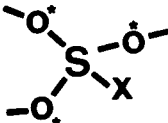
Point Group	ν_1	ν_2	ν_3	ν_4	ν_5	ν_6
C_{3v}	A_1	A_1	A_1	E	E	E
C_s	A_1	A_1	A_1	$A' + A''$	$A' + A''$	$A' + A''$

Reduction in point group symmetry from C_{3v} to C_s may occur through site-symmetry effects or anion coordination. The former effect arises from the crystalline environment affecting the local anion symmetry and usually gives rise to small splittings (for example, $4\text{--}18\text{ cm}^{-1}$ in $\text{Na}(\text{CH}_3\text{SO}_3)$ (37)). The latter effect of anion coordination, arises when the XSO_3^- coordinates through one or two of the oxygen atoms, i.e. uni- or bidentate anion coordination. This lowers the anion symmetry to C_s . If, on the other hand, the XSO_3^- anion is involved in terdentate coordination by equivalent bonding through each of the three oxygen atoms then the anion symmetry is again C_{3v} (see Fig. 3.2).

The splitting of the E modes observed when site-symmetry effects are involved is usually less than when anion coordination is the cause. Thus, the magnitude of the splitting is usually the only criterion for distinguishing these two possibilities.

We turn now to a general discussion of the type of spectra observed for $\text{Fe}(\text{XSO}_3)_2$ compounds and the structure proposed for these materials. If the XSO_3^- anion retains its C_{3v} symmetry, as observed in $\text{Fe}(\text{FSO}_3)_2$ (16), terdentate XSO_3^- bridging anions may be proposed, with each oxygen coordinating to a different metal centre. This results in FeO_6 octahedra in a polymeric layer structure (Fig. 1.1), a type of structure proposed for all of the $\text{Fe}(\text{XSO}_3)_2$ compounds. However, as will be seen from the Mossbauer spectra of these compounds, to be presented in Chapter 6, a distortion of the FeO_6 octahedron must be proposed to explain the

FIG. 3.2. BONDING AND SYMMETRY PROPERTIES OF THE XSO_3^- ANION

	<u>POINT GROUP</u>	<u>MODE OF COORDINATION</u>
	C_{3v}	Free uncoordinated anion
	C_s	Unidentate
	C_s	Bidentate
	C_{3v}	Terdentate

observed quadrupole splitting.

Two simple distortions of the FeO_6 octahedron may be proposed. Firstly, a tetragonal distortion along the C_4 axis of the octahedron in which four of the oxygen atoms would differ from the remaining two axial oxygen atoms. A tetragonal distortion of this type would lower the anion symmetry to C_2 , and this should be observable in the infrared spectrum as a removal of the degeneracy of the E vibrational modes.

The second type of distortion proposed is a trigonal distortion along the C_3 axis of the FeO_6 octahedron. Here, the six oxygen atoms surrounding the iron cation would remain equivalent and the anion would retain its C_{3v} symmetry.

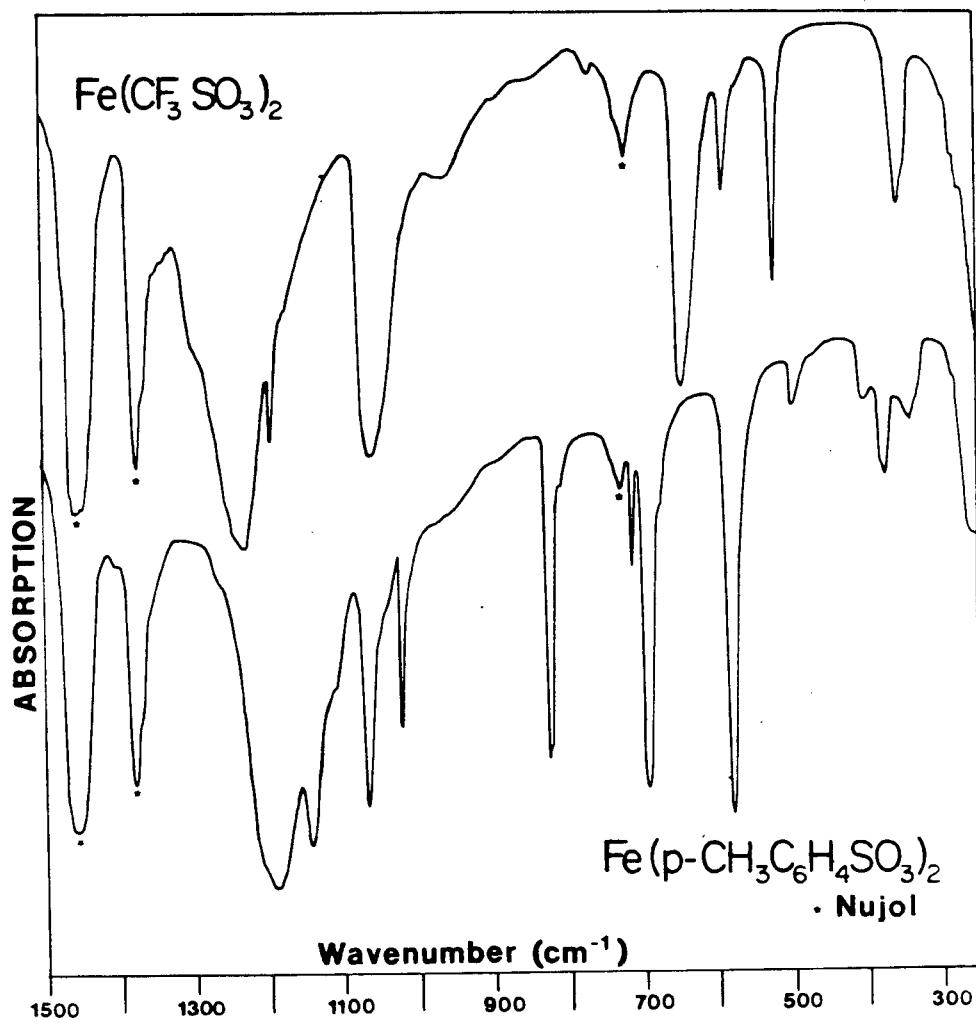
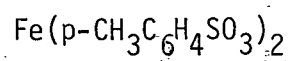
In this manner vibrational spectroscopy may be used to investigate structure in metal sulfonate compounds.

Table 3.2 shows the infrared frequencies for all the iron(II) sulfonates studied in this work and Fig. 3.3 shows the infrared spectra of $\text{Fe}(\text{CF}_3\text{SO}_3)_2$ and $\text{Fe}(\text{p-CH}_3\text{C}_6\text{H}_4\text{SO}_3)_2$. The infrared spectra of the α - and β -forms of $\text{Fe}(\text{CH}_3\text{SO}_3)_2$ are shown in Fig. 3.4. The following sections describe in some detail the spectra and assignments for the iron(II) sulfonates and $\text{M}(\text{CH}_3\text{SO}_3)_2$ compounds (where M is Co, Ni, Cu, Zn and Ca).

TABLE 3.2 INFRARED SPECTRAL DATA (cm^{-1}) FOR $\text{Fe}(\text{XSO}_3)_2$ COMPOUNDS

C_{3v} Assignment For XSO_3^- ANION	X			
	CF_3	$\alpha\text{-CH}_3$	$\beta\text{-CH}_3$	$\text{p-CH}_3\text{C}_6\text{H}_4$
ν_4 (E) SO_3 as. str.	1239 v.s.	1220 s 1175 s	1175 s	1195 s
ν_1 (A_1) SO_3 sym.str.	1062 m	1066 m	1072 m	1145 m
ν_2 (A_1) S-C str.	770 w	790 w	800 m	691 m
ν_5 (E) SO_3 as. def.	647 m	587 m 531 m	551 m	580 m
ν_3 (A_1) SO_3 sym. def.	523 m	513 m	507 m	493 w
ν_6 (E) S-C def. and internal vibrations of CF_3 , CH_3 and $\text{p-CH}_3\text{C}_6\text{H}_4$	<div style="display: inline-block; vertical-align: middle;"> <div style="font-size: 3em; vertical-align: middle;">}</div> <div style="display: inline-block; vertical-align: middle;"> 1300 w.sh 1201 m 965 w 592 w 360 m </div> </div>	<div style="display: inline-block; vertical-align: middle;"> <div style="font-size: 3em; vertical-align: middle;">}</div> <div style="display: inline-block; vertical-align: middle;"> 3030 w 2940 m 1430 m 1400 m 1330 m 970 v.w. 383 m 355 w </div> </div>	<div style="display: inline-block; vertical-align: middle;"> <div style="font-size: 3em; vertical-align: middle;">}</div> <div style="display: inline-block; vertical-align: middle;"> 3040 w 3030 w 2950 w 1425 m 1415 m 1405 m 1330 m 1260 m 975 v.w. 360 w 330 w </div> </div>	<div style="display: inline-block; vertical-align: middle;"> <div style="font-size: 3em; vertical-align: middle;">}</div> <div style="display: inline-block; vertical-align: middle;"> 3000-3100 v.w. 1270 v.w. 1112 v.w. 1070 m 1040 w 822 m 712 w 400 w 370 w 340 w </div> </div>

FIG. 3.3. INFRARED SPECTRA ($1500-250\text{ cm}^{-1}$) OF $\text{Fe}(\text{CF}_3\text{SO}_3)_2$ AND



3.3. INFRARED SPECTRUM OF $\text{Fe}(\text{CF}_3\text{SO}_3)_2$

Several papers (38-44) have provided considerable information regarding the vibrational spectrum of the trifluoromethanesulfonate anion and assignments have been made for both the CF_3 and SO_3 parts of the anion from infrared and Raman spectra.

The infrared spectrum of $\text{Fe}(\text{CF}_3\text{SO}_3)_2$ is shown in Fig. 3.3 and Table 3.3 compares the fundamental vibrations of the CF_3SO_3^- anion in various first-row transition metal compounds with those in $\text{Fe}(\text{CF}_3\text{SO}_3)_2$.

Previously the SO_3 asymmetric stretching vibration (ν_4) in trifluoromethanesulfonate compounds has been assigned a higher frequency than the SO_3 symmetric stretching frequency (ν_1). This result was based upon polarised Raman studies (39). This assignment is followed here and is reflected in Table 3.3. At the resolution of the spectrophotometer used, no splitting of the doubly degenerate SO_3 asymmetric stretching mode is observed. This result suggests that the anion retains its C_{3v} symmetry and that no significant anion distortion occurs in $\text{Fe}(\text{CF}_3\text{SO}_3)_2$.

The ν_2 vibration, described as the sulfur-carbon stretching frequency has not been assigned with certainty in any of these CF_3SO_3^- salts but has been tentatively assigned to a weak absorption at 775 cm^{-1} in the cobalt(II) and copper(II) compounds(14). A weak absorption at 770 cm^{-1} in the iron(II) compounds may be assigned to this vibration. Other assignments (38) have placed

TABLE 3.3 INFRARED SPECTRAL DATA (cm^{-1}) FOR $\text{M}(\text{CF}_3\text{SO}_3)_2$ COMPOUNDS

C_{3v} Assignment for CF_3SO_3^-	M				
	Fe	Co*	Ni ^x	Cu*	Zn ^x
ν_4	1239 s	1235 s	1230 s	1280 s 1225 s	1235 s
ν_1	1062 m	1042 s	1050 s	1058 s	1050 s
ν_5	647 m	630 s	630 s	640 s	640 s
ν_3	523 m	525 m	525 m	530 m	525 m

* Results from reference 14.

x R.C. Thompson, unpublished results.

the sulfur-carbon stretching frequency around 350 cm^{-1} and have assigned the band at approximately 770 cm^{-1} to the symmetric CF_3 deformation. It was noted, however that these two vibrations may be strongly coupled.

Table 3.3 shows that, with the exception of the copper(II) compound, the infrared spectra of the first-row transition metal trifluoromethanesulfonates are very similar. This may be indicative of similar structures for the Fe, Co, Ni and Zn compounds. The structure proposed has the anion retaining C_{3v} symmetry by acting as a terdentate bridging ligand, with each oxygen from a given anion involved in equivalent coordination to three different metal centres, resulting in a highly polymeric lattice (Fig. 1.1).

3.4. INFRARED SPECTRUM OF $\text{Fe}(\text{p-CH}_3\text{C}_6\text{H}_4\text{SO}_3)_2$

The infrared spectrum of iron(II) paratoluenesulfonate is shown in Fig. 3.3 and Table 3.4 compares the infrared frequencies of the anion vibrations with those of other previously studied first-row transition metal paratoluenesulfonates.

The fundamental modes of vibration of the anion have been assigned in Table 3.2. The ν_6 vibration remains unassigned due to the number of internal vibrations of the $\text{p-CH}_3\text{C}_6\text{H}_4$ part of the anion. These internal vibrations also remain unassigned.

The important observations again are that the SO_3 asymmetric stretching and deformation modes remain unsplit, indicating C_{3v} anion

TABLE 3.4 INFRARED SPECTRAL DATA (cm^{-1}) FOR $\text{M}(\text{p-CH}_3\text{C}_6\text{H}_4\text{SO}_3)_2$ COMPOUNDS

C_{3v} Assignment for $\text{p-CH}_3\text{C}_6\text{H}_4\text{SO}_3^-$	M				
	Fe	Co*	Ni ^x	Cu*	Zn ^x
ν_4	1195 s	1200 s	1190 s	$\left\{ \begin{array}{l} 1275 \text{ s} \\ 1266 \text{ sh} \\ 1240 \text{ sh} \\ 1160 \text{ s} \end{array} \right.$	1200 s
ν_1	1145 m	1143 m	1140 s	$\left\{ \begin{array}{l} 1130 \text{ s} \\ 1110 \text{ s} \end{array} \right.$	1142 s
ν_2	691 m	673 m	683 s	680 s	687 s
ν_5	580 m	570 m	574 m	$\left\{ \begin{array}{l} 588 \text{ m} \\ 575 \text{ m} \\ 560 \text{ m} \end{array} \right.$	575 s
ν_3	493 w	488 w	490 w	490 w	490 w

* Results from reference 14

x R.C. Thompson, unpublished results.

symmetry. From Table 3.4 it can be ascertained that, with the exception of the copper(II) compound, the infrared spectra of $M(p\text{-CH}_3\text{C}_6\text{H}_4\text{SO}_3)_2$ compounds, where M is Fe, Co, Ni and Zn, are virtually independent of the cation. The structure proposed for these compounds is one with the anions acting as terdentate bridging ligands resulting in a polymeric lattice as proposed for the trifluoromethanesulfonates.

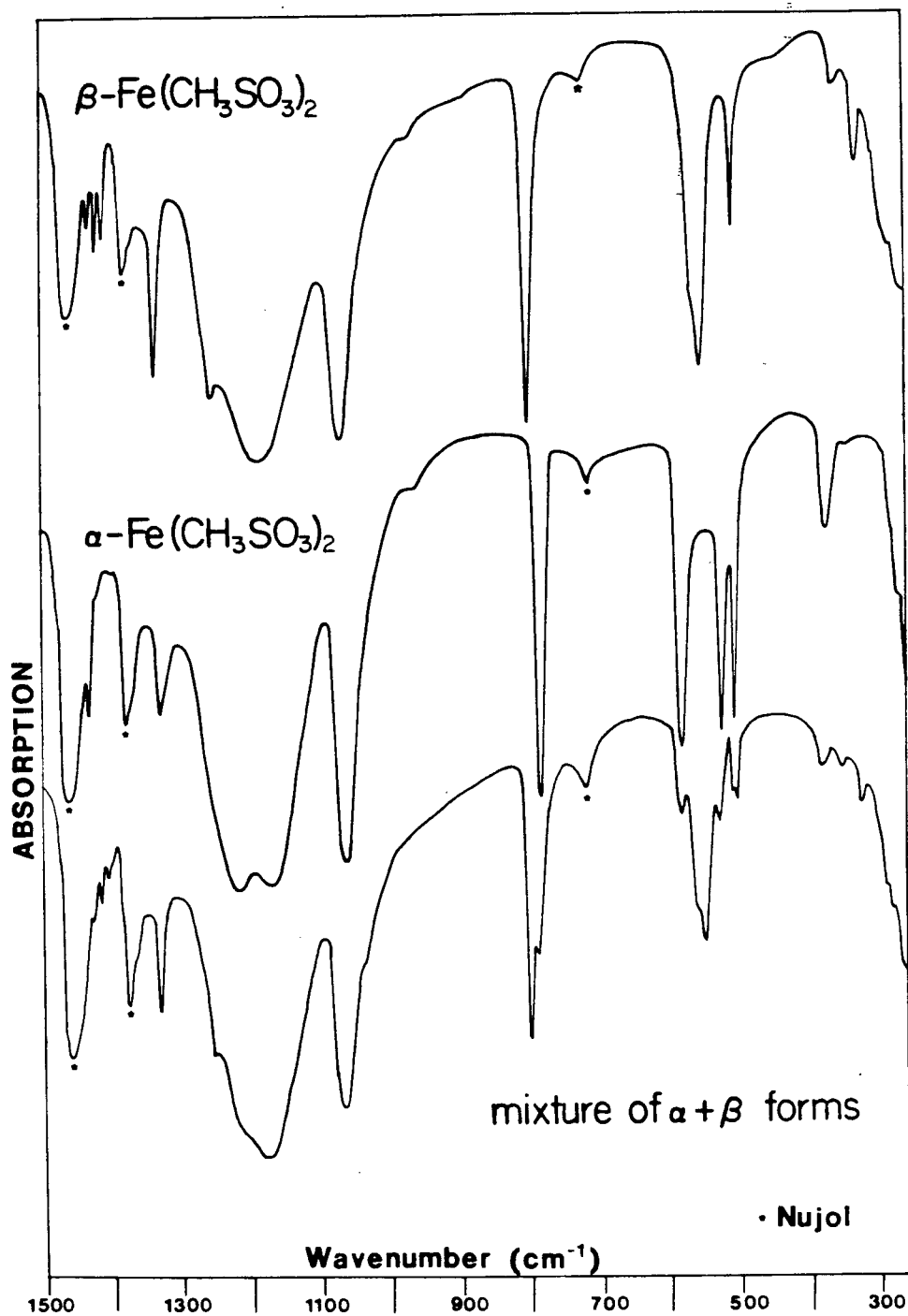
3. 5. INFRARED SPECTRA OF $\text{Fe}(\text{CH}_3\text{SO}_3)_2$

Two forms of this compound, α and β , have been isolated, and have been characterised by infrared spectroscopy. The vibrational frequencies of both forms are listed in Table 3.2 and the infrared spectra of the α and β - forms and of a mixture are shown in Fig. 3.4. Both Miles et al. (38) and Gillespie and Robinson (45) have concluded that the CH_3SO_3^- anion belongs to the C_{3v} point group and assignments made in Table 3.2 are based upon this conclusion.

3.5.1. Infrared Spectrum of α -Iron(II) Methanesulfonate

The α -isomer, the modification produced by thermal dehydration under vacuum, exhibits three absorptions in both the SO_3 bending and stretching regions (see Table 3.2). Both doubly degenerate E modes have been split and the magnitude of the splitting is 45 and 56 cm^{-1} for the ν_4 and ν_5 vibrations respectively. This indicates a distortion of the anion with a concomitant lowering

FIG. 3.4 INFRARED SPECTRA (1500-250 cm^{-1}) OF $\text{Fe}(\text{CH}_3\text{SO}_3)_2$

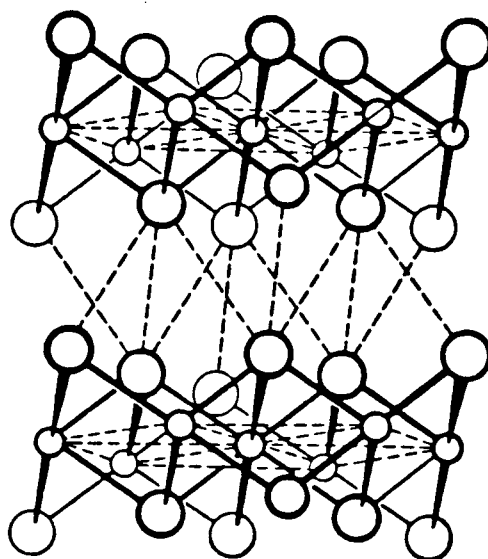


of anion symmetry below C_{3v} to C_s . As mentioned previously site-symmetry effects usually give splittings of a magnitude up to $\sim 20 \text{ cm}^{-1}$ and the splittings here appear to be too great to be explained by this mechanism alone.

The infrared spectrum of $\alpha\text{-Fe}(\text{CH}_3\text{SO}_3)_2$ is virtually identical to that of $\text{Co}(\text{CH}_3\text{SO}_3)_2$ reported previously (14). For cobalt(II) methanesulfonate Arduini et al. proposed that the anion symmetry was reduced below C_{3v} to C_s through nonequivalent bonding of oxygen atoms to cobalt ions, i.e. two of the oxygen atoms from a CH_3SO_3^- anion are bonded to cobalt ions more or less strongly than the third oxygen atom. This would lead to a distortion along the C_4 axis of the CoO_6 octahedron and a tetragonally distorted species. This may also account for the infrared spectrum of $\alpha\text{-Fe}(\text{CH}_3\text{SO}_3)_2$ but appears unlikely in light of Mossbauer spectroscopic studies. The Mossbauer results, to be discussed in more detail in Chapters 6 and 7, indicate that in $\alpha\text{-Fe}(\text{CH}_3\text{SO}_3)_2$ the FeO_6 octahedra are distorted by a trigonal compression. Another mechanism must be proposed to explain the anion having less than C_{3v} symmetry in $\alpha\text{-Fe}(\text{CH}_3\text{SO}_3)_2$.

If one looks at the proposed layer structure for these compounds, Fig. 3.5, as well as the interactions between anion and cation, represented by the solid black lines, there must also be an interaction between adjacent layers, i.e. anion-anion interactions, represented by the broken black lines. Such interactions could result in a displacement of the methyl groups from the C_3 axis of

FIG. 3.5 THE CADMIUM IODIDE LAYER STRUCTURE



the anion resulting in C_s anion symmetry.

Table 3.5 lists the infrared bands observed in the methyl stretching and bending regions - approximately 3000 and 1400 cm^{-1} respectively. The data in this table will be discussed in the subsequent section.

3.5.2. Infrared spectrum of β -Iron(II) methanesulfonate

The β -isomer, prepared by treatment of $\alpha\text{-Fe}(\text{CH}_3\text{SO}_3)_2$ with boiling D.M.P., shows only two absorptions in both the SO_3 stretching and bending regions (see Fig. 3.4 and Table 3.2). In contrast to $\alpha\text{-Fe}(\text{CH}_3\text{SO}_3)_2$ the β -isomer exhibits an infrared spectrum which indicates C_{3v} anion symmetry; no splitting of the ν_4 and ν_5 vibrations is observed. The β -isomer may be proposed to have a similar structure to the one described for the trifluoromethanesulfonate and paratoluenesulfonate analogues.

The infrared frequencies assigned to the XSO_3^- part of the anion are given in Table 3.2, and Table 3.5 lists the methyl stretching and bending modes for both the α - and β -isomers. Assignments for the XSO_3^- part of the anion may be made by comparison with previous infrared spectral studies (39,45). Assignments for the CH_3 vibrations are made on the basis of previously reported data for $\text{Ba}(\text{CH}_3\text{SO}_3)_2$ (38).

As in the SO_3 stretching and bending regions, the α - and β -isomers show distinct differences in the CH_3 stretching

TABLE 3.5 INFRARED SPECTRAL DATA (cm^{-1}) FOR $\text{Fe}(\text{CH}_3\text{SO}_3)_2$
 IN THE CH_3 STRETCHING AND BENDING REGIONS*

ASSIGNMENT	$\alpha\text{-Fe}(\text{CH}_3\text{SO}_3)_2$	$\beta\text{-Fe}(\text{CH}_3\text{SO}_3)_2$
CH_3 as. str. (E)	3030 w	3040 w 3030 w
CH_3 sym. str. (A_1)	2940 m	2950 m
CH_3 as. def. (E)	1430 s 1400 m	$\left\{ \begin{array}{l} 1425 \text{ m} \\ 1415 \text{ m} \\ 1405 \text{ m} \end{array} \right.$
CH_3 sym. def. (A_1)	1330 s	1330 s

* Infrared spectra were recorded in hexachlorobuta-1,3-diene.

and bending regions and this may possibly be due to differences in the anion-anion interactions in the two species. In the β -isomer the methyl group may be situated on the C_3 axis resulting in C_{3v} anion symmetry. It is not understood at the moment why the β -isomer, with a more regular anion symmetry, shows a more complex infrared spectrum in the 3000 and 1400 cm^{-1} regions of the spectrum than the α -isomer. Again it may be due to the differences in anion-anion interactions.

3.5.3. Infrared spectrum of a mixture of α - and β - $\text{Fe}(\text{CH}_3\text{SO}_3)_2$

As can be seen from the lower spectrum in Fig. 3.4, the infrared spectrum which one obtains after refluxing the α -isomer in D.M.P. for only a few hours is simply a superposition of the spectra of the individual α - and β - forms. This indicates that α converts directly to β and there appear to be no other structural isomers, detectable by infrared spectroscopy, present in the system.

3.5.4. Infrared spectrum of $\text{Fe}(\text{CH}_3\text{SO}_3)_2 \cdot \text{CH}_3\text{SO}_3\text{H}$

The infrared spectrum of iron(II) methanesulfonate solvate is listed in Table 3.6 and is compared with the infrared spectrum of α -iron(II) methanesulfonate and the parent acid, methanesulfonic acid (46). The major bands appearing in the infrared spectrum of the solvate can be correlated with the major bands in the infrared spectrum of α -iron(II) methanesulfonate and methanesulfonic acid. The infrared spectrum of $\text{Fe}(\text{CH}_3\text{SO}_3)_2 \cdot \text{CH}_3\text{SO}_3\text{H}$ is similar to that of $\text{Co}(\text{CH}_3\text{SO}_3)_2 \cdot 2\text{CH}_3\text{SO}_3\text{H}$ (26).

TABLE 3.6 INFRARED SPECTRAL DATA (cm^{-1}) FOR $\text{Fe}(\text{CH}_3\text{SO}_3)_2 \cdot \text{CH}_3\text{SO}_3\text{H}$
AND A COMPARISON WITH $\alpha\text{-Fe}(\text{CH}_3\text{SO}_3)_2$ AND $\text{CH}_3\text{SO}_3\text{H}$

C_{3v} ASSIGNMENT FOR ANION	$\alpha\text{-Fe}(\text{CH}_3\text{SO}_3)_2$	$\text{Fe}(\text{CH}_3\text{SO}_3)_2 \cdot \text{CH}_3\text{SO}_3\text{H}$	$\text{CH}_3\text{SO}_3\text{H}^*$	ASSIGNMENT FOR $\text{CH}_3\text{SO}_3\text{H}$
		1323 m	1338 m	SO_2 as. str.
SO_3 as. str.	1220 s 1175 s	1190 m.sh. 1150 s		
		1120 m	1122 m	SO_2 sym.str.
SO_3 sym. str.	1066 m	1066 s		
		990 s	980 s	CH_3 wag
		920 s	891 s	S-(O)H str
S-C str.	790 m	787 m		
		767 m	760 s	S-C str.
SO_3 as. def.	587 m 531 m	566 s 556 m		
SO_3 sym. def.	513 m	542 m		
		506 s	502 m	SO_2 rock
		484 w	473 w	S-O wag

* Results from reference 46.

3.6. STRUCTURAL ISOMERISM IN FeO_6 OCTAHEDRA

$\text{Fe}(\text{H}_2\text{O})_6 (\text{ClO}_4)_2$ exhibits a thermally induced phase transition which has been monitored by Mössbauer spectroscopy (47,48). The iron cation is surrounded by an octahedron of water molecules. In the high temperature form (temperatures greater than 250K) the octahedron is elongated along the trigonal axis and in the low temperature form (temperatures less than 220K) the octahedron is compressed along the trigonal axis. The two forms are interconvertible by changing the temperature. In the present case both forms of $\text{Fe}(\text{CH}_3\text{SO}_3)_2$ appear to be thermally stable between 4.2 - 300K and no phase transition occurs. The infrared results just presented and the Mössbauer results to be discussed in Chapters 6 and 7 suggest the FeO_6 octahedron in the α -isomer is similar to that in the low-temperature form of $\text{Fe}(\text{H}_2\text{O})_6 (\text{ClO}_4)_2$ and the FeO_6 chromophore in the β -isomer is similar to that in the high-temperature form.

The next sections (3.7 and 3.8) describe attempts made to isolate other isomeric forms of divalent metal sulfonates similar to the modifications found to exist in $\text{Fe}(\text{CH}_3\text{SO}_3)_2$.

3.7. THE SEARCH FOR STRUCTURAL ISOMERISM IN $\text{Fe}(\text{CF}_3\text{SO}_3)_2$
AND $\text{Fe}(\text{p-CH}_3\text{C}_6\text{H}_4\text{SO}_3)_2$ USING INFRARED SPECTROSCOPY

Further studies were carried out in order to ascertain whether or not the isomerism observed in iron(II) methanesulfonate is peculiar to this particular compound.

As noted previously, section 3.3, when $\text{Fe}(\text{CF}_3\text{SO}_3)_2$ was prepared under anhydrous conditions from the parent acid the anion retained C_{3v} symmetry. However, this compound may also be prepared by an aqueous method involving precipitation of silver(I) chloride from a reaction between stoichiometric proportions of $\text{FeCl}_2 \cdot 4\text{H}_2\text{O}$ and $\text{Ag}(\text{CF}_3\text{SO}_3)$. The compound resulting from the thermal dehydration of the aqueous solution of $\text{Fe}(\text{CF}_3\text{SO}_3)_2$ gave an identical infrared spectrum to the one reported in Table 3.2.

When both $\text{Fe}(\text{CF}_3\text{SO}_3)_2$ and $\text{Fe}(\text{p-CH}_3\text{C}_6\text{H}_4\text{SO}_3)_2$ were refluxed in .D.M.P. no changes were observed in their infrared spectra. Both anions retain C_{3v} symmetry.

From the observations made here it appears that the methanesulfonate anion is the only one to show structural isomerism in $\text{Fe}(\text{XSO}_3)_2$ compounds, where X is CF_3 , CH_3 and $\text{p-CH}_3\text{C}_6\text{H}_4$.

3.8. THE SEARCH FOR STRUCTURAL ISOMERISM IN $M(\text{CH}_3\text{SO}_3)_2$ COMPOUNDS USING INFRARED SPECTROSCOPY

A number of $M(\text{CH}_3\text{SO}_3)_2$ compounds were prepared where M is Co, Ni, Cu, Zn and Ca. They were investigated by infrared spectroscopy with particular interest in ascertaining whether or not structural isomerism occurs in these compounds. The results are discussed in sections 3.8.1 to 3.8.5.

3.8.1. Infrared spectrum of $\text{Co}(\text{CH}_3\text{SO}_3)_2$

The reported infrared data for cobalt(II) methanesulfonate are very similar to those of $\alpha\text{-Fe}(\text{CH}_3\text{SO}_3)_2$ (14). Section 3.5.1. discussed the proposed structures of these compounds. When $\text{Co}(\text{CH}_3\text{SO}_3)_2$ is boiled under reflux in D.M.P. the infrared spectrum shows several changes. The infrared spectral data are given in Table 3.7. The spectrum of the compound after treatment is more complex than that reported in reference 14 and is more complex than that of $\beta\text{-Fe}(\text{CH}_3\text{SO}_3)_2$ in that more than one absorption is seen in the SO_3 symmetric stretching region. This ν_1 vibration is of symmetry species A_1 and only one band is expected. Previously this doubling of A_1 modes has been explained by proposing nonequivalent anion sites. This may also be the case here.

We found that these infrared spectral changes could be reversed by heating the cobalt(II) compound under vacuum at 150°C , whereupon the initial infrared spectrum was observed. This type of reversal did not occur in $\beta\text{-Fe}(\text{CH}_3\text{SO}_3)_2$.

TABLE 3.7 INFRARED SPECTRAL DATA (cm^{-1}) FOR $\text{Co}(\text{CH}_3\text{SO}_3)_2$
BEFORE AND AFTER TREATMENT WITH 2,2-DIMETHOXYPROPANE

C_{3v} Assignment for CH_3SO_3^-	Before Treatment with D.M.P.*	After Treatment with D.M.P.
ν_4	1233 s 1170 s	1180 s.br
ν_1	1070 s	1070 s 1035 m
ν_2	787 s	800 m 780 w
ν_5	590 m 530 m	563 m 550 m
ν_3	512 m	500 w
ν_6 AND CH_3 INTERNAL VIBRATIONS }	{ 1330 w 970 w 385 w 373 w 350 w	{ 1330 w 1250 w.sh 420 w 390 w

* Results from reference 14

3.8.2. Infrared spectrum of $\text{Ni}(\text{CH}_3\text{SO}_3)_2$

Nickel(II) methanesulfonate has been previously prepared in this laboratory and the products from different preparations gave different infrared spectra. Further work as a part of the current study gave inconsistent results and infrared spectra which exhibited extremely broad absorption bands in the SO_3 bending and stretching regions. Treatment with D.M.P. produces no changes in the infrared spectrum. No interpretation as to the nature of the anion symmetry could be made for this compound.

3.8.3. Infrared spectrum of $\text{Cu}(\text{CH}_3\text{SO}_3)_2$

The reported infrared spectrum of copper(II) methanesulfonate is complex and the presence of more than one type of anion in the lattice was proposed to account for this (14). No changes were observed in the infrared spectrum when this compound was refluxed in D.M.P.

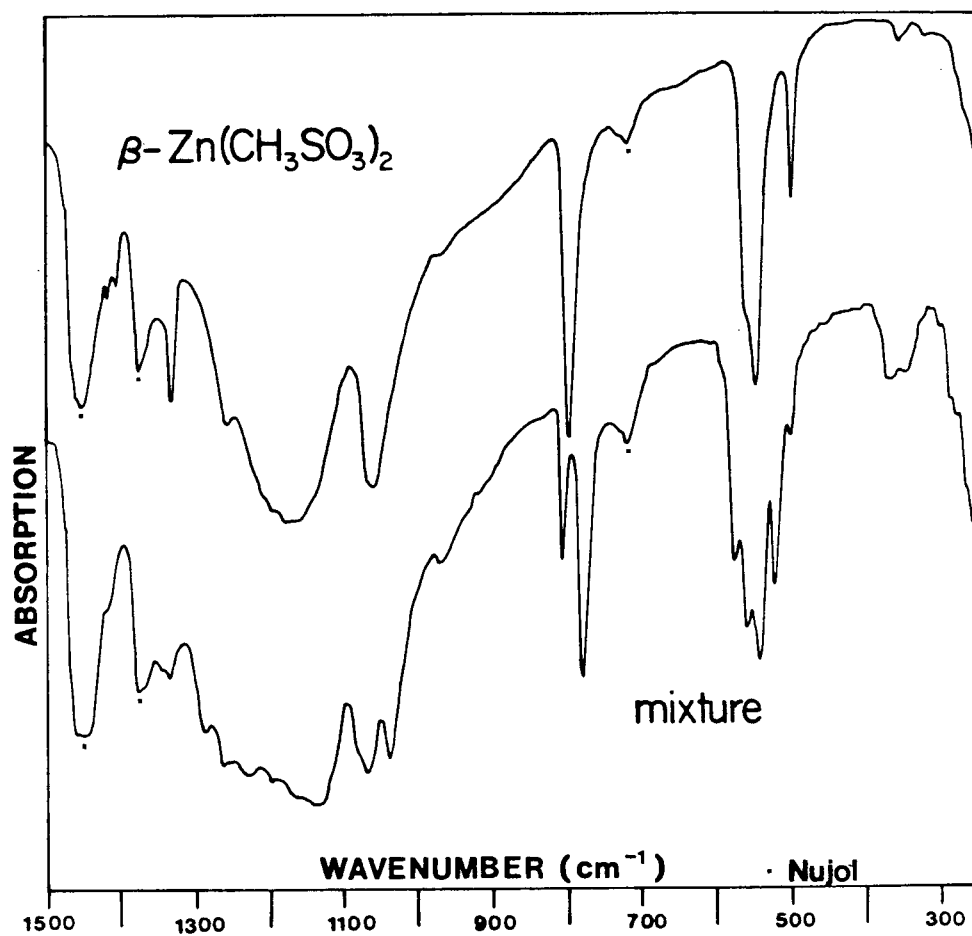
3.8.4. Infrared spectrum of $\text{Zn}(\text{CH}_3\text{SO}_3)_2$

Zinc(II) methanesulfonate was prepared previously in this laboratory but the infrared spectral data were not reported. The preparation has been repeated as a part of this study and the infrared data are given in Table 3.8. The spectrum obtained by thermal dehydration of a solution of $\text{Zn}(\text{CH}_3\text{SO}_3)_2$ is shown in the lower part of Fig.3.6. The spectrum is of a complex nature, some

TABLE 3.8 INFRARED SPECTRAL DATA (cm^{-1}) FOR $\text{Zn}(\text{CH}_3\text{SO}_3)_2$
BEFORE AND AFTER TREATMENT WITH 2,2-DIMETHOXYPROPANE

C_{3v} Assignment for CH_3SO_3^-	Before Treatment with D.M.P.	After Treatment with D.M.P.
ν_4	$\left\{ \begin{array}{l} 1288 \text{ m} \\ 1263 \text{ s} \\ 1230 \text{ s} \\ 1200 \text{ sh} \\ 1170 \text{ sh} \\ 1134 \text{ s} \end{array} \right.$	1170 s.br
ν_1	$\left\{ \begin{array}{l} 1070 \text{ m} \\ 1040 \text{ m} \end{array} \right.$	1063 s
ν_2	$\left\{ \begin{array}{l} 808 \text{ m} \\ 780 \text{ m} \end{array} \right.$	800 s
ν_5	$\left\{ \begin{array}{l} 580 \text{ m} \\ 561 \text{ m} \\ 545 \text{ m} \\ 524 \text{ m} \end{array} \right.$	$\left\{ \begin{array}{l} 560 \text{ sh} \\ 550 \text{ s} \end{array} \right.$
ν_3	503 w	502 m
ν_6 AND CH_3 INTERNAL VIBRATIONS	$\left\{ \begin{array}{l} 1420 \text{ w.br.} \\ 1334 \text{ w} \\ 1288 \text{ w} \\ 370 \text{ w} \\ 350 \text{ w} \end{array} \right.$	$\left\{ \begin{array}{l} 1429 \text{ w} \\ 1419 \text{ w} \\ 1406 \text{ w} \\ 1331 \text{ m} \\ 1259 \text{ m} \\ 360 \text{ w} \end{array} \right.$

FIG. 3.6 INFRARED SPECTRA (1500-250 cm^{-1}) OF $\text{Zn}(\text{CH}_3\text{SO}_3)_2$



consisting of a broad absorption in the asymmetric SO_3 stretching region and more than one absorption in the symmetric SO_3 stretching region. As mentioned previously the ν_1 vibration is of symmetry species A_1 and to explain the doubling of vibrations observed in this spectrum a single species with nonequivalent anion sites or a mixture of species must be proposed.

The upper spectrum of Fig. 3.7 shows the simplification as a result of refluxing a sample of $\text{Zn}(\text{CH}_3\text{SO}_3)_2$ in D.M.P. The modification produced in this way is called the β -isomer because of the infrared spectral similarities with $\beta\text{-Fe}(\text{CH}_3\text{SO}_3)_2$. For this form one anion site may be proposed with the anion retaining C_{3v} symmetry. The anion may have its symmetry slightly lowered below C_{3v} as seen by the small splitting (10 cm^{-1}) of the ν_5 mode and the broad ν_4 absorption. From the infrared spectrum of this β -form it appears that this modification is not present in the original sample (prior to refluxing in D.M.P.). When $\beta\text{-Zn}(\text{CH}_3\text{SO}_3)_2$ was heated under vacuum at 150°C no change was observed in the infrared spectrum.

3.8.5. Infrared spectrum of $\text{Ca}(\text{CH}_3\text{SO}_3)_2$

As noted previously a crystal structure has been reported for calcium(II) methanesulfonate (17). No infrared data or preparative method were given. The compound was prepared here by an analogous route to that used for the first-row transition metal methanesulfonates (see Chapter 2). The infrared spectrum is given in

Table 3.9. The doubling of the A_1 modes indicate again that more than one type of anion environment must exist in this compound. The crystal structure also shows the presence of nonequivalent anion sites, although because of the structural modifications observed in this type of compound, it is possible that the compound prepared by Charbonnier et al. is not structurally the same as the one prepared in this study. When $\text{Ca}(\text{CH}_3\text{SO}_3)_2$ was refluxed in D.M.P. no change was observed in its infrared spectrum.

3.9. SUMMARY OF RESULTS AND CONCLUSIONS

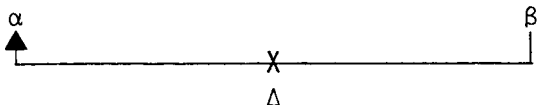
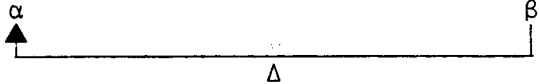
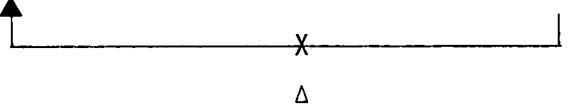
Infrared spectroscopy has been invaluable in this study in showing the presence or absence of structural isomers in $\text{M}(\text{XSO}_3)_2$ systems. A general structural model appropriate to all $\text{M}(\text{XSO}_3)_2$ compounds may be proposed in which anions act as terdentate bridging ligands and the metal ions are octahedrally coordinated by oxygen atoms from six different anions. Infrared spectroscopy is incapable of probing the detailed nature of the MO_6 chromophore, i.e. whether it is octahedral or tetragonally or trigonally distorted. To investigate the MO_6 environment one requires another technique, namely Mossbauer spectroscopy which will be discussed in Chapters 6 and 7.

Table 3.10 summarises the results concerning isomerism in $\text{M}(\text{CH}_3\text{SO}_3)_2$ compounds.

TABLE 3.9 INFRARED SPECIAL DATA (cm^{-1}) FOR $\text{Ca}(\text{CH}_3\text{SO}_3)_2$

C_{3v} Assignment for CH_3SO_3^-	ν
ν_4	1200 s. br
ν_1	1085 m.sh. 1070 s
ν_2	800 s 790 s
ν_5	557 s 542 s
ν_3	530 w.sh. 520 m
ν_6 AND CH_3 INTERNAL VIBRATIONS	$\left\{ \begin{array}{l} 1421 \text{ m} \\ 1330 \text{ m} \\ 1260 \text{ m} \\ 970 \text{ w} \\ 345 \text{ m} \end{array} \right.$

TABLE 3.10 SUMMARY OF RESULTS CONCERNING ISOMERISM IN
 $M(\text{CH}_3\text{SO}_3)_2$ COMPOUNDS

M	PRODUCT OBTAINED BY DEHYDRATION BETWEEN 100-150°C	PRODUCT OBTAINED UPON REFLUXING IN D.M.P.
Fe		
	COMPLEX I.R. SPECTRUM	
Co		
Ni	INCONCLUSIVE RESULTS	
Cu	COMPLEX I.R. SPECTRUM	NO CHANGE
Zn	COMPLEX I.R. SPECTRUM	
Ca	COMPLEX I.R. SPECTRUM	NO CHANGE

CHAPTER 4ELECTRONIC SPECTRA OF $\text{Fe}(\text{XSO}_3)_2$ COMPOUNDS4.1. INTRODUCTION

For a regular octahedral complex of iron(II) it is relatively simple to assign a value to $10Dq$. The free-ion ground term is 5D which represents a ground state d^6 electron configuration. An octahedral crystal field lifts the degeneracy of the 5D state as shown in Fig. 4.1, into a low energy $^5T_{2g}$ and a high energy 5E_g state, the energy difference being $10Dq$.

The compounds studied in this work are all high spin as evidenced by Mossbauer spectroscopy and magnetic susceptibility measurements. Hence the ground state in these compounds is $^5T_{2g}$ and they should all show only one spin-allowed d-d absorption arising from the $^5T_{2g} \longrightarrow ^5E_g$ transition.

4.2. RESULTS AND DISCUSSION

The electronic spectra of the anhydrous sulfonate species studied here are all very similar and the band positions are listed in Table 4.1. The spectra consist of a broad absorption maximum around 9000 cm^{-1} with a less intense shoulder at lower energy. A typical spectrum, that of $\text{Fe}(\text{CF}_3\text{SO}_3)_2$, is reproduced in Fig. 4.2. Here one can clearly observe the splitting of the band into two

FIG. 4.1. SPLITTING OF THE FREE-ION 5D GROUND TERM
IN AN OCTAHEDRAL CRYSTAL FIELD

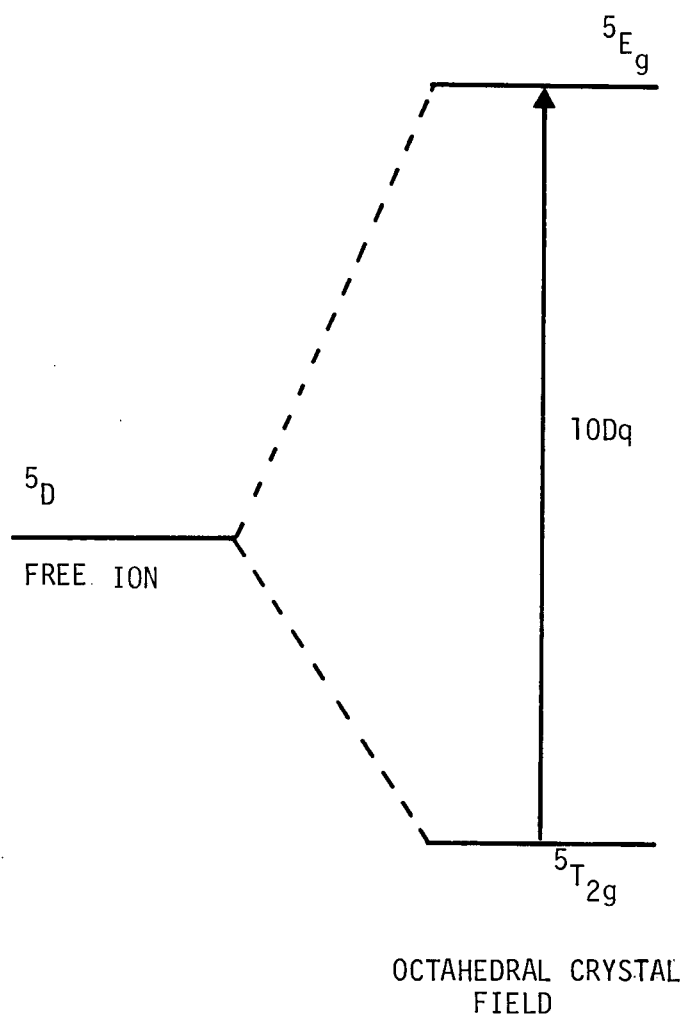
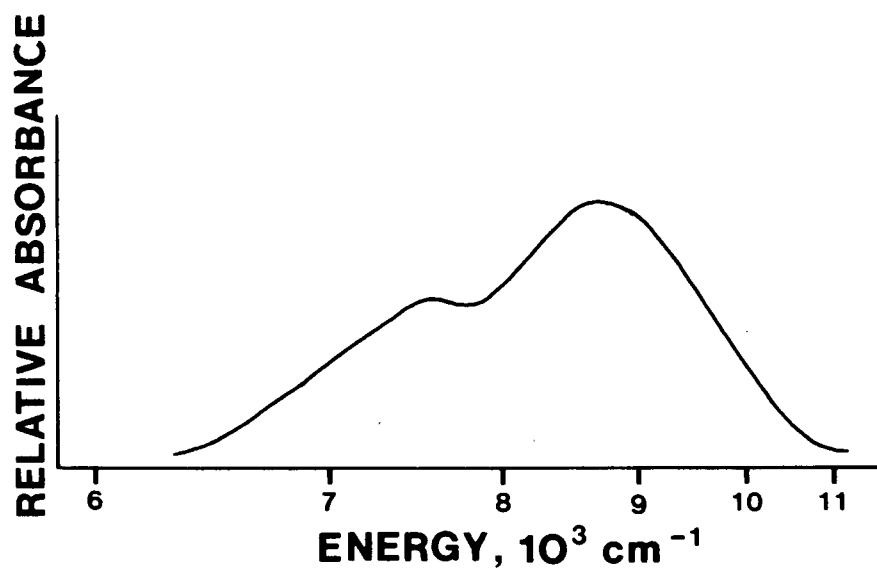


TABLE 4.1. ELECTRONIC SPECTRA OF $\text{Fe}(\text{XSO}_3)_2$ COMPOUNDS

X	BAND POSITIONS (cm^{-1})		10Dq
CF_3	8600	7600	8100
$\alpha\text{-CH}_3$	9000	7400	8200
$\beta\text{-CH}_3$	9000	7300	8150
$p\text{-CH}_3\text{C}_6\text{H}_4$	8700	7300	8000

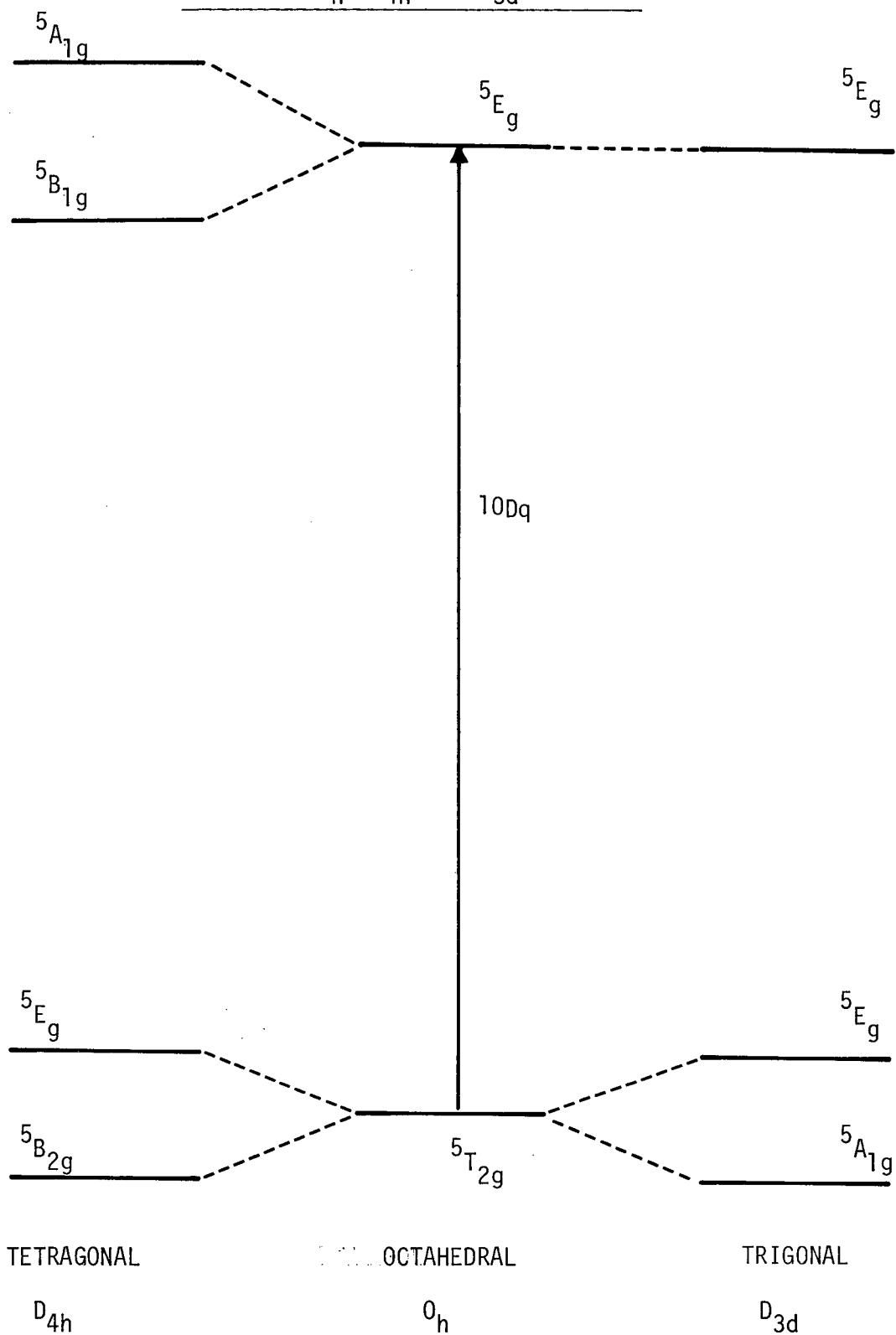
FIG. 4.2. ELECTRONIC SPECTRUM OF $\text{Fe}(\text{CF}_3\text{SO}_3)_2$



components. As mentioned in section 4.1, in regular octahedral symmetry only one band is expected in this region of the spectrum; however, there are several mechanisms by which a double peak may be observed.

- (i) As can be seen from Fig. 4.3 if the symmetry of the octahedron is lowered from O_h to D_{4h} the degeneracy of both the 5E_g and $^5T_{2g}$ states is lifted. Two absorptions would be expected due to transitions from the ground state to the $^5A_{1g}$ and $^5B_{1g}$ excited states. The splitting of the $^5T_{2g}$ state is too small, of the order of 300 cm^{-1} , to be observed in the electronic spectra of these compounds. A tetragonal distortion of the $\text{Fe}(\text{H}_2\text{O})_6^{2+}$ octahedron occurs in Tutton's salt, $(\text{NH}_4)_2\text{Fe}(\text{SO}_4)_2 \cdot 6\text{H}_2\text{O}$, where two absorptions are observed due to a splitting of the excited state by 2400 cm^{-1} (49,50). In the compounds studied here both the Mossbauer and infrared data indicate that the symmetry around the cation is not tetragonal but trigonal, D_{3d} . As can be seen from Fig. 4.3 the 5E_g excited state remains unsplit in this environment and although the ground state degeneracy is removed this splitting is too small to be observed in the electronic spectra. An alternative mechanism must be proposed.
- (ii) Spin-orbit coupling lifts the degeneracy of both the 5E_g and $^5T_{2g}$ levels, but for iron(II) the spin-orbit coupling constant is approximately 100 cm^{-1} (51) and is an order of magnitude too small to account for the observed splittings of greater than

FIG. 4.3. SPLITTING DIAGRAM FOR HIGH-SPIN IRON(II) IN CRYSTAL FIELDS OF O_h , D_{4h} AND D_{3d} SYMMETRY



1000 cm^{-1} .

- (iii) The mechanism which is most plausible and has been proposed to account for the band splitting in $\text{Fe}(\text{FSO}_3)_2$ (15) and $\text{Fe}(\text{SiF}_6)_2 \cdot 6\text{H}_2\text{O}$ (49) is a removal of the excited state degeneracy by a dynamic Jahn-Teller effect (52). The dynamic Jahn-Teller effect is an interconversion from one species to another, eg. tetragonal compression to tetragonal elongation, both configurations having a lower energy than that of the undistorted octahedron. Under such conditions the molecule may well oscillate between the two forms and the time-averaged form may be close to an octahedron.

If one assumes that the band splitting is due to this dynamic Jahn-Teller effect, the value of $10Dq$ for the compounds studied here may be estimated from the approximate centre of the split absorption band. This enables us to calculate values of Dq which are presented in Table 4.2. and are seen to be comparable to the values given previously (14,15).

A correlation between the base strengths of the particular anion, XSO_3^- , and Dq might be expected. This, however, is not observed. If one compares the values of Dq for compounds of the type $\text{M}(\text{XSO}_3)_2$ given in Table 4.2, the values are all very similar, approximately 800 cm^{-1} . It appears that the estimation of ligand field strength from electronic spectroscopy is simply not sufficiently sensitive to detect small differences that exist between the various

TABLE 4.2 Dq VALUES (cm^{-1}) FOR $\text{M}(\text{XSO}_3)_2$ COMPOUNDS

M	X			
	F	CF_3	$\alpha\text{-CH}_3$	$\text{p-CH}_3\text{C}_6\text{H}_4$
Co	765	780	765	780
Fe	800	810	820	800

Dq value for $\text{Fe}(\text{FSO}_3)_2$ from reference 15

Dq value for $\text{Co}(\text{XSO}_3)_2$ compounds from reference 14

XSO_3^- anions.

The magnitude of $10Dq$ observed in these compounds is not unreasonable when compared, for example, with that of $\text{Fe}(\text{H}_2\text{O})_6^{2+}$, where $10Dq$ is approximately $10,000\text{ cm}^{-1}$ (49), and is consistent with a greater ligand field strength for water as compared with the XSO_3^- anions.

Comparison of the Dq values of $\text{Fe}(\text{XSO}_3)_2$ compounds with those of the corresponding cobalt(II) analogues is also informative, Table 4.2. The Dq values for the iron salts are approximately 5% greater than those of the corresponding cobalt(II) species as is generally expected (53).

CHAPTER 5MAGNETIC SUSCEPTIBILITIES OF $\text{Fe}(\text{XSO}_3)_2$ COMPOUNDS5.1. INTRODUCTION

Inorganic coordination chemists have long used magnetic properties of d-transition metal complexes as a means of determining oxidation states and stereochemistries. Magnetic susceptibility measurements between liquid nitrogen and room temperature are routinely performed in this laboratory; and in other establishments low temperature cryostats have extended the temperature range below 4.2K, enabling the chemist to extract even more information.

Studies involving magnetic susceptibility measurements include the investigation of magnetic anisotropies using single crystals (54), investigation of spin cross-over phenomena (55) and magnetic exchange interactions (56).

This chapter discusses the origins of the magnetic effects observed and includes a brief description of the theory of paramagnetism as derived by Van Vleck. In particular the application of this theory to the case of high-spin iron(II) will be considered.

The magnetic susceptibility measurements made in this study will be discussed and analysed using a model developed by Figgis and Lewis (57).

5.2. ORIGINS OF THE MAGNETIC EFFECTS

The electron has a magnetic moment approximately 1000 times as large as that of the proton and hence the various types of magnetic effects considered here arise only from the electrons. However, these nuclear paramagnetic effects have great significance for the Mossbauer and n.m.r. spectroscopist.

When the electrons are in closed shells the magnetic effect is known as diamagnetism and unpaired electrons give rise to the magnetic behaviour known as paramagnetism. The nature of the paramagnetism exhibited by a given compound is determined by the number and orbital arrangements of the unpaired electrons.

The magnetic behaviour of a compound is investigated by measuring the magnetic polarisation of the substance by an applied magnetic field. This can be achieved by a variety of experimental techniques, including force methods (for example, the Gouy or Faraday technique (58, 59)) and induction methods (using, for example, a vibrating sample magnetometer (60)).

5.3. DIAMAGNETISM

This is a property of all forms of matter and arises from field-induced electron circulation which generates a field opposed to the applied magnetic field. In classical terms the lines of force inside a diamagnetic sample are less concentrated than outside and so such a material when placed in a heterogeneous magnetic field will move

to regions of minimum field strength. An important feature of diamagnetism is that its magnitude does not vary with temperature. The induced moment only depends upon the electron configuration which is not temperature dependent.

5.4. PARAMAGNETISM

This arises as a consequence of the interaction of orbital and/or spin angular momentum of the unpaired electron density with the applied magnetic field. In classical terms it is the reverse of diamagnetism; magnetic lines of force are concentrated in the paramagnetic sample and when placed in a heterogeneous magnetic field the sample moves to regions of relatively high field strength.

Paramagnetic susceptibilities are field independent in the case of magnetically dilute systems. Such systems are those where the paramagnetic centres are too far removed from each other to transmit any cooperative effects. (Ferro- and antiferromagnetism are cases of magnetic concentration where the spins of one paramagnetic ion are aligned with or opposed to those of adjacent ions, respectively.

Paramagnetic susceptibilities are temperature dependent and this temperature dependence may be thought of as arising from two opposing forces; the applied magnetic field tends to align the moments of the paramagnetic ions and the thermal energy of the sample tends to randomise these aligned moments.

Paramagnetic susceptibilities are usually several orders of magnitude greater than diamagnetic susceptibilities. Hence, materials with unpaired electron spin densities almost always have a net paramagnetic susceptibility. By determining the measured susceptibility, χ_M and estimating the diamagnetic contributions, χ_{DIA} , one can obtain the desired paramagnetic susceptibility, χ_A , from the relationship,

$$\chi_A = \chi_M - \chi_{DIA} \quad (5.1)$$

Diamagnetic contributions may be obtained from Pascal's constants (30,31,32), which allow the diamagnetic contributions to be calculated by summing the contributions from all the atoms, i , χ_{Ai} and all the bonds, j , χ_{Bj}

$$\chi_{DIA} = \sum_i \chi_{Ai} + \sum_j \chi_{Bj} \quad (5.2)$$

5.5. THEORY OF PARAMAGNETIC SUSCEPTIBILITY, THE VAN VLECK EQUATION AND ITS APPLICATION TO HIGH-SPIN IRON(II) SYSTEMS

Magnetic susceptibility may be defined in the following way:

$$B = H + 4\pi I \quad (5.3)$$

where B is the magnetic induction or flux, H is the applied magnetic field and I is the intensity of magnetisation.

The ratio B/H is the magnetic permeability of the substance

and is given by:

$$B/H = 1 + 4\pi I/H \quad (5.4)$$

$$= 1 + 4\pi\chi_v \quad (5.5)$$

where χ_v is the magnetic susceptibility per unit volume.

The molar susceptibility may then be defined thus:

$$\chi_M = \chi_v (M.W./\rho) \quad (5.6)$$

where M.W. is the molecular weight and ρ the density of the material under investigation. The paramagnetic susceptibility may then be corrected for the diamagnetic effects of the atoms and ions present and χ_A may be evaluated from equation 5.1. The effective magnetic moment, μ_{Eff} may then be calculated:

$$\mu_{Eff} = \left[\frac{3k \chi_A T}{N\beta^2} \right]^{1/2} \quad (5.7)$$

where k is the Boltzman constant, N is Avagadro's number and β is the Bohr Magnetron. Evaluation of these constants gives the familiar equation:

$$\mu_{Eff} = 2.828(\chi_A T)^{1/2} \quad (5.8)$$

Paramagnetism may be considered to arise from changes in the thermally accessible energy levels of an atom when it is subjected to a magnetic field. Studies of paramagnetism in atoms enable the magnetochemist to probe the ground state and thermally

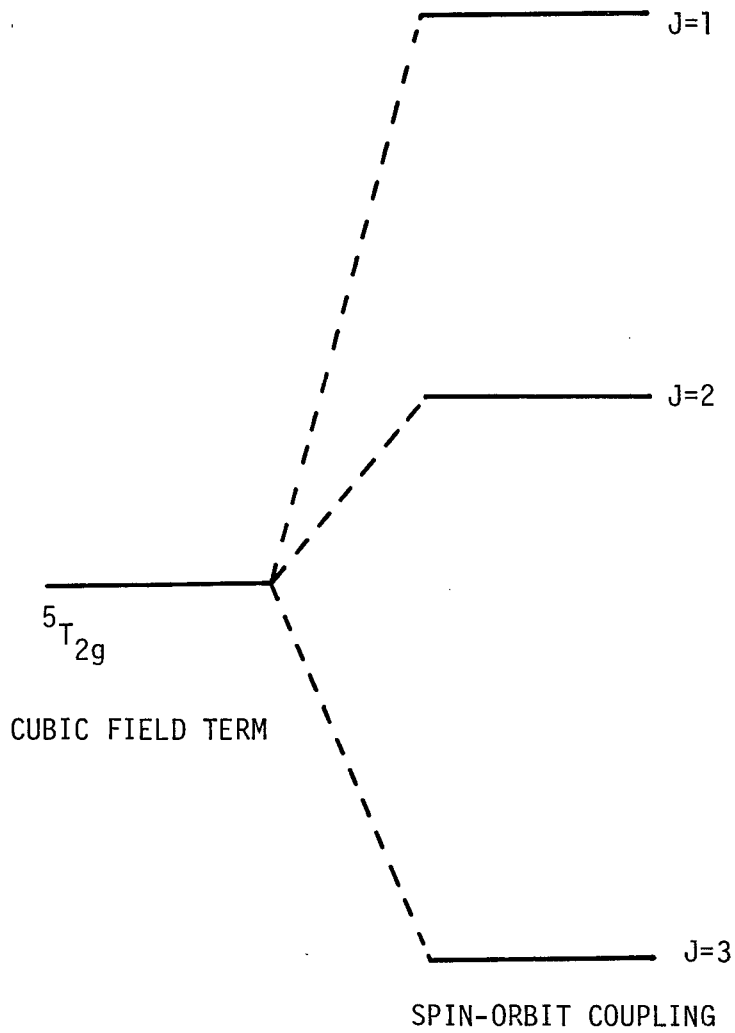
accessible excited states. Van Vleck (61) solved the problem of evaluating the new energy levels of the individual atoms and ions in the magnetic field and then, using Boltzman statistics, deriving the susceptibility per mole of atoms from the thermal distribution of atoms among the available energy states. This led to Van Vleck's equation of paramagnetism which is derived in standard texts (62,63) and is given here to second order:

$$\chi_A = \frac{N \sum_i (W_i^{(1)2} / kT - 2W_i^{(2)}) \exp(-W_i^{(0)} / kT)}{\sum_i \exp(-W_i^{(0)} / kT)} \quad (5.9)$$

The calculation of χ_A depends upon the evaluation of $W_i^{(0)}$, $W_i^{(1)}$ and $W_i^{(2)}$, where $W_i^{(0)}$ is the energy of the level in the absence of an applied field and $W_i^{(1)}$ and $W_i^{(2)}$ are the first and second order Zeeman coefficients respectively.

The case of interest here is iron(II) a d^6 electron configuration and a 5D high-spin free-ion ground term. As mentioned in the previous chapter and illustrated in Fig. 4.1 an octahedral crystal field lifts the degeneracy of this 5D term. The low energy $^5T_{2g}$ term is further split by spin-orbit coupling as shown in Fig. 5.1. The resulting J-states are separated by a few hundred wavenumbers and thus will be thermally populated; (kT at room temperature is approximately 200 cm^{-1}). The applied magnetic field further lifts the degeneracy of each J-state into a multiplet of $2J+1$ levels.

FIG. 5.1 THE EFFECT OF SPIN-ORBIT COUPLING ON THE
 $^5T_{2g}$ GROUND TERM



The magnitude of the magnetic moment can be estimated from a knowledge of the free-ion ground term and assuming no spin-orbit coupling is given by:

$$\mu = (L(L+1) + 4S(S+1))^{\frac{1}{2}} \text{ B.M.} \quad (5.10)$$

For high-spin iron(II) the total spin and orbital angular momentum quantum numbers, S and L respectively, are both equal to two, and the calculated magnetic moment is 5.48 B.M.

It is found that the values of μ calculated from this expression are often greater than the experimentally determined values and a value of μ assuming no orbital contribution to the moment may be calculated from the "spin-only" expression:

$$\mu_{s.o.} = (4S(S+1))^{\frac{1}{2}} \text{ B.M.} \quad (5.11)$$

and $\mu_{s.o.}$ is 4.89 B.M. for high-spin iron(II). This mathematical expression may be represented physically by assuming that the orbital contribution to the moment present in the free-ion has been "quenched" by the crystal field upon formation of the complex. A qualitative picture of this quenching of orbital angular momentum proposes that for an electron in a particular orbital to possess orbital angular momentum about a specified axis it must be possible, by rotation about that axis, to convert that orbital into an identical degenerate orbital which has a vacancy for the electron concerned. Therefore, in the free ion, a 45° rotation about the z-axis will convert the d_{xy} into the $d_{x^2-y^2}$ orbital. A similar rotation about the z-axis will

interchange the d_{xz} and d_{yz} orbitals, and orbital contributions may arise from electrons occupying these orbitals. However, in an octahedral (or tetrahedral) crystal field the t_{2g} and e_g orbitals are no longer degenerate and hence the orbital contribution about the z-axis arising from the d_{xy} and $d_{x^2-y^2}$ pair of orbitals vanishes. The e_g orbitals now produce no orbital contribution to the magnetic moment. For a high-spin d^6 electron configuration we may still expect some contribution from the t_{2g} set of orbitals.

The next section will now discuss the three-parameter model of Figgis and Lewis (57) used to analyse the experimentally determined magnetic moment data.

5.6. THE FIGGIS AND LEWIS MODEL

A theoretical treatment of the magnetic properties of the d^6 high-spin ion has been given by Figgis and Lewis (57). This model has successfully parameterised several iron(II) compounds in terms of Δ , κ and λ . The model has also been used in the treatment of the magnetic properties of other first-row transition metal complexes (64).

The model simultaneously considers the effects of an axial (tetragonal or trigonal) crystal field and a spin-orbit coupling perturbation on the $^5T_{2g}$ cubic field ground term and does not consider any interactions with higher excited terms.

Δ is defined as the splitting of the orbital degeneracy of the $^5T_{2g}$ term into a doublet and a singlet by the asymmetric ligand field component and is taken to be positive when the orbital singlet is lower in energy relative to the doublet.

κ is the orbital reduction factor and takes into account the covalent bond character. It appears in the effective magnetic moment operator:

$$\hat{\mu} = \hat{\mu}_B (\kappa \hat{L} + 2\hat{S}) \quad (5.12)$$

κ can take values up to a maximum of 1 which indicates no electron delocalisation.

Electron delocalisation is also taken into account by allowing the spin-orbit coupling constant to vary from its free-ion value, λ_0 (for iron(II), $\lambda_0 = -103\text{cm}^{-1}$) (51).

The operator $V_{AXIAL} + \lambda \hat{L} \cdot \hat{S}$ operates on the fifteen wavefunctions, $|M_L, M_S\rangle$, in trigonal or tetragonal symmetry. This results in a secular determinant which is solved numerically on a computer. The energies and wavefunctions resulting from the perturbation by the low symmetry crystal field and spin-orbit coupling are also perturbed by the effects of the magnetic field. The first-order Zeeman coefficients are found for each individual level by constructing the appropriate secular determinant. The second-order Zeeman coefficients are then found by evaluating the matrix elements of the magnetic moment operator between levels

which were not degenerate with each other in the absence of an applied field. The magnetic susceptibilities may then be calculated by substituting these coefficients into Van Vleck's equation, (5.9).

5.7. RESULTS AND DISCUSSION

Magnetic susceptibilities have been measured between 80 and 310K for the compounds studied, $\text{Fe}(\text{XSO}_3)_2$, where X is CF_3 , $\alpha\text{-CH}_3$, $\beta\text{-CH}_3$ and $p\text{-CH}_3\text{C}_6\text{H}_4$. Where X is F the magnetic susceptibility data were previously reported (15).

Fig. 5.2 shows the temperature dependence of the magnetic moments and includes the data for the $\text{Fe}(\text{FSO}_3)_2$ compound for comparison. Tables 5.1 to 5.4 show the magnetic susceptibilities and effective magnetic moments for the compounds studied. Tabulated are results obtained from the Gouy balance over a range of temperatures and results obtained from the Faraday balance in three magnetic field strengths at room temperature.

It can be seen that the effective magnetic moments range from a minimum of 4.71 B.M. for $\beta\text{-Fe}(\text{CH}_3\text{SO}_3)_2$ at low temperature (80K), to a maximum of 5.49 B.M. for $\text{Fe}(\text{CF}_3\text{SO}_3)_2$.

Section 5.7.1 discusses the magnetic moment data for the $\text{Fe}(\text{CF}_3\text{SO}_3)_2$ and $\text{Fe}(p\text{-CH}_3\text{C}_6\text{H}_4\text{SO}_3)_2$ compounds, the analysis of the data using the Figgis and Lewis model, and a comparison of these two compounds with $\text{Fe}(\text{FSO}_3)_2$. Section 5.7.2 discusses the magnetic moment data for the α - and β -isomers of iron(II) methanesulfonate.

FIG. 5.2 TEMPERATURE DEPENDENCE OF THE MAGNETIC MOMENT FOR $\text{Fe}(\text{XSO}_3)_2$ COMPOUNDS.

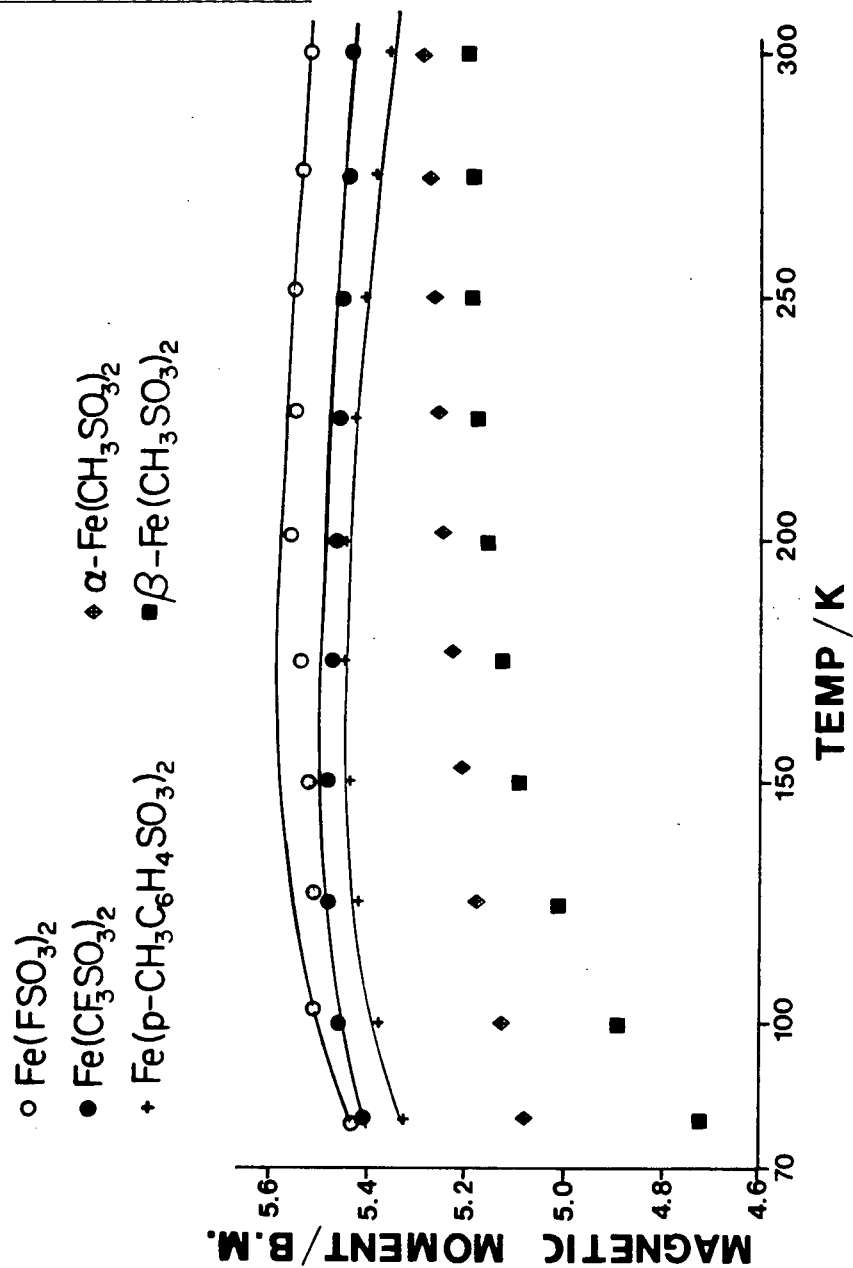


TABLE 5.1 MAGNETIC SUSCEPTIBILITY DATA FOR $\text{Fe}(\text{CF}_3\text{SO}_3)_2$

TEMP (K)	$10^6 \chi_A (\text{cm}^3 \text{mol}^{-1})$	$\mu_{\text{EFF}} (\text{B.M.})$
300	12290	5.43
275	13450	5.44
250	14850	5.45
225	16570	5.46
200	18770	5.48
175	21530	5.49
150	25120	5.49
125	30150	5.49
100	37270	5.46
80	45240	5.38

FARADAY RESULTS AT 295K

$\frac{\text{HdH}}{\text{dx}} (\text{T}^2 \text{cm}^{-1})$	$10^6 \chi_A (\text{cm}^3 \text{mol}^{-1})$	$\mu_{\text{EFF}} (\text{B.M.})$
253	12600	5.45
526	12570	5.44
869	12630	5.45

Diamagnetic corrections $-105 \times 10^{-6} \text{cm}^3 \text{mol}^{-1}$

TABLE 5.2 MAGNETIC SUSCEPTIBILITY DATA FOR α -Fe(CH₃SO₃)₂

TEMP (K)	$10^6 \chi_A (\text{cm}^3 \text{mol}^{-1})$	$\mu_{\text{EFF}} (\text{B.M.})$
300	11620	5.28
275	12670	5.28
250	13890	5.27
225	15370	5.26
200	17230	5.25
175	19540	5.23
150	22630	5.21
125	26840	5.18
100	32910	5.13
80	40330	5.08

FARADAY RESULTS AT 295K

$\frac{HdH}{dx} (\text{T}^2 \text{cm}^{-1})$	$10^6 \chi_A (\text{cm}^3 \text{mol}^{-1})$	$\mu_{\text{EFF}} (\text{B.M.})$
253	11840	5.28
526	11850	5.28
869	11870	5.29

Diamagnetic corrections $-83 \times 10^{-6} \text{ cm}^3 \text{mol}^{-1}$

TABLE 5.3 MAGNETIC SUSCEPTIBILITY DATA FOR β -Fe(CH₃SO₃)₂

TEMP(K)	$10^6 \chi_A (\text{cm}^3 \text{mol}^{-1})$	$\mu_{\text{EFF}} (\text{B.M.})$
300	11270	5.20
275	12250	5.19
250	13470	5.19
225	14910	5.18
200	16650	5.16
175	18800	5.13
150	21930	5.09
125	25310	5.03
100	30140	4.91
80	34670	4.71

FARADAY RESULTS AT 295K

$\frac{HdH}{dx} (\text{T}^2 \text{cm}^{-1})$	$10^6 \chi_A (\text{cm}^3 \text{mol}^{-1})$	$\mu_{\text{EFF}} (\text{B.M.})$
253	11650	5.24
526	11680	5.25
869	11750	5.26

Diamagnetic corrections $-83 \times 10^{-6} \text{ cm}^3 \text{mol}^{-1}$

TABLE 5.4 MAGNETIC SUSCEPTIBILITY DATA FOR $\text{Fe}(\text{p-CH}_3\text{C}_6\text{H}_4\text{SO}_3)_2$

TEMP (K)	$10^6 \chi_A (\text{cm}^3 \text{mol}^{-1})$	$\mu_{\text{EFF}} (\text{B.M.})$
300	11970	5.36
275	13210	5.39
250	14640	5.41
225	16380	5.43
200	18570	5.45
175	21220	5.45
150	24670	5.44
125	29380	5.42
100	36190	5.38
80	44400	5.33

FARADAY RESULTS AT 294K

$\frac{HdH}{dx} (\text{T}^2 \text{cm}^{-1})$	$10^6 \chi_A (\text{cm}^3 \text{mol}^{-1})$	$\mu_{\text{EFF}} (\text{B.M.})$
253	12390	5.40
526	12350	5.39
869	12340	5.39

Diamagnetic corrections $-191 \times 10^{-6} \text{ cm}^3 \text{mol}^{-1}$

5.7.1. Magnetic moment data for $\text{Fe}(\text{CF}_3\text{SO}_3)_2$ and $\text{Fe}(\text{p-CH}_3\text{C}_6\text{H}_4\text{SO}_3)_2$

The magnetic moments of both the trifluoromethanesulfonate and paratoluenesulfonate compounds initially exhibit an increase with decrease in temperature. They pass through a maximum and decrease as the temperature decreases to 80K. As can be seen from Fig. 5.2 this behaviour is very similar to that of the fluorosulfonate compound previously discussed (15).

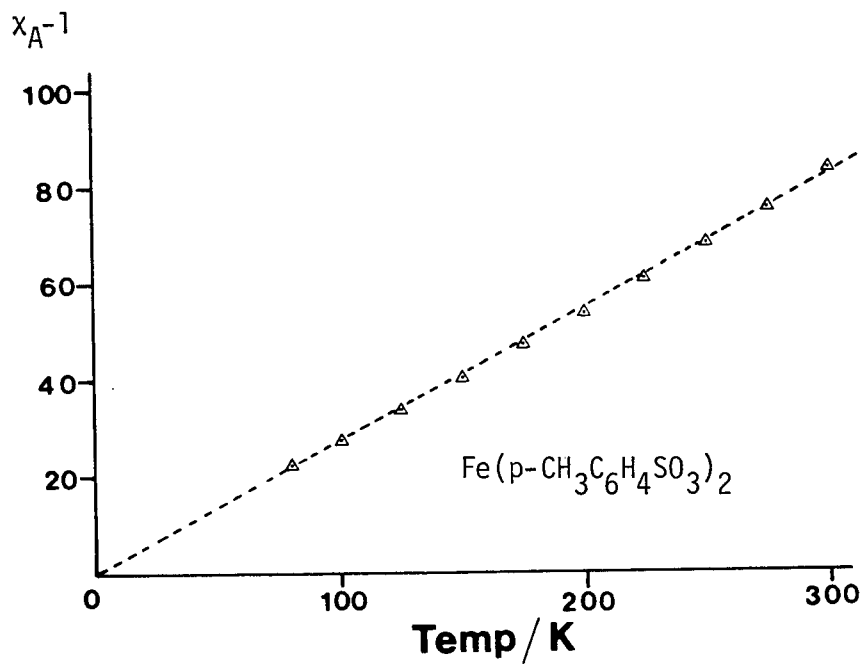
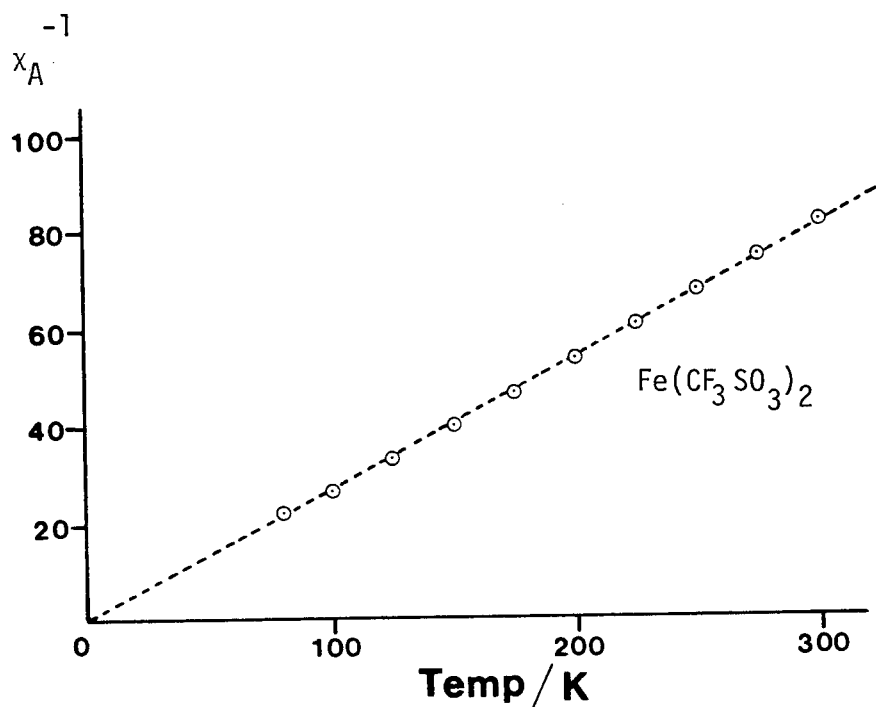
Plots of reciprocal susceptibility against temperature (Fig. 5.3) show a slight curvature, hence a small deviation from Curie Law behaviour, represented by the straight broken lines.

These results are typical for a high-spin d^6 ion in an octahedral crystal field. Measurements in three different magnetic field strengths using a Faraday magnetic balance are given in Tables 5.1 and 5.4. These results show that the magnetic moments are field independent at room temperature, indicating that the materials are not ferromagnetically ordered and that the presence of any ferromagnetic impurity is unlikely.

For $\text{Fe}(\text{CF}_3\text{SO}_3)_2$ and $\text{Fe}(\text{p-CH}_3\text{C}_6\text{H}_4\text{SO}_3)_2$ it is possible to analyse the experimental data using the three parameter model discussed in section 5.6.

The experimental data were analysed by plotting magnetic moment against kT/λ ; various values of λ were chosen, $100 > -\lambda > 70$. A suitable value of k was determined from the absolute magnitude of

FIG. 5.3 PLOTS OF RECIPROCAL SUSCEPTIBILITY AGAINST
TEMPERATURE FOR $\text{Fe}(\text{CF}_3\text{SO}_3)_2$ AND $\text{Fe}(\text{p-CH}_3\text{C}_6\text{H}_4\text{SO}_3)_2$



the magnetic moment and then the temperature dependence was fitted by adjusting the value of ν , where $\nu = \Delta/\lambda$.

Values of the three parameters used to generate the solid lines in Fig. 5.2 are given in Table 5.5 and were obtained by a visual comparison of experimental and theoretical plots.

The value of κ is determined to a large extent by the absolute magnitude of the magnetic moment. The larger the value of μ at any given temperature the larger is the magnitude of κ . The values of κ given in Table 5.5 are probably accurate to ± 0.05 units as the magnitude of the magnetic moment is determined to an accuracy of 1-2%.

It can be seen that the values of κ decrease in the order, $\text{FSO}_3^- > \text{CF}_3\text{SO}_3^- > \text{p-CH}_3\text{C}_6\text{H}_4\text{SO}_3^-$. This may be attributed qualitatively to an increase in the covalency of the iron-oxygen bond, that is, the anions from the stronger acids, namely FSO_3H and $\text{CF}_3\text{SO}_3\text{H}$, are involved in more ionic Fe-O bonds than is the anion from paratoluenesulfonic acid.

The variation of calculated magnetic moment with temperature is determined to a large extent by the values of Δ and λ . In fact the sign of Δ (a positive value indicates a singlet ground state and a negative value indicates an orbital doublet ground state) may be determined from magnetic moment measurements. However, in the compounds studied here the variations of magnetic moment with temperature are too small to determine the sign of Δ with any degree of certainty.

TABLE 5.5 CRYSTAL-FIELD SPLITTING PARAMETERS FOR IRON(II)
SULFONATE COMPOUNDS

COMPOUND	κ	$\Delta(\text{cm}^{-1})$	$\lambda(\text{cm}^{-1})$
$\text{Fe}(\text{FSO}_3)_2^*$	0.95	290	-90
$\text{Fe}(\text{CF}_3\text{SO}_3)_2$	0.80	180	-90
$\alpha\text{-Fe}(\text{CH}_3\text{SO}_3)_2$	0.70	500	-100
$\beta\text{-Fe}(\text{CH}_3\text{SO}_3)_2$	0.50	160	-80
$\text{Fe}(\text{p-CH}_3\text{C}_6\text{H}_4\text{SO}_3)_2$	0.75	270	-90

* Results from reference 15

Equally good fits may be obtained with positive or negative values of Δ . Hence, it is difficult to identify with certainty the nature of the ground state from magnetic moment data alone. However, as will be seen in Chapter 6 the temperature dependence of the Mössbauer quadrupole splittings is definitive as to the orbital properties of the ground state and for $\text{Fe}(\text{CF}_3\text{SO}_3)_2$ and $\text{Fe}(\text{p-CH}_3\text{C}_6\text{H}_4\text{SO}_3)_2$ the ground states have been identified as orbital doublets. Hence $\Delta < 0$ and only fits for negative values of Δ are given in Table 5.5.

Note must be made here that the Δ value of the Figgis and Lewis model is the same as the parameter $3D_5$ used in the analysis of the Mössbauer spectral data.

The magnitude of the axial distortion, as measured by Δ , is of the same order for $\text{Fe}(\text{p-CH}_3\text{C}_6\text{H}_4\text{SO}_3)_2$ and $\text{Fe}(\text{FSO}_3)_2$, approximately 300cm^{-1} , reflecting similar axial field strengths in these compounds. The value of Δ for $\text{Fe}(\text{CF}_3\text{SO}_3)_2$ is the lowest of the three reflecting perhaps, a less distorted environment around the metal ion in this compound. There is some uncertainty regarding this parameter, however, as will be seen later, the same parameter derived from Mössbauer data shows all three compounds to have approximately equal values of Δ . This difference in Δ values, apparent from the interpretation of the magnetic moment data, may simply reflect the relative insensitivity of magnetic moments, when compared with Mössbauer spectral data, to variations in axial field strengths. This may be especially true when the magnetic moments

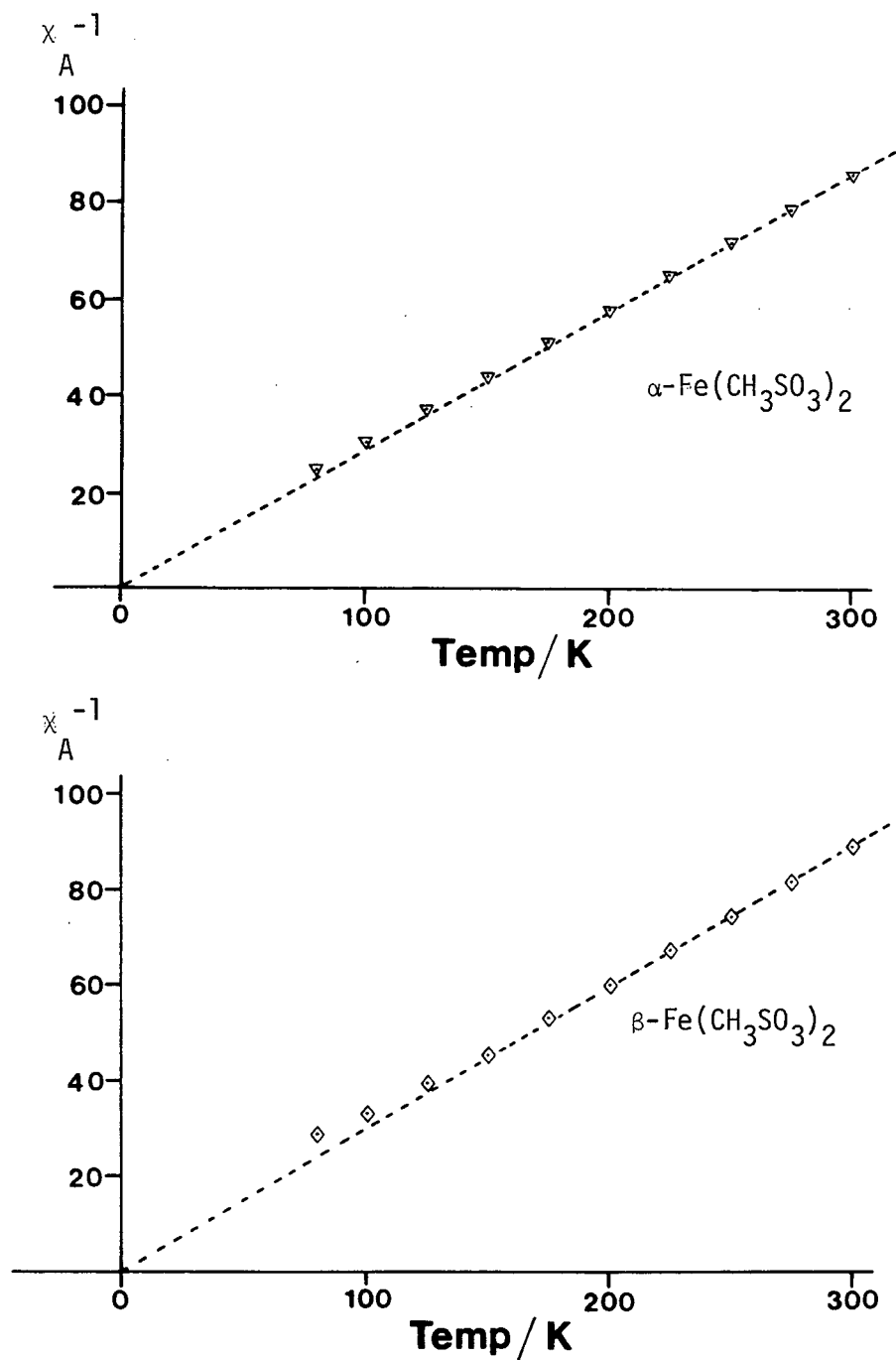
show only a very small temperature dependence as in the present case.

A reduction in the value of the spin-orbit coupling constant below the free-ion value of -103 cm^{-1} is indicated for all these compounds. This is indicative of the presence of some metal-anion covalency associated with $\text{Fe}(\text{CF}_3\text{SO}_3)_2$ and $\text{Fe}(\text{p-CH}_3\text{C}_6\text{H}_4\text{SO}_3)_2$.

5.7.2. Magnetic moment data for α - and β - $\text{Fe}(\text{CH}_3\text{SO}_3)_2$

The magnetic moment data for these two isomers are given in Tables 5.2 and 5.3 and illustrated in Fig. 5.2. It may be observed that there are differences between the iron(II) methanesulfonate compounds and the iron(II) sulfonate compounds discussed in the previous section. Firstly, the absolute magnitudes of the magnetic moments of the iron(II) methanesulfonates are significantly smaller than those of $\text{Fe}(\text{FSO}_3)_2$, $\text{Fe}(\text{CF}_3\text{SO}_3)_2$ or $\text{Fe}(\text{p-CH}_3\text{C}_6\text{H}_4\text{SO}_3)_2$. Secondly, the two iron(II) methanesulfonate isomers show a difference in that no maximum is observed in the magnetic moment against temperature plot; instead the moments decrease monotonically with decreasing temperature. Plots of reciprocal susceptibility against temperature are shown in Fig. 5.4. Both show deviations from Curie Law behaviour, represented by the broken lines. This deviation is particularly noticeable for the β -isomer at temperatures below 150K.

FIG. 5.4 PLOTS OF RECIPROCAL SUSCEPTIBILITY AGAINST
TEMPERATURE FOR α -AND β -Fe(CH₃SO₃)₂

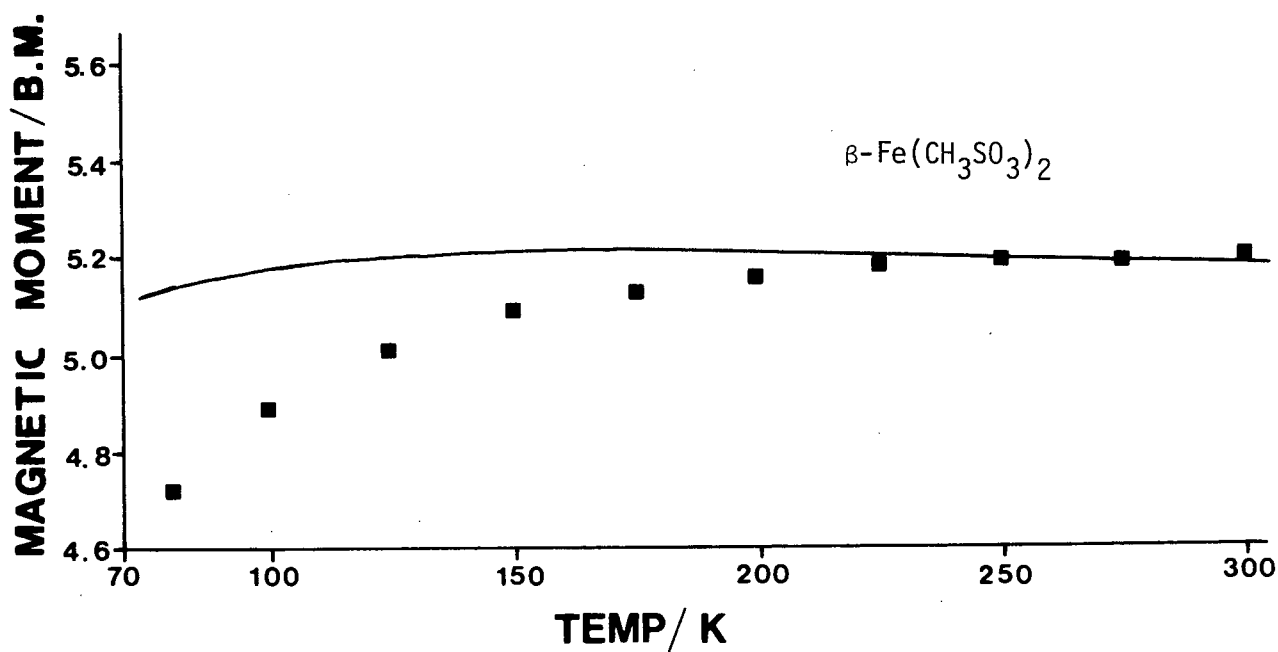
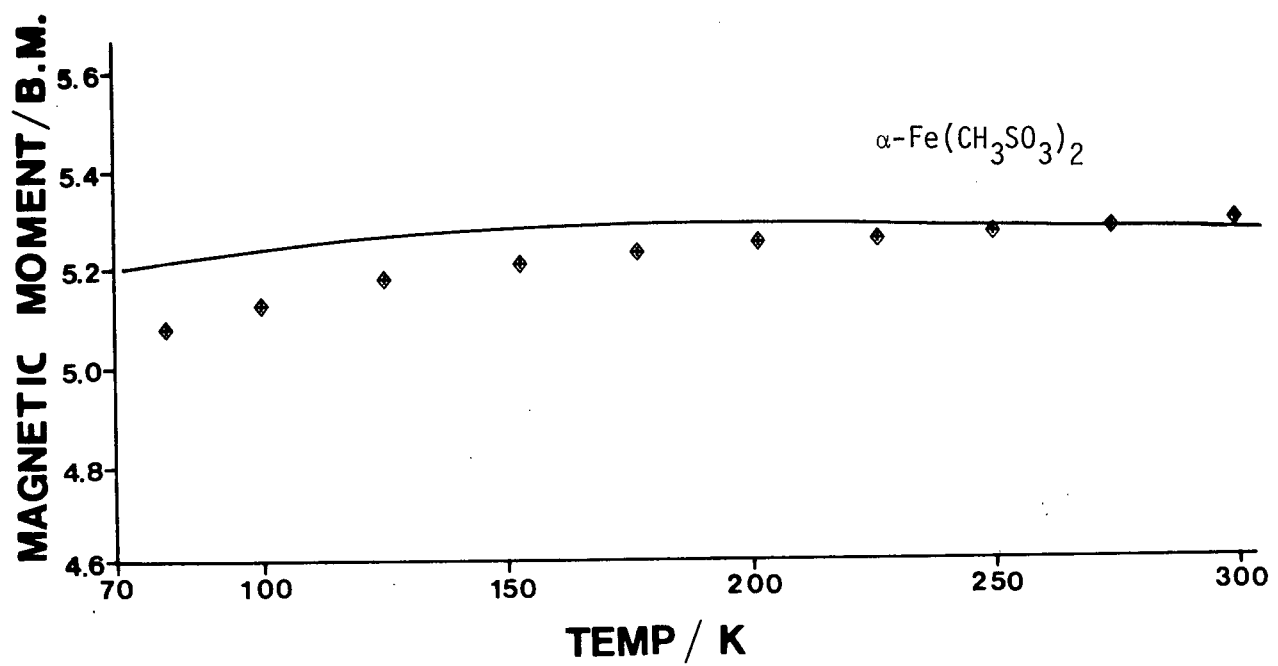


Tables 5.2 and 5.3 show the results obtained in three different magnetic field strengths and indicate that the magnetic moment is independent of magnetic field at room temperature, as found for $\text{Fe}(\text{CF}_3\text{SO}_3)_2$ and $\text{Fe}(\text{p-CH}_3\text{C}_6\text{H}_4\text{SO}_3)_2$. α - and β - $\text{Fe}(\text{CH}_3\text{SO}_3)_2$ are not ferromagnetically ordered.

Attempts were made to analyse the magnetic moment data for both forms of iron(II) methanesulfonate using the model which was successful for $\text{Fe}(\text{CF}_3\text{SO}_3)_2$ and $\text{Fe}(\text{p-CH}_3\text{C}_6\text{H}_4\text{SO}_3)_2$. But due to the magnitude and temperature dependence of the magnetic moment data no reasonable fits could be obtained. Satisfactory fits could only be obtained between about 200K and room temperature, whilst at lower temperatures the decrease in magnetic moment, especially for the β -isomer, is appreciably more than that predicted from the theoretical model.

The parameters used to generate the solid lines in Fig. 5.5 are given in Table 5.5. It can be seen that to allow for the absolute magnitude of the room temperature moment one has to employ κ values of 0.7 and 0.5 for the α - and β -isomers respectively. These κ values, especially the latter, indicate an anomalously high degree of electron delocalisation in these two compounds. This seems unreasonable in light of the fact that the Mössbauer isomer shifts (see Table 6.3) for these compounds and other iron(II) sulfonates are similar, which would indicate a similar degree of covalency.

FIG. 5.5 TEMPERATURE DEPENDENCE OF THE MAGNETIC
MOMENT FOR α - AND β - $\text{Fe}(\text{CH}_3\text{SO}_3)_2$



Another mechanism by which such low magnetic moments may arise is by antiferromagnetic exchange coupling between adjacent iron centres, rather than as a consequence of abnormal electron delocalisation effects. This proposal seems more reasonable, especially for the β -isomer, as Mössbauer results to be discussed later indicate a magnetic phase transition to an antiferromagnetically ordered state in this compound.

At the present time no model of antiferromagnetic exchange coupling has been used to analyse the magnetic moment data of the iron(II) methanesulfonate compounds. Due to the polymeric nature of these compounds in which each anion bridges to three different iron centres it is obviously a complex situation.

There is no evidence for magnetic exchange in $\text{Fe}(\text{FSO}_3)_2$, $\text{Fe}(\text{CF}_3\text{SO}_3)_2$ or $\text{Fe}(\text{p-CH}_3\text{C}_6\text{H}_4\text{SO}_3)_2$ and magnetic exchange in the methanesulfonate compounds is somewhat surprising not only because of the number of bridging atoms through which an exchange would have to be transmitted but also because of the highly ionic nature of the compounds as indicated by the high isomer shift values. Nevertheless magnetic exchange was proposed to occur through the FSO_3^- anion in $\text{Fe}(\text{FSO}_3)_3$ (22).

Magnetic exchange through bridging carboxylate anions, RCO_2^- , has been proposed previously (65). Carboxylates are, however, more basic than the methanesulfonate anion and form compounds which are more highly covalent.

5.8. SUMMARY OF RESULTS AND CONCLUSIONS

From the magnetic moment data the $\text{Fe}(\text{XSO}_3)_2$ compounds appear to fall into two categories:

- (i) Where X is F, CF_3 or $\text{p-CH}_3\text{C}_6\text{H}_4$. In these cases a reasonable analysis of the magnetic moment data is possible using the Figgis and Lewis model, and values of the parameters κ , Δ and λ give an indication of the electron delocalisation and axial field strengths in these compounds. No magnetic exchange seems likely.

- (ii) Where X is $\alpha\text{-CH}_3$ or $\beta\text{-CH}_3$. The analysis of magnetic moment data using the Figgis and Lewis approach is poor and the parameters derived from it may have little significance. Magnetic exchange between iron centres is proposed here but no detailed analysis has yet been undertaken.

CHAPTER 6

MÖSSBAUER SPECTROSCOPY

6.1. INTRODUCTION

In 1957 R.L. Mössbauer observed recoilless nuclear gamma resonance which has become known as the Mössbauer effect (66). The effect in the ^{57}Fe nucleus was not observed until 1959 but since 1961 the technique has been widely applied in chemistry and other diverse applications using various isotopes (e.g. nuclear and solid state physics (67), electronic structure of impurity atoms in alloys (68), mineralogical and geological applications (69), and the nature of active centres in iron porphyrins (70)). The majority of work has involved the ^{57}Fe and ^{119}Sn nuclei; however, over 50 other isotopes show the effect.

A brief discussion of the Mössbauer effect will follow and the treatment focusses on the nature of the interactions responsible for the observed spectra. The isomer shift and quadrupole splitting, and the chemical information to be derived from these parameters, are discussed in sections 6.2.1 and 6.2.3. Magnetic hyperfine interactions are discussed in Chapter 7. For detailed theoretical treatments the reader is referred to standard texts (71, 72). After this discussion of the theory, sections 6.3 and 6.4 present the results obtained in this study.

6.2. THEORY OF MÖSSBAUER SPECTROSCOPY

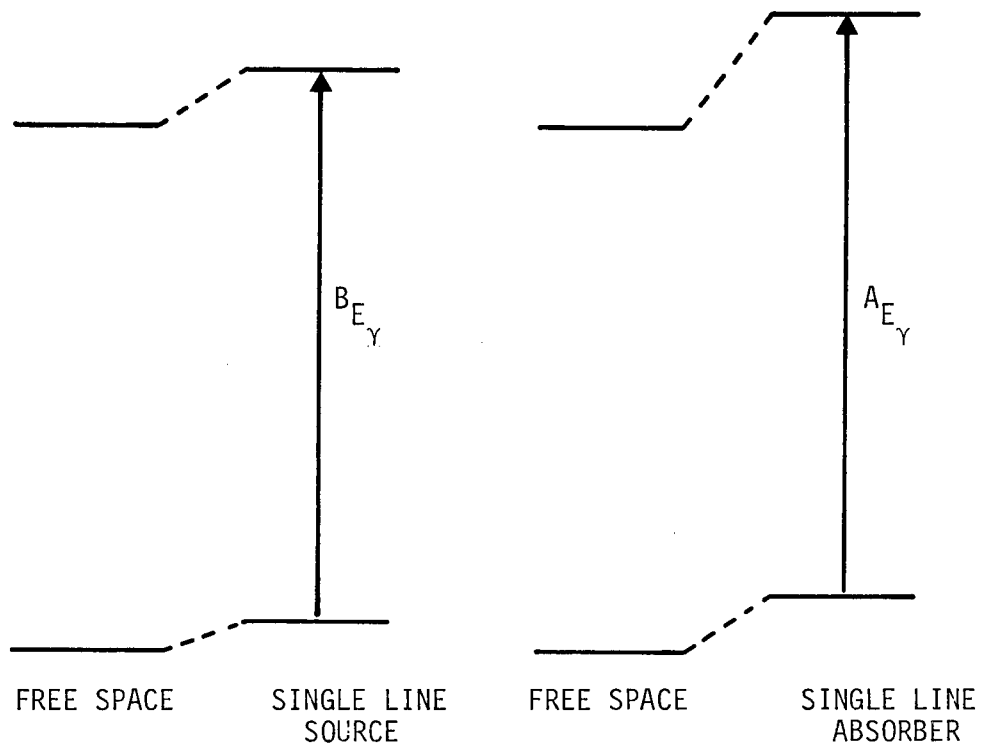
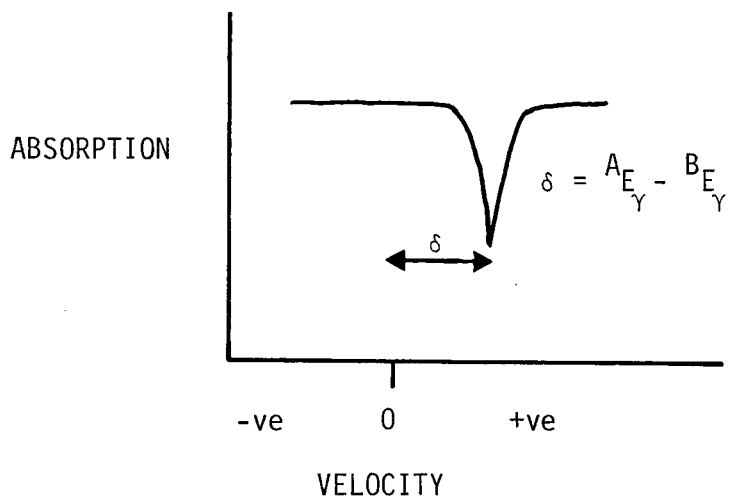
6.2.1. Electric monopole interaction, the isomer shift

The nucleus has a finite volume and the isomer shift arises because of the penetration of the nuclear volume by electrons which have a finite probability of being found in the region of the nucleus. During a nuclear γ -transition it is usual for the effective nuclear size to change, thereby slightly altering the nucleus-electron interaction energy. This interaction does not lead to a splitting of nuclear energy levels but results in a shift of energy levels which, in general, will be different in source(B) and absorber(A) as shown in Fig. 6.1.

If nucleus B is chosen as a reference and the relative energy of nucleus A is measured with respect to B, then the difference in γ -ray energies may be expressed as the chemical isomer shift, δ , where δ is given by:

$$\delta = \frac{4}{5} \pi z e^2 r^2 \left\{ \frac{dr}{r} \right\} \left[|\psi_s(0)_A|^2 - |\psi_s(0)_B|^2 \right] \quad (6.1)$$

where z is the atomic number, e is the positive elementary charge, r is the mean nuclear radius, dr is equal to $r_e - r_g$, the difference in nuclear radii of the excited and ground states. $|\psi_s(0)_A|^2$ and $|\psi_s(0)_B|^2$ are the s-electron densities in the nuclear volume for A and B respectively.

FIG. 6.1 (i) SOURCE AND ABSORBER NUCLEAR ENERGY LEVELS(ii) RESULTANT MÖSSBAUER SPECTRUM

The term $\frac{4}{5} \pi Ze^2 r^2 (dr/r)$ is a constant for a given nucleus and hence the isomer shift is largely dependent upon the s-electron density. In particular for ^{57}Fe the 4s electrons primarily determine the isomer shift. Other electrons have some effect on isomer shifts also, since s-electron density is sensitive to changes in p- and d-electron density as a result of screening effects.

For ^{57}Fe the nucleus expands as it goes from the excited state to the ground nuclear state with the emission of a gamma ray. Hence, dr/r is negative (73). For this isotope an increase in s-electron density at the nucleus results in a decrease in isomer shift. In other words, the higher the value of the isomer shift the more ionic is the material under investigation. This fact has enabled the determination of oxidation states and electron configurations of iron in some of its complexes, as well as the relative electronegativities of some ligands to be determined (74).

6.2.2. Second-order Doppler effect

It is experimentally observed that the isomer shift is temperature dependent. This arises from the thermal motion of the Mössbauer atoms, i.e. a temperature dependence of the lattice vibrational modes. This effect is small compared to the isomer shift and is not chemically significant.

6.2.3. Electric quadrupole interaction, the quadrupole splitting

The electric quadrupole moment of the nucleus can interact with the chemical environment around the nucleus. Nuclei with a spin quantum number I greater than $\frac{1}{2}$ have a non-spherical charge distribution, the magnitude of the charge distortion being measured by Q , the nuclear quadrupole moment. The sign of Q may be positive, corresponding to a prolate charge distribution elongated along the spin axis, or negative, corresponding to an oblate charge distribution flattened along the spin axis.

The interaction of the nuclear quadrupole moment with the electronic environment may be expressed by the following Hamiltonian:

$$\mathcal{H} = - \frac{1}{6} e Q \nabla^2 E \quad (6.2)$$

where $\nabla^2 E$ represents the electric field gradient, E.F.G. at the nucleus. The E.F.G. at the nucleus is a tensor quantity whose elements are the negative second derivatives of the electrostatic potential, V

$$V_{ij} = \frac{d^2 V}{dx_i dx_j} \quad (6.3)$$

In order to express $\nabla^2 E$ in a Cartesian axis system there are nine values of V_{ij} . A principal axis system may be defined such that all V_{ij} terms with $i \neq j$ are zero, resulting in a diagonal matrix. Following convention the principal axes are chosen such that $|V_{zz}| \geq |V_{yy}| \geq |V_{xx}|$. Also the tensor is traceless, i.e. $V_{xx} + V_{yy} + V_{zz} = 0$.

In order to specify the electric field gradient tensor only two parameters are necessary in the principal axis system. They are η the asymmetry parameter, and V_{zz} the principal component of the E.F.G. tensor. Where η and V_{zz} may be defined as follows:

$$\eta = \frac{(V_{xx} - V_{yy})}{V_{zz}} \quad (6.4)$$

$$V_{zz} = eq \quad (6.5)$$

The asymmetry parameter may take values between the following limits, $0 \leq \eta \leq 1$.

The nuclear quadrupole coupling Hamiltonian for a nucleus of spin I can be written as:

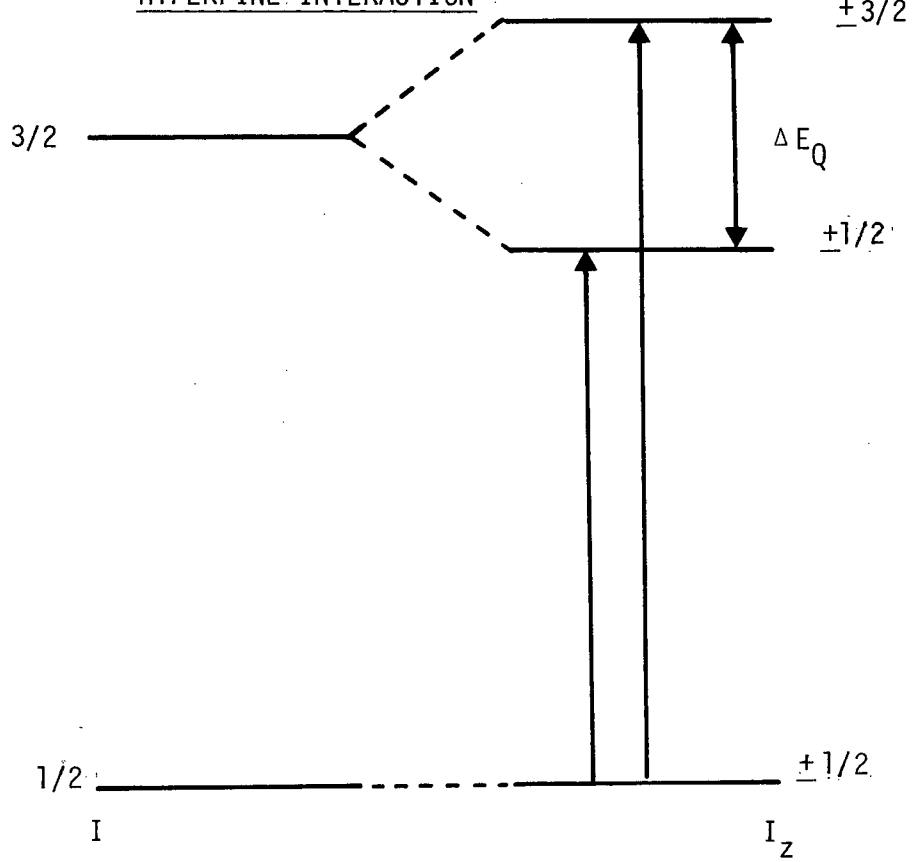
$$\mathcal{H}_Q = \frac{e^2 q Q}{4I(2I-1)} \left[3\hat{I}_z^2 - I(I+1) + \frac{\eta}{2} (\hat{I}_+^2 + \hat{I}_-^2) \right] \quad (6.6)$$

where \hat{I}_z is the nuclear spin operator, and \hat{I}_+ , \hat{I}_- are shift operators (75). ^{57}Fe has a ground state with $I = \frac{1}{2}$ and hence zero quadrupole moment, and a first excited state with $I = 3/2$. In the presence of an E.F.G. the latter is split into two substates with $I_z = \pm 3/2$ and $\pm 1/2$, for $\eta = 0$. The separation of these substates is the quadrupole splitting ΔE_Q and is given by:

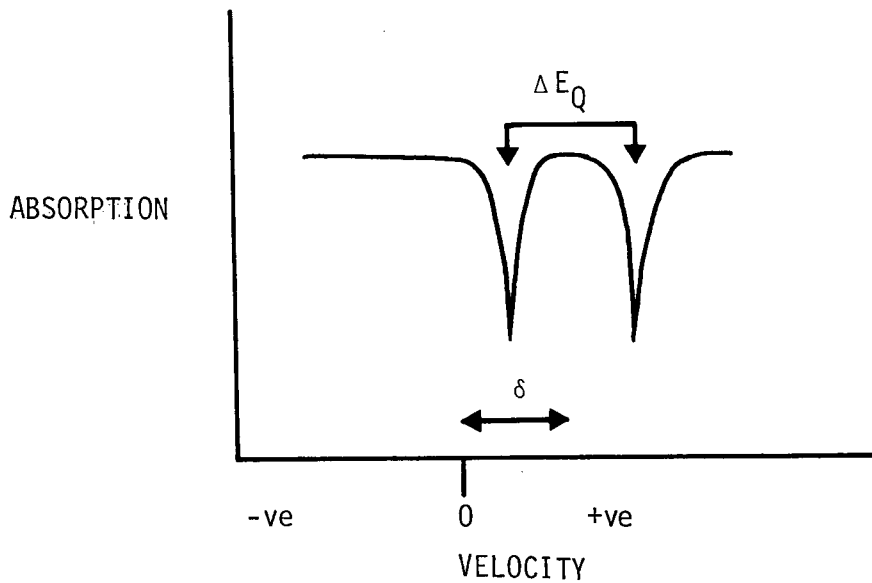
$$\Delta E_Q = \frac{1}{2} e^2 q Q (1 + \eta^2/3)^{\frac{1}{2}} \quad (6.7)$$

Both possible transitions are allowed as shown in Fig. 6.2 and a two line spectrum is observed. ΔE_Q is taken as being positive

FIG. 6.2 (i) ENERGY LEVEL SCHEME INCLUDING QUADRUPOLE HYPERFINE INTERACTION



(ii) RESULTANT MOSSBAUER SPECTRUM



when the $\pm\frac{1}{2}$ state is lower in energy than the $\pm\frac{3}{2}$ state. From such symmetric two line spectra only the isomer shift and quadrupole splitting may be evaluated, neither the sign of V_{zz} nor the magnitude of η may be determined.

The case of high-spin iron(II) will now be discussed in more detail as much information about the orbital ground state and orbital occupations can be obtained using Mössbauer spectroscopy.

The 5D free-ion spectroscopic state for high-spin iron(II) arises from a d^6 electron configuration. In a perfectly octahedral crystal field the d orbitals split as shown in Fig. 6.3 and the degeneracy of the t_{2g} levels is not removed, the sixth electron equally populates the three t_{2g} orbitals and hence no finite E.F.G. is experienced by the iron nucleus and no quadrupole splitting is observed. The same conclusion may be arrived at by consulting Table 6.1 and using the Townes-Dailey approximation (73,76). Table 6.1 gives the contributions to the E.F.G. from a single electron in each of the d orbitals (71) and the Townes-Dailey approximation discusses the valence contribution to the E.F.G. in terms of the effective population of the p and d orbitals. Thus

$$q_{VAL} = \frac{4}{5} \langle r^{-3} \rangle_p \left[-N_{pz} + \frac{1}{2} (N_{px} + N_{py}) \right] \\ + \frac{4}{7} \langle r^{-3} \rangle_d \left[N_{d_{x^2-y^2}} - N_{d_{z^2}} + N_{d_{xy}} - \frac{1}{2} (N_{d_{xz}} + N_{d_{yz}}) \right] \quad (6.8)$$

FIG. 6.3 3d ORBITAL SPLITTINGS IN OCTAHEDRAL, AXIAL AND RHOMBIC FIELDS

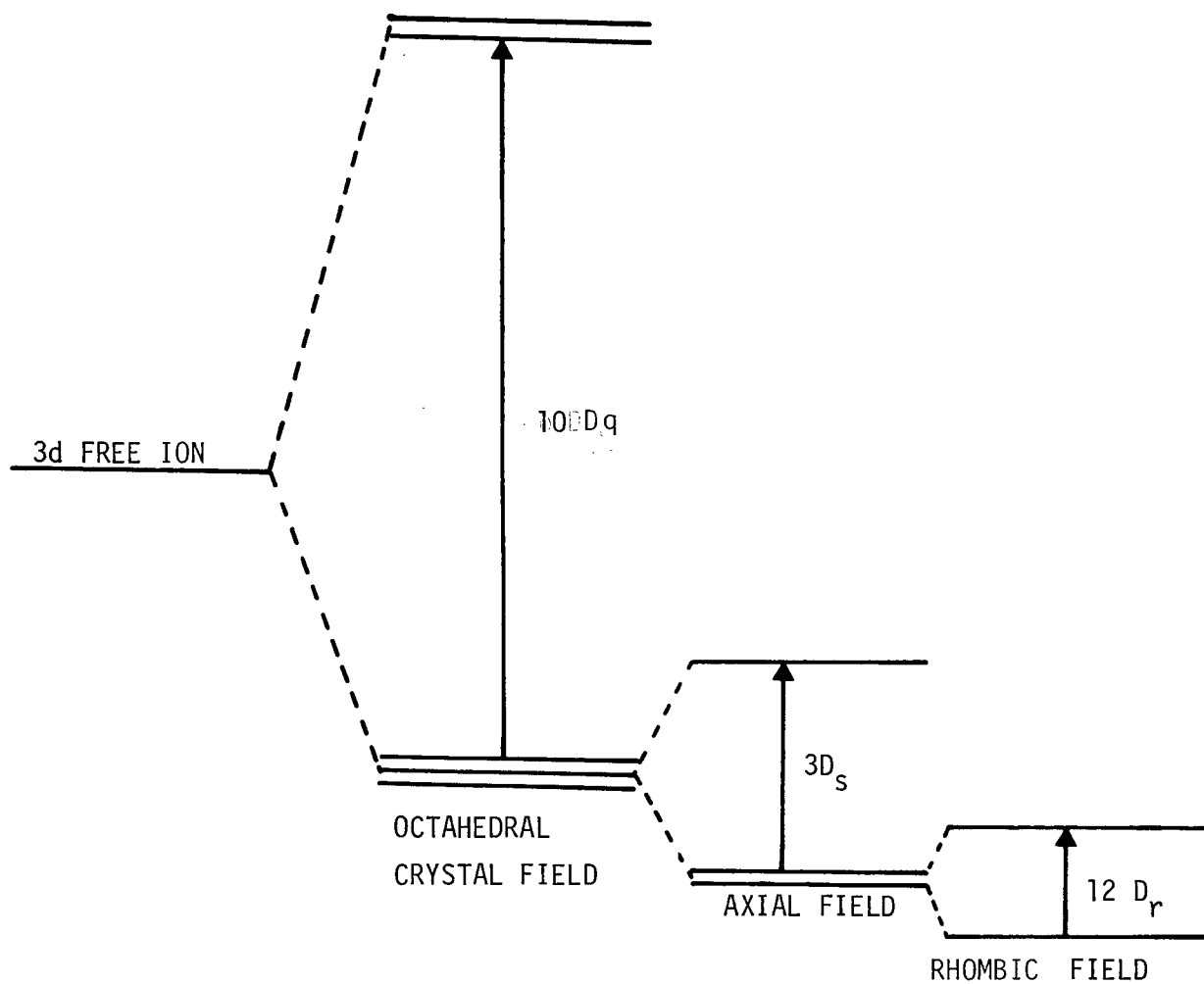


TABLE 6.1 VALUES OF q_{VAL} FOR THE 3d ORBITALS

3d ORBITAL	q_{VAL}
$d_{x^2-y^2}$	$+ \frac{4}{7} \langle r^{-3} \rangle$
d_{z^2}	$- \frac{4}{7} \langle r^{-3} \rangle$
d_{xy}	$+ \frac{4}{7} \langle r^{-3} \rangle$
d_{xz}	$- \frac{2}{7} \langle r^{-3} \rangle$
d_{yz}	$- \frac{2}{7} \langle r^{-3} \rangle$

where N_{pi} and N_{di} are the effective populations of the appropriate 4p and 3d iron orbitals, respectively, and $\langle r^{-3} \rangle$ the expectation value of $1/r^3$ taken over the appropriate 4p or 3d radial function.

However, iron(II) compounds are inherently subject to a Jahn-Teller distortion which removes the degeneracy of the t_{2g} orbitals as shown in Fig. 6.3 and the sixth electron occupies the lowest level. For example, if the axial ligands are compressed slightly relative to the equatorial ligands the electron preferentially occupies the d_{xy} orbital and generates an E.F.G. in proportion to $+4/7 \langle r^{-3} \rangle$.

As can be seen from Fig. 6.3 the axial field (D_{4h} or D_{3d}) splits the t_{2g} orbitals into a singlet and a doublet separated by $3D_s$. If this splitting is of the order of kT the quadrupole splitting will show a large temperature dependence caused by a Boltzman distribution between these two levels. A rhombic field will remove the remaining degeneracy of the t_{2g} orbitals, splitting the doublet by $12D_r$ (Fig.6.3).

If the fourfold axis (C_4) is taken as the quantisation axis, the d orbitals transform as those shown in Fig. 6.4. However, if the threefold axis (C_3) of the octahedron is assumed to be the axis of quantisation, then, in terms of the real d orbitals, one has those as shown in Fig. 6.5 (77). In the tetragonal case the singlet is $|xy\rangle$ and in the trigonal case it is the $|z^2\rangle$ orbital.

FIG. 6.4 C_4 QUANTISATION AXIS AND d ORBITALS

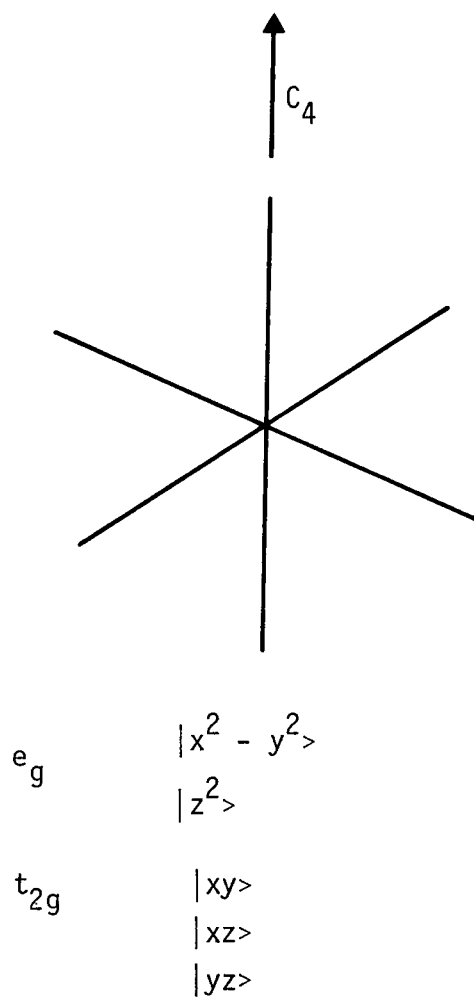
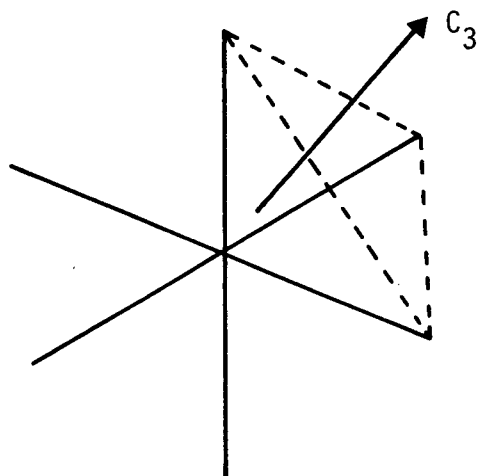


FIG. 6.5 C_3 QUANTISATION AXIS AND d ORBITALS

$$e_g \quad (1/3)^{1/2} |x^2-y^2\rangle + (2/3)^{1/2} |xz\rangle$$

$$(1/3)^{1/2} |xy\rangle - (2/3)^{1/2} |yz\rangle$$

$$t_{2g} \quad |z^2\rangle$$

$$(2/3)^{1/2} |x^2-y^2\rangle - (1/3)^{1/2} |xz\rangle$$

$$(2/3)^{1/2} |xy\rangle + (1/3)^{1/2} |yz\rangle$$

6.3 ISOMER SHIFTS AND QUADRUPOLE SPLITTINGS FOR IRON(II) SULFONATES

"Mössbauer spectra have been recorded for all the iron(II) sulfonates studied from 4.2K to room temperature. The Mössbauer parameters, isomer shift (δ), quadrupole splitting (ΔE_Q) and line widths (Γ) are given in Table 6.2 (i-iv).

6.3.1. Isomer shift values

The isomer shift values normally observed for octahedral high-spin iron(II) compounds are of the order $1.1 - 1.3 \text{ mm s}^{-1}$ at 80K (71). As can be seen from Table 6.3 the compounds studied here all have relatively high isomer shifts, $1.4 - 1.5 \text{ mm s}^{-1}$ at 80K. This is indicative of a high degree of ionic character in the metal-ligand bonds in these compounds. The isomer shift values are in fact comparable with those of known "highly ionic" compounds. These include some iron(II) fluorides FeF_2 (78), CsFeF_2 (79) and Rb_2FeF_4 (80) which have isomer shift values of 1.48 mm s^{-1} at 78K, 1.49 mm s^{-1} at 4.2K and 1.45 mm s^{-1} at 78K, respectively. Using the Walker-Wertheim-Jaccarino model (81) which relates isomer shift values to electron configurations, a derived electron configuration for the iron(II) cation in these compounds may be derived as $3d^{6.00}4s^{0.00}$.

The differences in isomer shift values shown in Table 6.3 are only small and as they are a function of lattice dynamics as well as the s-electron density any attempt at a correlation between isomer shifts and the base strengths of the anions is tenuous.

TABLE 6.2 ⁵⁷MOSSBAUER EFFECT DATA FOR IRON(II) SULFONATES

Note units of δ , ΔE_Q and Γ are all given in mm s^{-1}

(i) $\text{Fe}(\text{CF}_3\text{SO}_3)_2$

TEMP(K)	δ	ΔE_Q	Γ_1	Γ_2
6.5	1.46	2.01	0.49	0.52
17.7	1.46	1.98	0.52	0.54
38.8	1.45	1.95	0.55	0.55
64.4	1.45	1.91	0.51	0.49
78.8	1.39	1.82	0.28	0.31
80.0	1.45	1.84	0.47	0.44
104	1.46	1.88	0.50	0.50
115	1.43	1.81	0.33	0.33
131	1.42	1.78	0.55	0.54
183	1.40	1.68	0.41	0.39
233	1.37	1.59	0.46	0.44
272	1.35	1.51	0.45	0.41
293	1.32	1.44	0.28	0.26

* All isomer shift values are quoted relative to the centroid of an iron foil spectrum.

TABLE 6.2 Continued

(ii) $\alpha\text{-Fe}(\text{CH}_3\text{SO}_3)_2$

TEMP (K)	δ	ΔE_Q	Γ_1	Γ_2
4.2	1.35	3.31	0.52	0.54
10.5	1.21	3.39	0.40	0.40
35.2	1.44	3.34	0.55	0.51
60.0	1.42	3.35	0.56	0.54
84.7	1.45	3.37	0.41	0.37
110	1.44	3.36	0.41	0.38
140	1.42	3.30	0.47	0.44
170	1.41	3.29	0.39	0.36
200	1.40	3.24	0.40	0.38
235	1.37	3.19	0.40	0.37
264	1.36	3.12	0.44	0.41
293	1.34	2.95	0.41	0.39

TABLE 6.2 Continued

(iii) $\beta\text{-Fe}(\text{CH}_3\text{SO}_3)_2$

TEMP (K)	δ	ΔE_Q	Γ_1	Γ_2
25.3	1.37	1.54	0.41	0.39
30.0	1.49	1.55	0.39	0.37
80.0	1.48	1.41	0.45	0.44
109	1.46	1.38	0.35	0.34
139	1.46	1.33	0.35	0.33
169	1.43	1.28	0.34	0.33
209	1.43	1.20	0.33	0.33
239	1.41	1.14	0.34	0.32
260	1.40	1.10	0.33	0.32
293	1.31	0.94	0.28	0.33

TABLE 6.2 continued

(iv) $\text{Fe}(\text{p-CH}_3\text{C}_6\text{H}_4\text{SO}_3)_2$

TEMP (K)	δ	ΔE_Q	Γ_1	Γ_2
3.9	1.30	1.99	0.32	0.34
9.0	1.45	2.03	0.41	0.42
33.5	1.44	1.92	0.32	0.30
55.7	1.43	1.91	0.31	0.30
78.6	1.42	1.91	0.36	0.35
96.0	1.42	1.88	0.34	0.33
110	1.41	1.84	0.35	0.34
115	1.42	1.83	0.33	0.32
135	1.40	1.79	0.33	0.31
165	1.39	1.72	0.32	0.31
195	1.37	1.66	0.32	0.31
225	1.36	1.58	0.31	0.31
260	1.34	1.51	0.30	0.30
291	1.32	1.39	0.30	0.28

TABLE 6.3 ISOMER SHIFT VALUES FOR $\text{Fe}(\text{XSO}_3)_2$ COMPOUNDS AT 80K

X	δ (mm s^{-1})
F^*	1.49
CF_3	1.45
$\alpha\text{-CH}_3$	1.45
$\beta\text{-CH}_3$	1.48
$p\text{-CH}_3\text{C}_6\text{H}_4$	1.42

* Reference 15

The temperature dependence of the isomer shift values in these compounds may be assigned to a second-order Doppler effect. This may be confirmed in $\text{Fe}(\text{p-CH}_3\text{C}_6\text{H}_4\text{SO}_3)_2$ as the isomer shift value at 3.9K was measured with the source and absorber at the same temperature and is of a comparable value to the isomer shift measured at 291K.

6.3.2. Quadrupole splitting values

Mössbauer spectra of the compounds studied all show a two-line symmetric spectrum over the temperature range studied. The exceptions are $\text{Fe}(\text{CF}_3\text{SO}_3)_2$ which shows some asymmetry and magnetic hyperfine structure below 8K; also $\beta\text{-Fe}(\text{CH}_3\text{SO}_3)_2$ exhibits a complex hyperfine spectrum below $\sim 25\text{K}$. These observations will be discussed in Chapter 7.

The temperature dependence of the quadrupole splittings is shown in Fig. 6.6 and typical spectra are illustrated for $\text{Fe}(\text{p-CH}_3\text{C}_6\text{H}_4\text{SO}_3)_2$ at various temperatures in Fig. 6.7. The two modifications of $\text{Fe}(\text{CH}_3\text{SO}_3)_2$ were first identified by Mössbauer spectroscopy and spectra of the α -, β -forms and a mixture of $\text{Fe}(\text{CH}_3\text{SO}_3)_2$ are shown in Fig. 6.8.

$\alpha\text{-Fe}(\text{CH}_3\text{SO}_3)_2$ has a quadrupole splitting substantially greater than 2 mm s^{-1} and since a singlet ground state is expected to give an E.F.G. in proportion to $4/7\langle r^{-3} \rangle$ (see Table 6.1) the quadrupole splitting values for the α -isomer are only consistent with a singlet ground state. In trigonal symmetry this orbital

FIG. 6.6 TEMPERATURE DEPENDENCE OF THE QUADRUPOLE SPLITTING

FOR $\text{Fe}(\text{XSO}_3)_2$ COMPOUNDS

(Solid lines are generated using parameters listed in Table 6.4)

- ◆ $\alpha\text{-Fe}(\text{CH}_3\text{SO}_3)_2$
- $\text{Fe}(\text{CF}_3\text{SO}_3)_2$
- ▲ $\text{Fe}(\text{p-CH}_3\text{C}_6\text{H}_4\text{SO}_3)_2$
- △ $\text{Fe}(\text{FSO}_3)_2$
- $\beta\text{-Fe}(\text{CH}_3\text{SO}_3)_2$

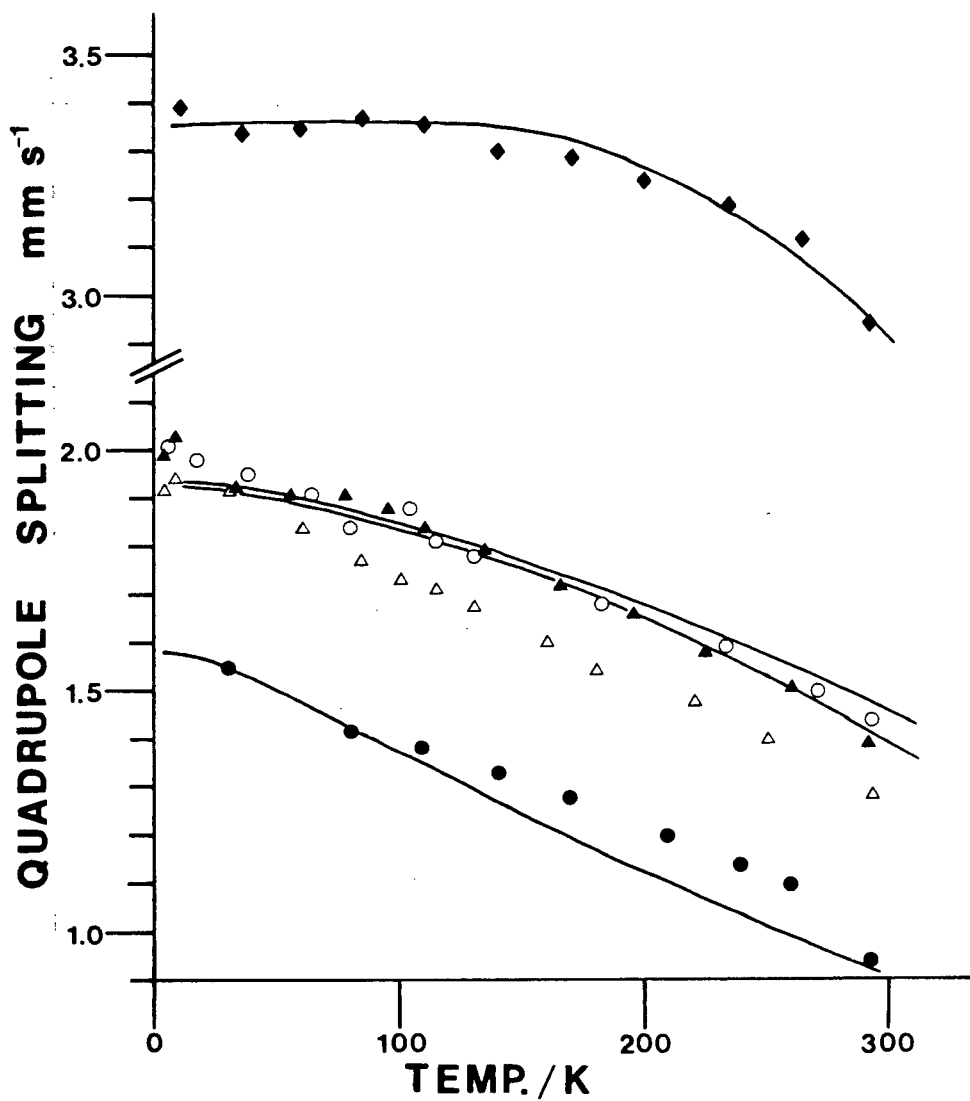


FIG. 6.7 ^{57}Fe MOSSBAUER SPECTRA OF $\text{Fe}(\text{p-CH}_3\text{C}_6\text{H}_4\text{SO}_3)_2$
AT VARIOUS TEMPERATURES

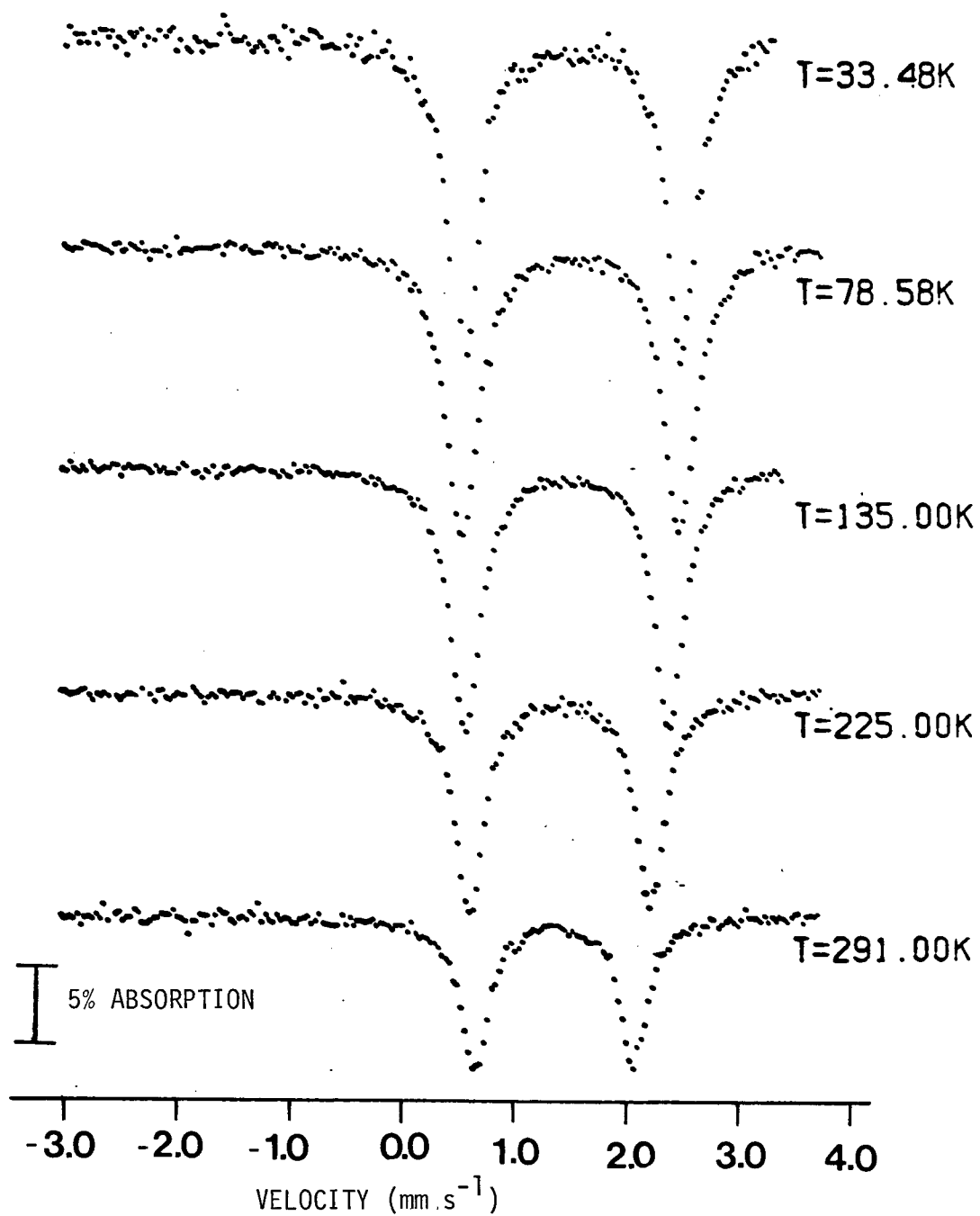
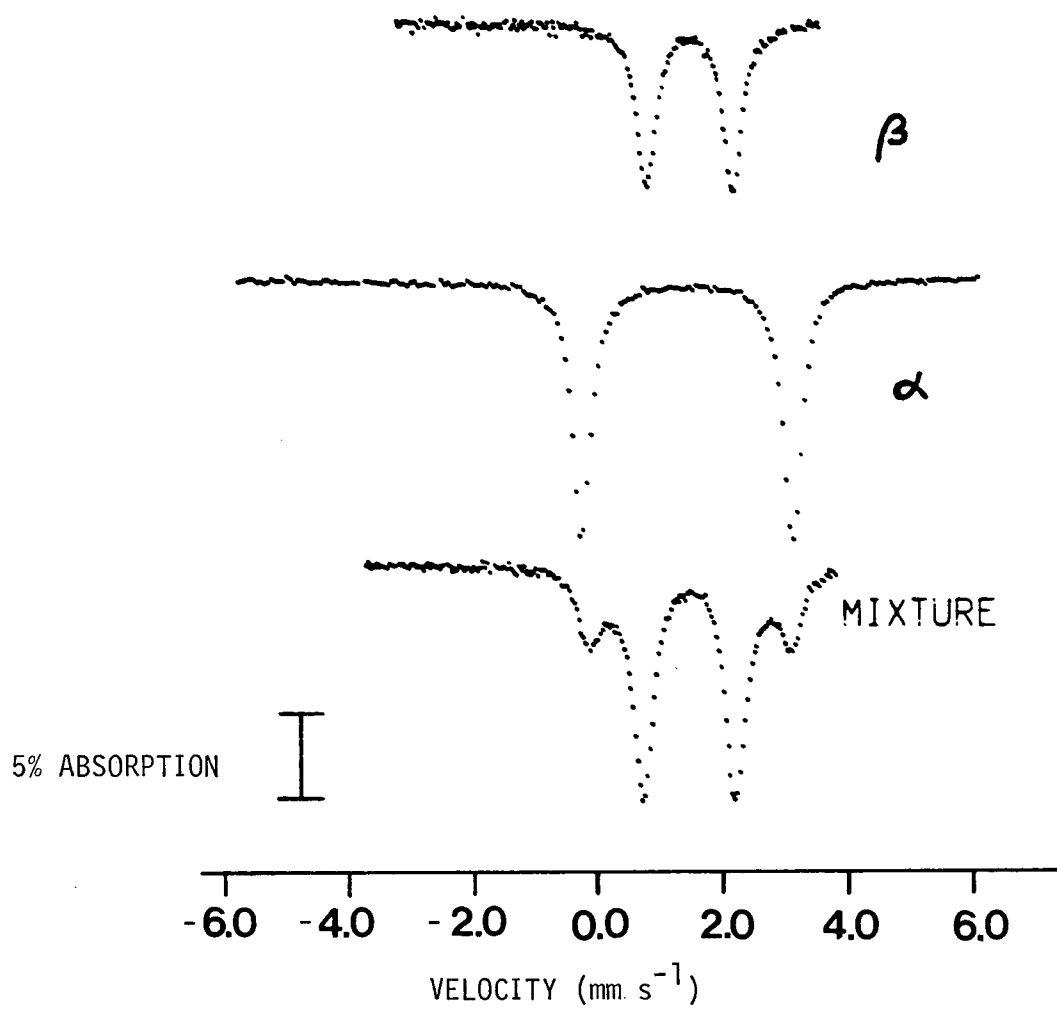


FIG. 6.8 ^{57}Fe MOSSBAUER SPECTRA OF $\text{Fe}(\text{CH}_3\text{SO}_3)_2$ AT 78K



singlet ground state would be $|z^2\rangle$ and in tetragonal symmetry the $|xy\rangle$ orbital ground state. For $\alpha\text{-Fe}(\text{CH}_3\text{SO}_3)_2$ the infrared data, presented in Chapter 3, indicates C_s anion symmetry and we initially thought that the α -species contained tetragonally distorted FeO_6 octahedra. However, Mössbauer spectral measurements in an applied magnetic field (Chapter 7) show V_{zz} to be negative. Thus the combination of a negative E.F.G. and a singlet ground state indicate a $|z^2\rangle$ and not an $|xy\rangle$ orbital ground state, and in $\alpha\text{-Fe}(\text{CH}_3\text{SO}_3)_2$ we have FeO_6 octahedra which are compressed along the threefold trigonal axis.

As can be seen from Fig. 6.6, $\text{Fe}(\text{CF}_3\text{SO}_3)_2$, $\beta\text{-Fe}(\text{CH}_3\text{SO}_3)_2$ and $\text{Fe}(\text{p-CH}_3\text{C}_6\text{H}_4\text{SO}_3)_2$ all exhibit similar temperature dependencies of their quadrupole splittings, comparable with the previously studied $\text{Fe}(\text{FSO}_3)_2$ (15). The major difference appears to be that for the β -isomer the quadrupole splitting has a considerably smaller value than for $\text{Fe}(\text{CF}_3\text{SO}_3)_2$ and $\text{Fe}(\text{p-CH}_3\text{C}_6\text{H}_4\text{SO}_3)_2$. At 80K the value of ΔE_Q is 1.41 mm s^{-1} for $\beta\text{-Fe}(\text{CH}_3\text{SO}_3)_2$ compared with $\Delta E_Q = 1.84$ and 1.91 mm s^{-1} for $\text{Fe}(\text{CF}_3\text{SO}_3)_2$ and $\text{Fe}(\text{p-CH}_3\text{C}_6\text{H}_4\text{SO}_3)_2$ respectively. This difference in ΔE_Q values has been analysed in terms of the crystal-field model discussed in section 6.4.

$\text{Fe}(\text{CF}_3\text{SO}_3)_2$, $\beta\text{-Fe}(\text{CH}_3\text{SO}_3)_2$ and $\text{Fe}(\text{p-CH}_3\text{C}_6\text{H}_4\text{SO}_3)_2$ all have ΔE_Q values of less than 2.1 mm s^{-1} over all temperatures studied. This indicates either an orbital doublet ground state or possibly an orbital singlet ground state if $3D_s/k$ is not much greater than 300K; in the latter case the thermal population of the doublet would

be significant and ΔE_Q would be expected to show a pronounced increase as the temperature was lowered and the electron was localised in the singlet. For the compounds studied here this is not the case, and a detailed analysis of the quadrupole splittings show these compounds to have orbital doublet ground states as was found for the $\text{Fe}(\text{FSO}_3)_2$ compound. The infrared data for these compounds are only consistent with a trigonal distortion and results from magnetically-perturbed Mössbauer spectra show these compounds to have a positive value of V_{zz} . Hence the ground state is the orbital doublet and the FeO_6 octahedra are distorted by a trigonal elongation.

6.4. CRYSTAL-FIELD, SPIN-ORBIT AND SPIN-SPIN SPLITTING PARAMETERS FOR IRON(II) SULFONATES

The temperature dependence of the quadrupole splitting has been analysed using a model formulated by Ingalls (82) and Gibb (83). The theoretical approach is based upon the crystal-field model; the effect of the non-cubic part of the crystal field is treated in terms of the perturbation Hamiltonian:

$$\mathcal{H} = V_T + V_R + V_{s.o.} + V_{s.s.} \quad (6.9)$$

where V_T is the axial field term (tetragonal or trigonal), V_R the rhombic term, $V_{s.o.}$ the spin-orbit coupling parameter and $V_{s.s.}$ the intraionic spin-spin coupling parameter. The last term was omitted by Ingalls and Gibb in their treatments but was included

in the model of Sams and Tsin (84) in order to account for the behaviour of the quadrupole splittings below 80K. If $V_{s.s.}$ is omitted the computed values of ΔE_Q decrease with decreasing temperature below 80K and this behaviour is contrary to what is observed experimentally (see Fig. 6.6).

In operator notation equation 6.9 can be written:

$$\mathcal{H} = D_s (\hat{L}_z^2 - 2) + D_r (\hat{L}_+^2 + \hat{L}_-^2) - \lambda (\hat{L}_z \hat{S}_z + \frac{1}{2} (\hat{L}_+ \hat{S}_- + \hat{L}_- \hat{S}_+)) - D_\sigma (\hat{S}_z^2 - 2) \quad (6.10)$$

Here the small fourth-order axial and rhombic terms are ignored; \hat{L}_i and \hat{S}_i are the orbital and spin angular momentum operators respectively, D_s and D_r are the axial and rhombic field parameters and λ and D_σ are the spin-orbit and spin-spin coupling parameters respectively.

Optical spectra of these compounds, presented in Chapter 4, show that for the sulfonates studied here $10Dq$ has a value of approximately 9000 cm^{-1} and so in order to minimise the computation time it is assumed that there is no appreciable mixing of the t_{2g} and e_g orbitals. Hence a 25×25 matrix may be truncated to a 15×15 matrix. This truncation had no adverse effects on the results obtained by Sams and Tsin (84).

For the trigonally distorted complexes the basis set of $15 t_{2g}$ wavefunctions used was:

$$|2,0\rangle \quad |M_S\rangle$$

$$(2/3)^{1/2} |2,\pm 2\rangle \mp (1/3)^{1/2} |2,\mp 1\rangle \quad |M_S\rangle$$

where in the $|L, M_L\rangle \quad |M_S\rangle$ notation, M_L is the z-component of the total orbital angular momentum, L , and M_S is the z-component of the spin angular momentum which can take values of 0, ± 1 , ± 2 .

The quantities D_S/λ , D_T/λ and D_O/λ were treated as independent parameters which were read into the computer. The matrix was diagonalised to obtain the eigenvalues, ϵ_i/λ and corresponding eigenvectors, $|i\rangle$, which were then used to calculate the quadrupole splittings.

The contributions to the nine components V_{ij} of the E.F.G. tensor were calculated for each eigenvector $|i\rangle$, and the ensemble averages formed:

$$Z^{-1} \sum_{i=1}^{15} \langle i | V_{ij} / e | i \rangle \exp(-\epsilon_i/kT) \quad (6.11)$$

where $Z = \sum \exp(-\epsilon_i/kT)$ is the partition function. The E.F.G. matrix was diagonalised to obtain the tensor elements in the principal axis system. The quadrupole splitting may be written as:

$$\Delta E_Q = \frac{1}{2} e^2 Q (1-R) \left[q^2 + \frac{1}{3} (\eta q)^2 \right]^{1/2} \quad (6.12)$$

$$= \frac{1}{2} e^2 Q (1-R) \left(\frac{4}{7} \langle r^{-3} \rangle \right) (F_q^2 + \frac{1}{3} F_{\eta q}^2)^{1/2} \quad (6.13)$$

where $(1-R)$ is the Sternheimer correction for core polarisation and F_q and F_{nq} are given in terms of the principal components of the E.F.G. tensor from reference 82. The quantity $4/7 e^2 Q(1-R)\langle r^{-3} \rangle$ has been estimated to have a numerical value of 4.5 mm s^{-1} (85), whence:

$$\Delta E_Q = 4.5 (F_q^2 + 1/3 F_{nq}^2)^{1/2} \text{ mm s}^{-1} \quad (6.14)$$

Various values of the parameters D_s , D_r , D_σ and λ were used to generate plots of ΔE_Q as a function of temperature. The parameters obtained to generate the solid lines in Fig. 6.6 are given in Table 6.4.

Since the crystal-field treatment that has been employed here is only approximate, the derived parameters should be viewed accordingly. However, several comments on the results shown in Table 6.4 are relevant here. Firstly, the magnitude of the axial field, as measured by $3D_s$, is very similar for $\text{Fe}(\text{CF}_3\text{SO}_3)_2$ and $\text{Fe}(\text{p-CH}_3\text{C}_6\text{H}_4\text{SO}_3)_2$, 320 and 300 cm^{-1} respectively and is comparable to $\text{Fe}(\text{FSO}_3)_2$ but considerably smaller for $\beta\text{-Fe}(\text{CH}_3\text{SO}_3)_2$, a value of only 160 cm^{-1} . The axial field produced in the trigonally compressed $\alpha\text{-Fe}(\text{CH}_3\text{SO}_3)_2$ species is considerably larger and may be a function of ligand geometry in the α -isomer.

Secondly, the values of λ , the spin-orbit coupling constant, are approximately 80-90% of the free-ion value ($\lambda_0 = -103 \text{ cm}^{-1}$), suggesting a slight delocalisation of the 3d electrons towards the ligands.

TABLE 6.4 CRYSTAL-FIELD SPLITTING PARAMETERS DERIVED
FROM QUADRUPOLE SPLITTING DATA

COMPOUND	$3D_S (\text{cm}^{-1})$	$\lambda (\text{cm}^{-1})$	$D_\sigma (\text{cm}^{-1})$	$D_r (\text{cm}^{-1})$
$\text{Fe}(\text{FSO}_3)_2^*$	288	-90	22	0
$\text{Fe}(\text{CF}_3\text{SO}_3)_2$	320	-80	20	0
$\alpha\text{-Fe}(\text{CH}_3\text{SO}_3)_2$	510	-100	25	0
$\beta\text{-Fe}(\text{CH}_3\text{SO}_3)_2$	160	-80	16	0
$\text{Fe}(\text{p-CH}_3\text{C}_6\text{H}_4\text{SO}_3)_2$	300	-80	24	0

*Reference 15

As stated previously the temperature dependence of ΔE_Q in the low temperature region can only be reproduced when the spin-spin coupling parameter is included. The values of D_σ obtained here are similar to those obtained for other transition metal complexes from e.s.r. measurements (86) and from previous use of this model (84). At the present moment it is not understood why $\beta\text{-Fe}(\text{CH}_3\text{SO}_3)_2$, the compound which shows magnetic exchange between iron centres, has the lowest value of D_σ for the compounds studied. Although it must be noted here that the theoretical fit for the ΔE_Q against temperature data is the least satisfactory for this compound.

It is interesting to compare the parameters obtained from the temperature dependence of the quadrupole splittings with those derived from the Figgis and Lewis model. The relevant parameters are contained in Tables 5.5 and 6.4. Both $3D_S$, which is equal to Δ in the Figgis and Lewis model, and λ are quite similar as derived from the two methods, with the exception of the axial distortion in $\text{Fe}(\text{CF}_3\text{SO}_3)_2$. As noted in section 5.7.1 this is probably due to the rather small temperature dependence of the magnetic moment data and the lack of any such data below 80K.

CHAPTER 7

MAGNETICALLY-PERTURBED ^{57}Fe MOSSBAUER SPECTRA

7.1 INTRODUCTION

^{57}Fe Mossbauer spectra have been recorded at 2.4 and 4.2K in longitudinally applied magnetic fields of up to 5.6T. The spectra obtained for these paramagnetic iron(II) complexes are complicated but a theoretical analysis of the data has enabled a great deal of information to be deduced about the electronic environment of the iron nucleus. This type of information is usually not available from e.s.r. measurements.

The compounds $\text{Fe}(\text{XSO}_3)_2$, where X is CF_3 , $\alpha\text{-CH}_3$, $\beta\text{-CH}_3$ and $p\text{-CH}_3\text{C}_6\text{H}_4$ have been studied and they exhibit a surprising diversity of behaviour at low temperatures and in applied magnetic fields.

Section 7.2 will discuss $\text{Fe}(p\text{-CH}_3\text{C}_6\text{H}_4\text{SO}_3)_2$ and the successful analysis of the observed spectra using a spin Hamiltonian model. The experimental spectra were compared with computed spectra generated by a programme written by A.R. Hulme which was based upon one by Lang (34). The computer analysis was performed by J.R. Sams. In the case of $\text{Fe}(\text{CF}_3\text{SO}_3)_2$ this model has yet to provide a complete analysis but some general observations may be made (section 7.3). Sections 7.4 and 7.5 are

concerned with the α - and β -forms of $\text{Fe}(\text{CH}_3\text{SO}_3)_2$. Section 7.4 discusses the α -isomer and the model proposed by Varret (34) is used to treat the observed spectra. The β -isomer undergoes an antiferromagnetic phase transition at $\sim 23\text{K}$ and this will be the topic of section 7.5.

7.2. MAGNETICALLY-PERTURBED ^{57}Fe MOSSBAUER SPECTRA OF $\text{Fe}(\text{p-CH}_3\text{C}_6\text{H}_4\text{SO}_3)_2$

^{57}Fe Mossbauer spectra have been recorded in applied magnetic fields of up to 5.6T at temperatures of 2.4 and 4.2K and are illustrated in Figs. 7.1 and 7.2 respectively. At these temperatures in the absence of an applied magnetic field the ^{57}Fe Mossbauer spectra remain, within experimental error, symmetric quadrupole doublets with no evidence for line broadening.

The general features of the ^{57}Fe Mossbauer spectra as the applied magnetic field is increased may be qualitatively described as follows. In Fig. 7.1 a comparison of the 1.13T spectrum with the spectrum obtained in zero field shows that the effect of this small applied field is to broaden the low velocity line, whilst the high velocity line splits into a doublet. This is indicative of a positive value for V_{zz} and that the z-axis of the E.F.G. and the internal magnetic field are parallel. The ^{57}Fe Mossbauer spectra obtained at higher magnetic field strengths are more complex and show substantial magnetic splittings. The spectra in these larger magnetic fields may best be described as consisting of a six-line

FIG. 7.1 MAGNETICALLY-PERTURBED ^{57}Fe MOSSBAUER SPECTRA OF
 $\text{Fe}(\text{p-CH}_3\text{C}_6\text{H}_4\text{SO}_3)_2$ AT 2.4K

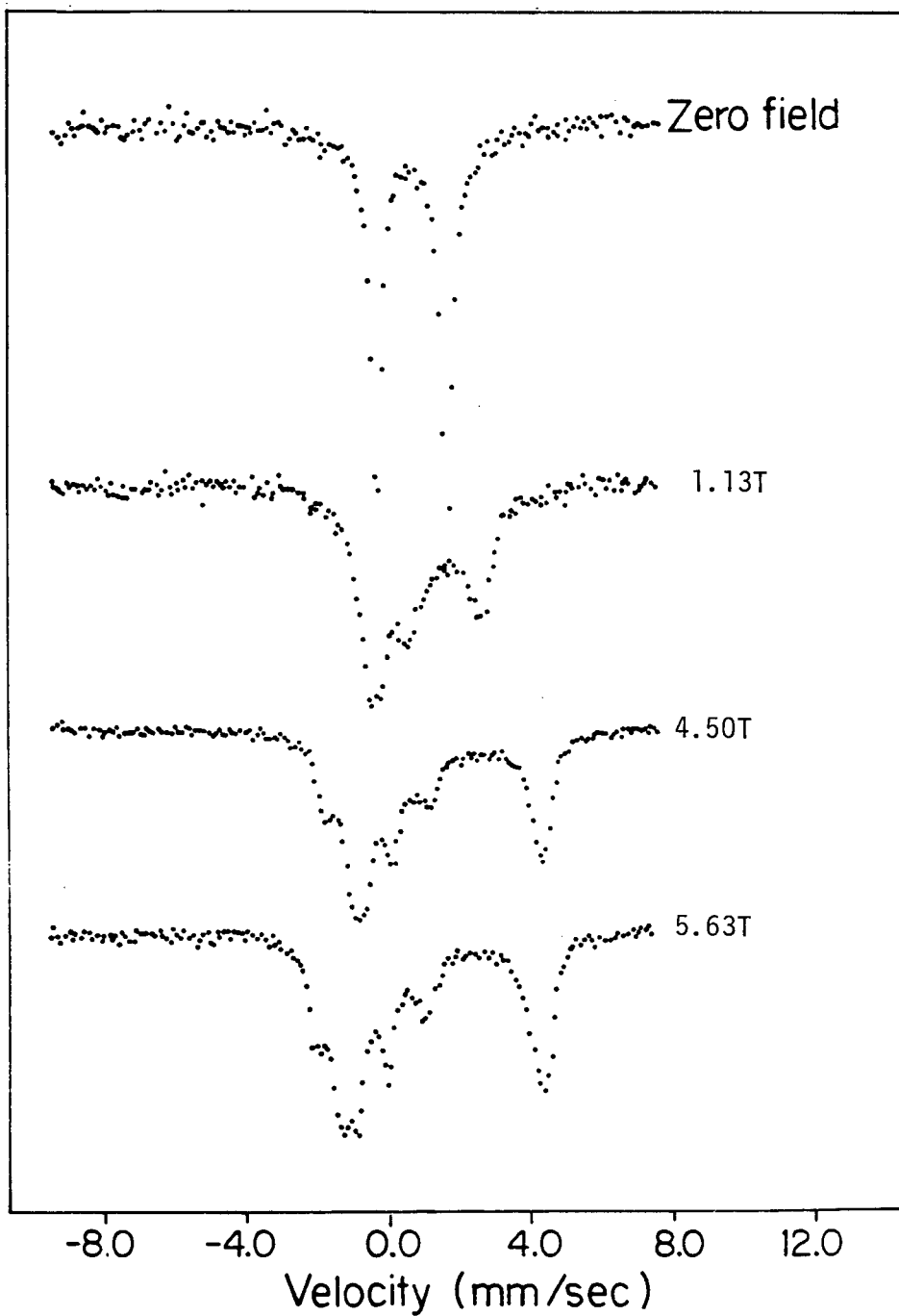
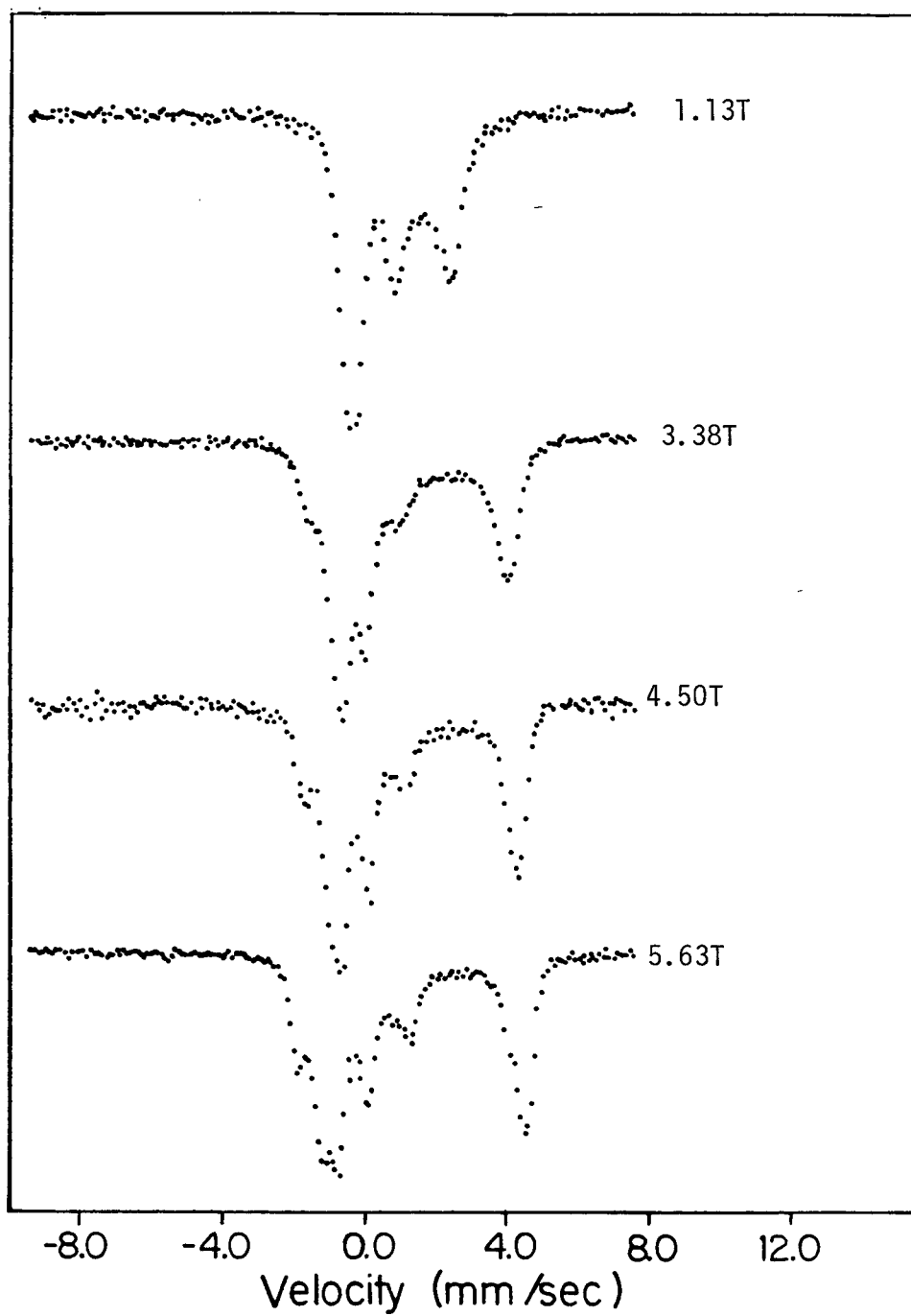


FIG. 7.2

MAGNETICALLY-PERTURBED MOSSBAUER SPECTRA OF
 $\text{Fe}(\text{p-CH}_3\text{C}_6\text{H}_4\text{SO}_3)_2$ AT 4.2K



pattern with the four inner lines shifted to lower energy by a positive quadrupole interaction.

At 4.2K in applied magnetic fields greater than $\sim 3T$ the overall magnetic splitting appears to change only as a function of the applied field, indicating that the internal magnetic hyperfine field has been saturated under these conditions.

7.2.1 Determination of the sign of e^2qQ

For a paramagnetic complex such as $\text{Fe}(\text{p-CH}_3\text{C}_6\text{H}_4\text{SO}_3)_2$ there are certain difficulties associated with the usual technique for determining the sign of V_{zz} . For diamagnetic complexes a magnetic-perturbation technique has been used previously (87, 88). At low temperatures where the magnetic susceptibility becomes large the effective magnetic field H_{EFF} , experienced by the iron nucleus may be very different from the applied field H_{APP} . H_{EFF} and H_{APP} may be related thus:

$$H_{\text{EFF}} = H_{\text{APP}} + \langle s \rangle / S H_{\text{INT}}^0 \quad (7.1)$$

where $\langle s \rangle$ is the average value of the total electronic spin and H_{INT}^0 is the saturation value of the internal hyperfine field.

These difficulties may be overcome by maintaining the specimen at elevated temperature so that the magnetisation $\langle s \rangle$ produced by the applied field is negligible and $H_{\text{EFF}} \sim H_{\text{APP}}$. This situation is then similar to that for a diamagnetic complex (88),

where the line of the quadrupole doublet which arises from the $|\pm\frac{1}{2}\rangle_g \rightarrow |\pm\frac{1}{2}\rangle_e$ transition splits into an apparent triplet, and that from the $|\pm\frac{1}{2}\rangle_g \rightarrow |\pm\frac{3}{2}\rangle_e$ splits into a doublet.

A spectrum of $\text{Fe}(\text{p-CH}_3\text{C}_6\text{H}_4\text{SO}_3)_2$ obtained at 298K in an applied magnetic field of 2.82T showed that the triplet was at lower energy relative to the doublet, and hence that e^2qQ is positive in this complex.

7.2.2 The spin Hamiltonian model

This section discusses the analysis of the magnetically-perturbed Mössbauer spectra in terms of a spin Hamiltonian model (89). This model will be discussed here.

In the eigenvalue spectrum, obtainable from the crystal-field parameters, the orbital doublet ground state is well isolated from higher spin-orbit split states and at 4.2K there will be no appreciable mixing of higher terms into the ground doublet. This orbital doublet may then be treated as containing three electrons or a single hole. The latter view is advantageous since one can now treat the system as a pseudo-Kramers doublet by assigning the hole an effective spin $S=\frac{1}{2}$.

A spin Hamiltonian may be used to describe the hyperfine interactions in the presence of an applied magnetic field (62).

$$\mathcal{H} = \beta \cdot \underline{H} \cdot \underline{g} \cdot \underline{\hat{S}} + \underline{\hat{I}} \cdot \underline{A} \cdot \underline{\hat{S}} - g_n \beta_n \underline{\hat{I}} \cdot \underline{H} + \frac{eqV_{zz}}{4\hat{I}(\hat{I}-1)} \left[3\hat{I}_z^2 - \hat{I}(\hat{I}+1) \right] \quad (7.2)$$

where g_n is the nuclear g-factor, β the Bohr magneton and β_n the nuclear magneton. The four terms in 7.2 describe respectively:

(i) the electronic Zeeman interaction between the applied field, H and the electronic spin, S via the g-tensor, (ii) the coupling of the electron spin and the nuclear spin, I via the magnetic hyperfine tensor, A , (iii) the direct nuclear Zeeman interaction and (iv) the interaction of the nuclear quadrupole moment with the E.F.G. at the iron nucleus. This quadrupole interaction assumes a zero value of the asymmetry parameter, η .

To use the Hamiltonian given above to calculate Mossbauer spectra requires the knowledge of the following parameters: (i) the sign and magnitude of the quadrupole coupling constant and the Mossbauer line width (these values can be obtained from the zero field spectrum and the high temperature magnetic perturbation result described in section 7.2.1), (ii) the magnitude and direction of the applied magnetic field, (iii) the three components of the g-tensor, (iv) the three components of the A-tensor and (v) the temperature. Also the isomer shift and an assumption about the spin-relaxation rate (spectra may be calculated in either a fast or slow spin-relaxation limit). In view of the high symmetry around iron in this complex it is assumed that the g , A and E.F.G.

tensors will have the same principal axis system and we may write:

$$g_x = g_y = g_{\perp} \quad ; \quad g_z = g_{\parallel}$$

$$A_x = A_y = A_{\perp} \quad ; \quad A_z = A_{\parallel}$$

" Mossbauer spectra recorded at 2.4 and 4.2K in applied magnetic fields of 3.38, 4.50 and 5.63T have been successfully analysed using one set of parameter values. The parameters are listed in Table 7.1 and the experimental and computed spectra (solid lines) are illustrated in Figs. 7.3 - 7.5. All theoretical spectra were computed assuming a fast spin-relaxation limit, as poor agreement between experimental and theoretical spectra were obtained assuming a slow relaxation rate, especially in small applied magnetic fields. A fast relaxation rate was also indicated by the symmetric quadrupole doublet observed in zero field.

As can be seen from Table 7.1 the g-values employed are highly anisotropic. This is as predicted by Griffith (62) and indicates that the effective hyperfine field of the ground doublet is parallel to the trigonal z-axis with only a very small spin density in the perpendicular direction.

As a consequence of the large g_{\parallel} value the theoretical spectra are extremely sensitive to the value of A_{\parallel} . This is the parameter largely responsible for determining the overall width of the spectrum. A value of -1.79 mm s^{-1} for A_{\parallel} gives

TABLE 7.1 MAGNETICALLY-PERTURBED MOSSBAUER SPECTRALPARAMETERS FOR $\text{Fe}(\text{p-CH}_3\text{C}_6\text{H}_4\text{SO}_3)_2$

H_{APP} (T)	TEMP (K)	Γ (mm s^{-1})	g_{\perp}	g_{\parallel}	A_{\perp} (mm s^{-1})	A_{\parallel} (mm s^{-1})
5.63	2.4	0.35	1	9	2.05	-1.79
5.63	4.2	0.30	1	9	2.05	-1.79
4.50	2.4	0.35	1	9	2.05	-1.79
4.50	4.2	0.25	1	9	2.05	-1.79
3.38	4.2	0.25	1	9	2.05	-1.79
1.13	4.2	0.30	1	9	2.05	-1.18

For all spectra axial symmetry was assumed, $\eta=0$

$$g_x = g_y = g_{\perp} \quad ; \quad g_z = g_{\parallel}$$

$$A_x = A_y = A_{\perp} \quad ; \quad A_z = A_{\parallel}$$

$$\Delta E_Q = 1.98 \text{ mm s}^{-1} \quad ; \quad \delta = 1.35 \text{ mm s}^{-1}$$

FIG. 7.3 COMPARISON OF COMPUTED AND EXPERIMENTAL SPECTRA FOR
 $\text{Fe}(\text{p-CH}_3\text{C}_6\text{H}_4\text{SO}_3)_2$ AT 2.4 AND 4.2K IN AN APPLIED MAGNETIC
FIELD OF 5.63T

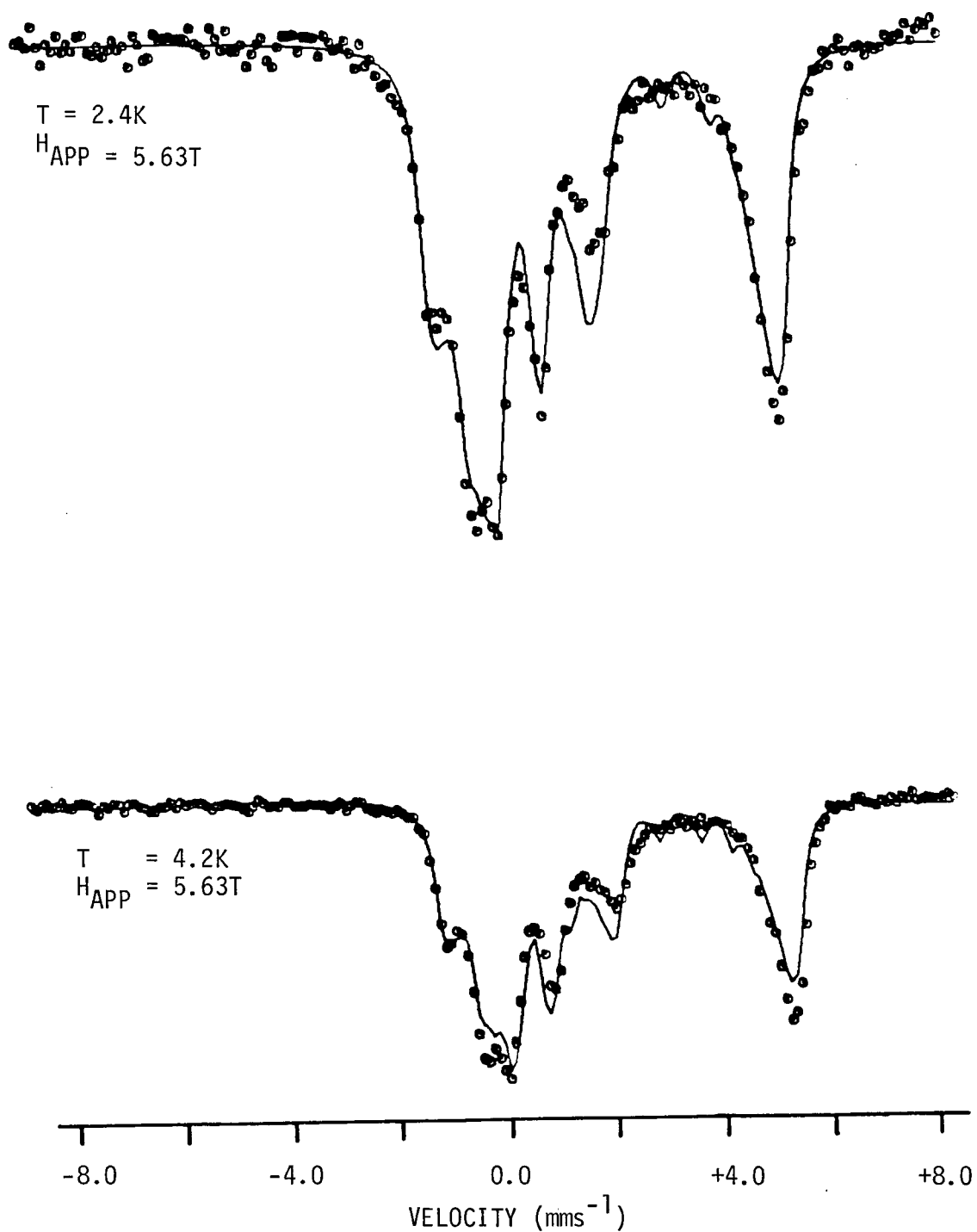


FIG. 7.4 COMPARISON OF COMPUTED AND EXPERIMENTAL SPECTRA FOR
 $\text{Fe}(\text{p-CH}_3\text{C}_6\text{H}_4\text{SO}_3)_2$ AT 2.4 AND 4.2K IN AN APPLIED
MAGNETIC FIELD OF 4.50T

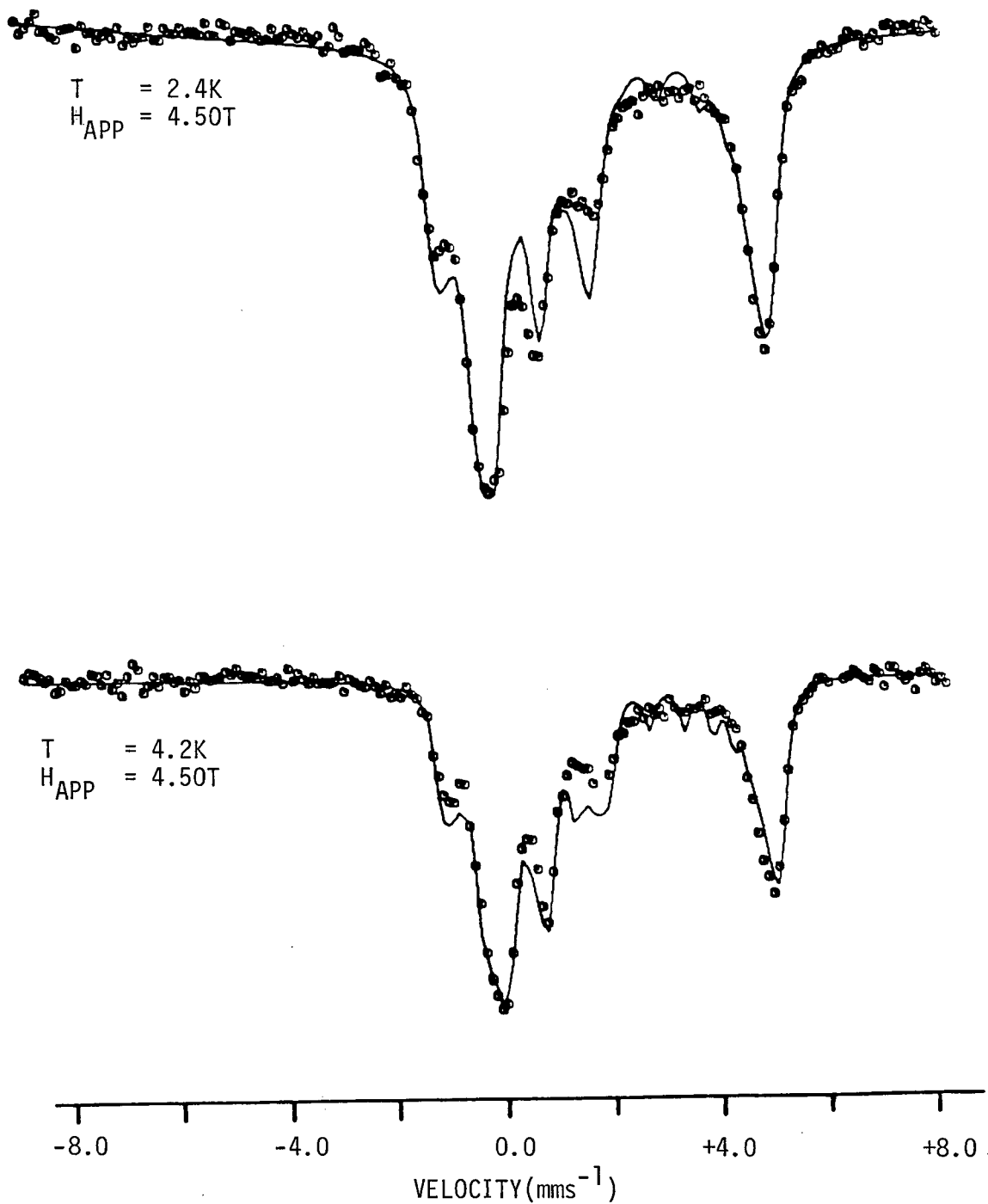
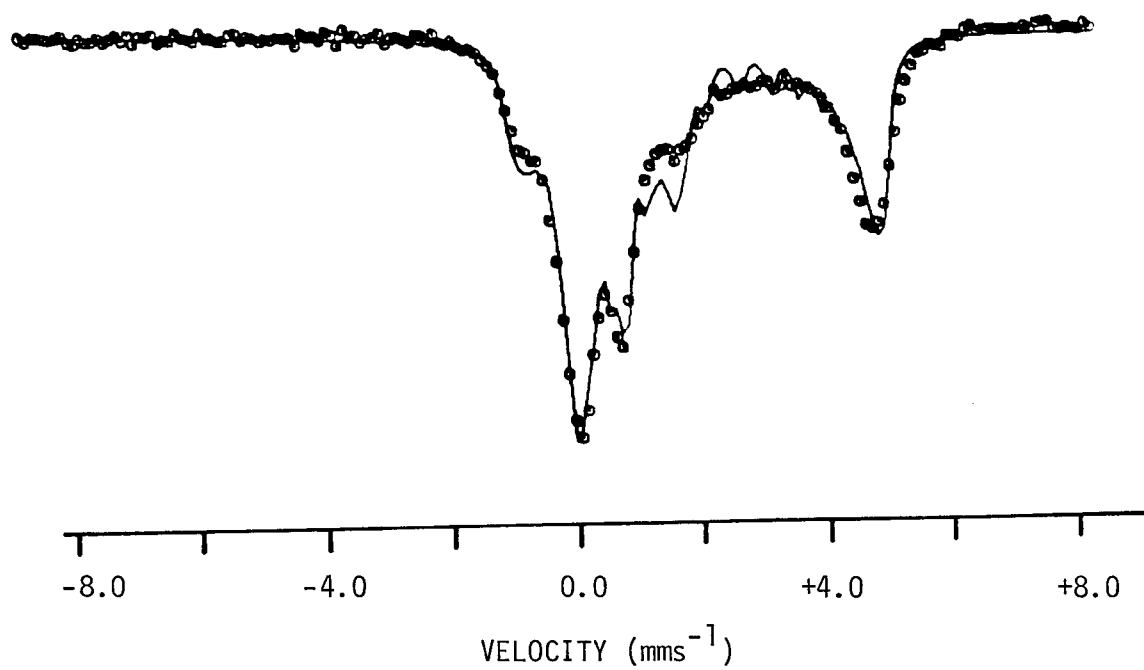


FIG. 7.5 COMPARISON OF COMPUTED AND EXPERIMENTAL SPECTRA
FOR $\text{Fe}(\text{p-CH}_3\text{C}_6\text{H}_4\text{SO}_3)_2$ AT 4.2K IN AN APPLIED MAGNETIC
FIELD OF 3.38T



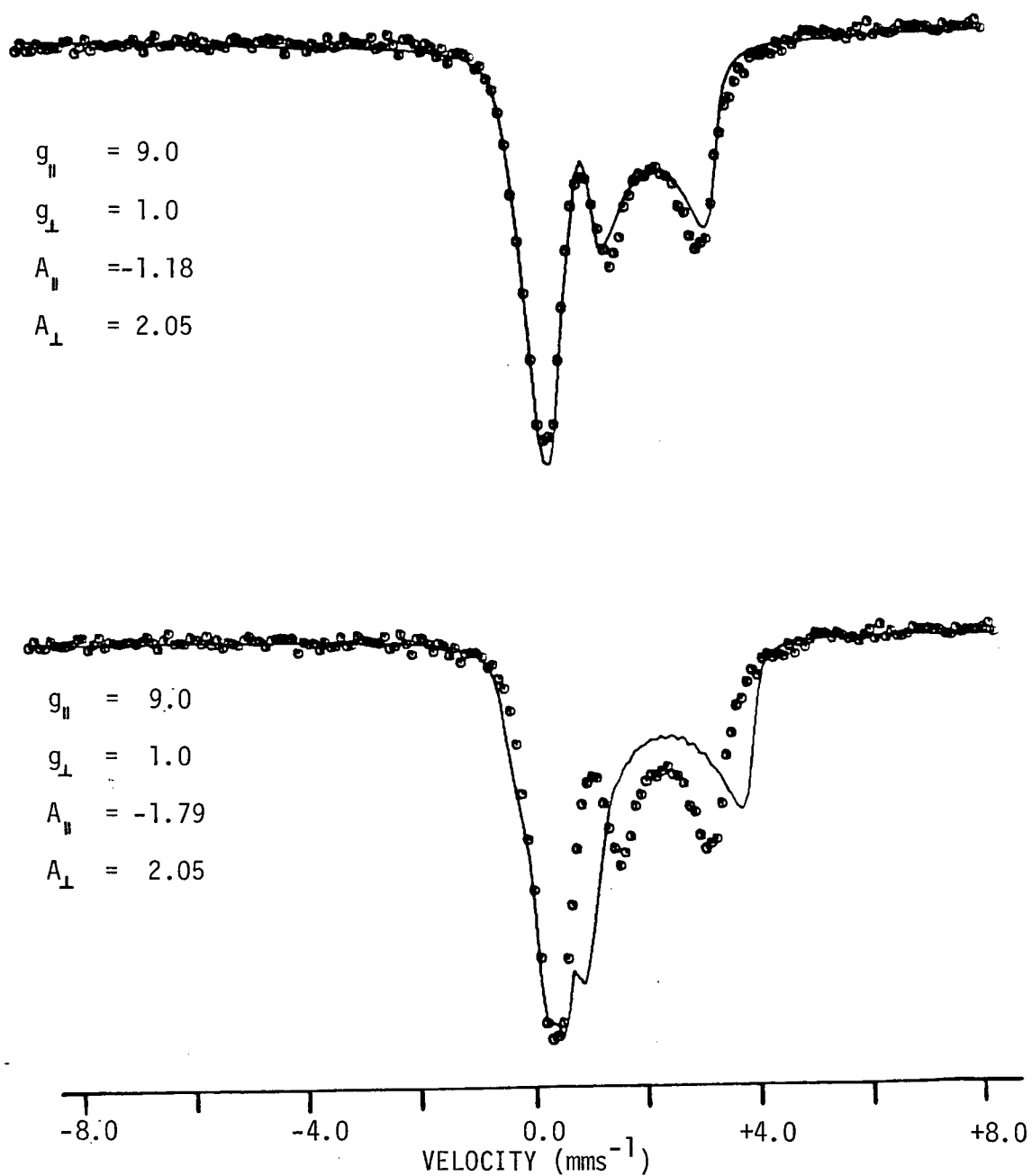
reasonable fits; this is equivalent to a field of 13.0T. The computed spectra are less sensitive to the value of A_{\perp} and a value of 2.05 mm s^{-1} fits the spectra satisfactorily.

Attempts to fit the spectrum of $\text{Fe}(\text{p-CH}_3\text{C}_6\text{H}_4\text{SO}_3)_2$ at a temperature of 4.2K in an applied magnetic field of 1.13T are shown in Fig. 7.6. The lower spectrum employs the parameters used to analyse the high field spectra (3.38, 4.50 and 5.60T). As can be seen these parameters give an unsatisfactory reproduction of the experimental spectrum. However, an excellent fit may be achieved by reducing the magnitude of A_{\parallel} to -1.18 mm s^{-1} (8.6T). This indicates that the internal hyperfine field has not reached saturation under these experimental conditions.

Hence, to obtain meaningful parameters from such spectra it is important to ensure that the applied magnetic field (or value of H/T) is large enough so that the internal fields are saturated. When the internal hyperfine fields are saturated a unique set of values may be defined to describe the g - and A tensors.

The previously reported (89) g - and A parameters of $\text{Fe}(\text{C}_5\text{H}_5\text{NO})_6 (\text{ClO}_4)_2$ are very similar to those obtained in this analysis of $\text{Fe}(\text{p-CH}_3\text{C}_6\text{H}_4\text{SO}_3)_2$. This may be rationalised on the basis of the environment around the iron nucleus. Both compounds consist of trigonally elongated FeO_6 octahedra with orbital doublet ground states and similar crystal-field splitting parameters.

FIG. 7.6 COMPARISON OF COMPUTED AND EXPERIMENTAL SPECTRA FOR
 $\text{Fe}(\text{p-CH}_3\text{C}_6\text{H}_4\text{SO}_3)_2$ AT 4.2K IN AN APPLIED MAGNETIC FIELD OF
1.13T



However, $\text{Fe}(\text{C}_5\text{H}_5\text{NO})_6 (\text{ClO}_4)_2$ was shown to have a slow spin-lattice relaxation rate which is not the case for $\text{Fe}(\text{p-CH}_3\text{C}_6\text{H}_4\text{SO}_3)_2$. These differences in spin-lattice relaxation rates are probably related to the differences which may be envisaged for the solid-state structure of these compounds. Whereas the proposed structure of $\text{Fe}(\text{p-CH}_3\text{C}_6\text{H}_4\text{SO}_3)_2$ consists of a polymeric lattice in which layers of iron(II) cations are sandwiched by layers of anions; $\text{Fe}(\text{C}_5\text{H}_5\text{NO})_6 (\text{ClO}_4)_2$ is probably isomorphous to the cobalt(II) analogue, whose single crystal X-ray structure has been determined as containing discrete CoO_6 octahedral cations and noncoordinated ClO_4^- anions (90). The more rigid polymeric lattice in the former compound should increase the spin-lattice relaxation rate.

At the present time $\text{Fe}(\text{FSO}_3)_2$ has only been examined at 4.2K in an applied magnetic field of 5.0T (15). Only two broad poorly resolved absorptions were observed rather than the well defined hyperfine spectra observed for $\text{Fe}(\text{p-CH}_3\text{C}_6\text{H}_4\text{SO}_3)_2$. A more extensive study of $\text{Fe}(\text{FSO}_3)_2$ is necessary before any conclusions and comparisons may be made.

7.3. MAGNETICALLY-PERTURBED ^{57}Fe MOSSBAUER SPECTRA OF $\text{Fe}(\text{CF}_3\text{SO}_3)_2$

^{57}Fe Mossbauer spectra have been recorded in applied magnetic fields of up to 5.6T at a temperature of 4.2K and are illustrated in Fig. 7.7. In comparison to the zero field spectrum of $\text{Fe}(\text{p-CH}_3\text{C}_6\text{H}_4\text{SO}_3)_2$ the $\text{Fe}(\text{CF}_3\text{SO}_3)_2$ compound exhibits asymmetric

FIG. 7.7 MAGNETICALLY-PERTURBED MÖSSBAUER SPECTRA OF
 $\text{Fe}(\text{CF}_3\text{SO}_3)_2$ AT 4.2K

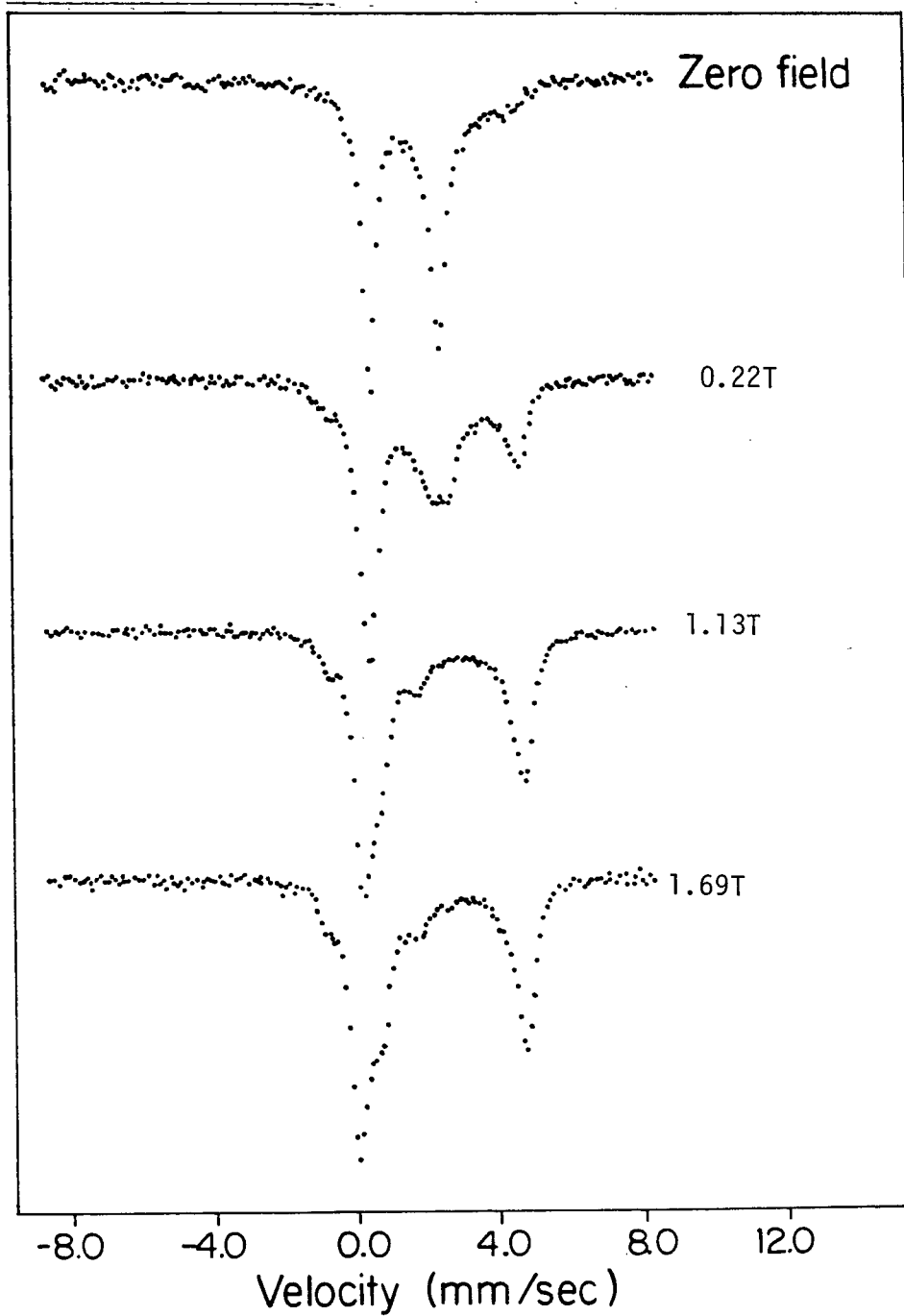
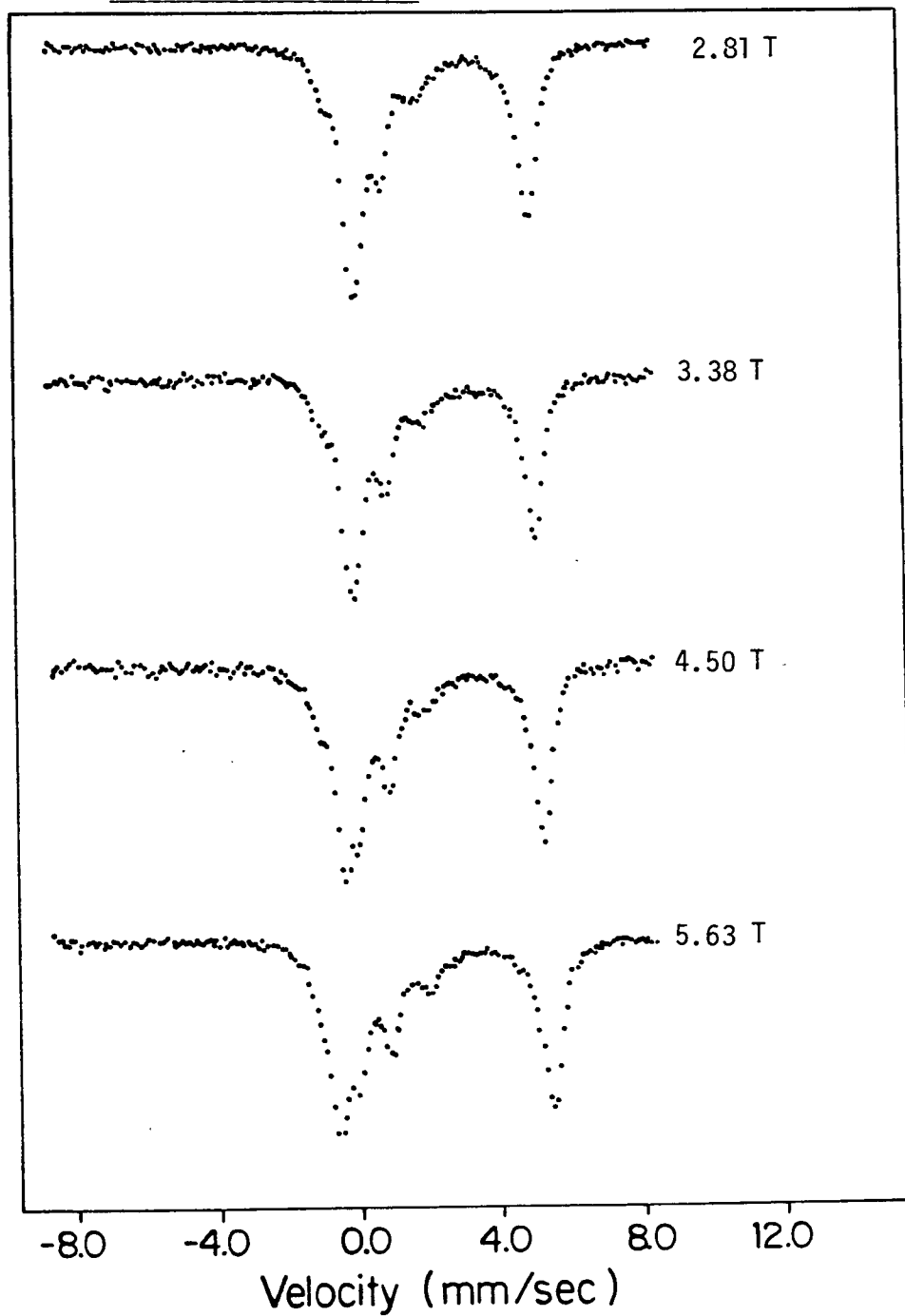


FIG. 7.7 - Contd. MAGNETICALLY-PERTURBED ^{57}Fe MOSSBAUER SPECTRA OF $\text{Fe}(\text{CF}_3\text{SO}_3)_2$ AT 4.2K



line broadening at 4.2K and there is evidence for some magnetic hyperfine structure as illustrated by the weak absorption around 5 mm s^{-1} . As the magnetic field is increased two observations may be made, (i) at 0.22T the low velocity quadrupole split line appears to broaden, whereas the high velocity line seems to be splitting into a doublet, and (ii) the weak line observed at high velocity in the zero field spectrum has gained in intensity.

These observations may indicate the possibility of two different spin-relaxation rates in this compound. This phenomenon has been proposed to explain the behaviour of $\text{Fe}(\text{C}_5\text{H}_5\text{NO})_6 (\text{ClO}_4)_2$ (89). The weak absorption at high velocity coming from a slow spin relaxation rate while the remainder of the spectrum results from a somewhat faster spin-relaxation rate.

As the applied magnetic field is increased the high velocity line intensifies and the overall width of the spectrum only appears to be a function of the applied magnetic field. Thus in $\text{Fe}(\text{CF}_3\text{SO}_3)_2$ the internal hyperfine field becomes fully saturated at very low applied magnetic field strength.

The line broadening observed in the zero field spectrum may arise through one of several mechanisms: (i) preferential ordering of the crystallites (91). This mechanism may be eliminated as the samples were thoroughly ground prior to use and different samples showed the same asymmetry. This effect should be present at all temperatures which is not the case for $\text{Fe}(\text{CF}_3\text{SO}_3)_2$.

(ii) Slow spin-spin relaxation between Kramers' doublets (92, 93, 94). However, unlike iron(III), iron(II) is not a Kramers' ion and the observed asymmetry should increase with increasing temperature. This possibility can be eliminated.

(iii) Another possible explanation of line broadening is the Gol'danskii Karyagin effect (95, 96) which arises from the anisotropy of the recoil-free fraction but again this phenomenon has a temperature dependence opposite to that observed here.

(iv) The only explanation consistent with the observed spectra is a decrease in the spin-lattice relaxation rate as the temperature decreases (93, 97). The spin-lattice relaxation rate is temperature dependent and decreases with decreasing temperature. It is thought that it is this mechanism which leads to the observed asymmetry and the onset of hyperfine splitting observed in zero field.

This mechanism has been proposed to explain the observed spectra in $\text{Fe}(\text{C}_5\text{H}_5\text{NO})_6 (\text{ClO}_4)_2$ (89), the mineral gillespite, $\text{BaFeSi}_4\text{O}_{10}$ (98, 99), and a tetrakis (1,8-naphthyridine) complex, $\text{Fe}(\text{C}_8\text{H}_6\text{N}_2)(\text{ClO}_4)_2$ (100).

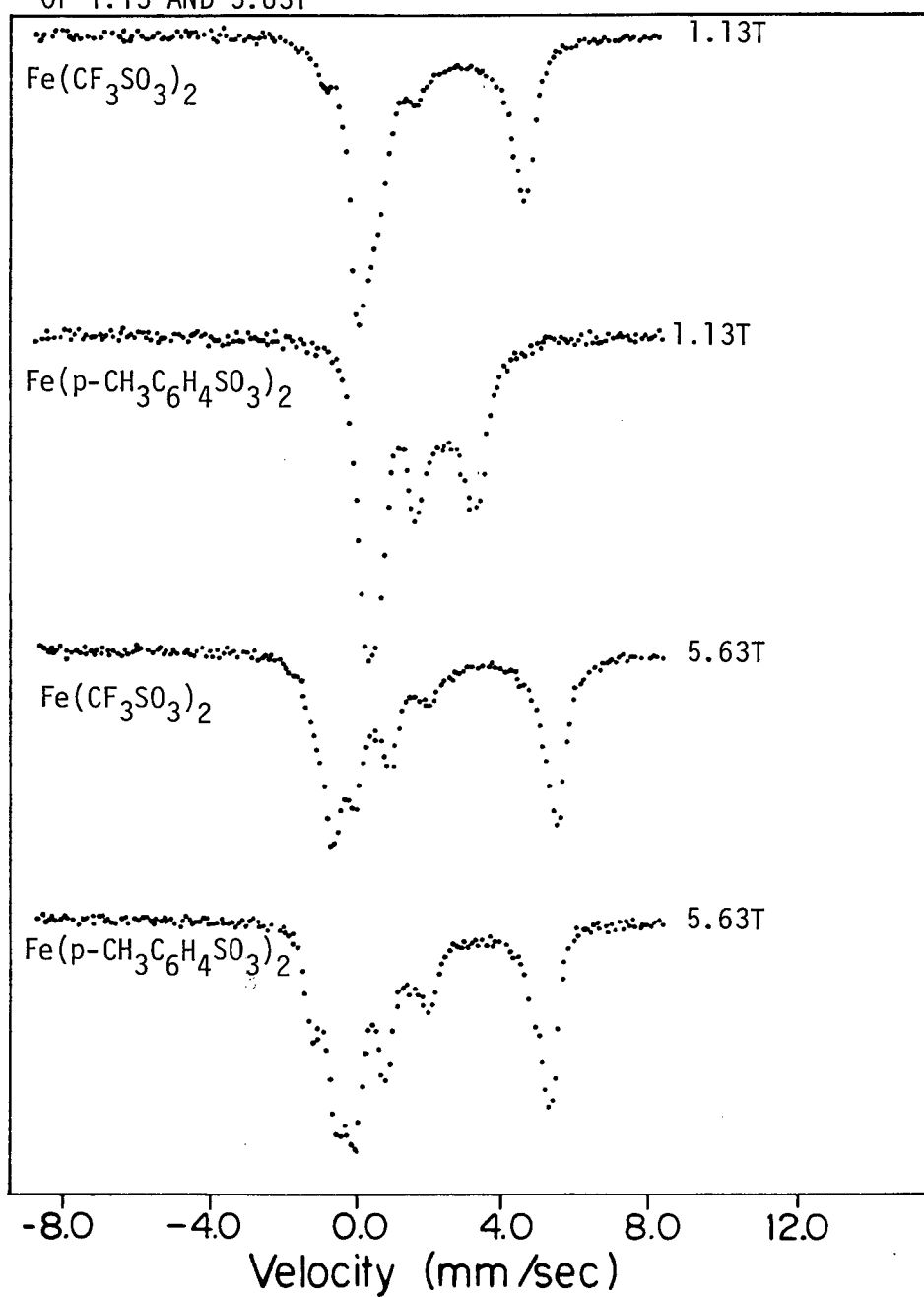
Attempts were made to analyse the experimental spectra obtained in applied magnetic fields using the spin Hamiltonian model which proved successful for $\text{Fe}(\text{p-CH}_3\text{C}_6\text{H}_4\text{SO}_3)_2$. At the present time no detailed parameter values are available due to the model being unable to reproduce some of the features in

the experimental spectra. From Fig. 7.8 it appears that the spectra of $\text{Fe}(\text{CF}_3\text{SO}_3)_2$ and $\text{Fe}(\text{p-CH}_3\text{C}_6\text{H}_4\text{SO}_3)_2$ in a magnetic field of 5.63T are very similar. However, there are some subtle differences especially in relative line intensities. The line at $\sim 2 \text{ mm s}^{-1}$ is less intense in the case of $\text{Fe}(\text{CF}_3\text{SO}_3)_2$ and as can be seen from Fig. 7.3 the fits of the spectra for $\text{Fe}(\text{p-CH}_3\text{C}_6\text{H}_4\text{SO}_3)_2$ compound are poorest in this region.

A few general observations may be made about the qualitative nature of the g- and A- tensors in this compound. Firstly, as in the case of $\text{Fe}(\text{p-CH}_3\text{C}_6\text{H}_4\text{SO}_3)_2$ and $\text{Fe}(\text{C}_5\text{H}_5\text{NO})_6 (\text{ClO}_4)_2$, the g-tensor must be highly anisotropic to reproduce the general features of the experimentally observed spectra.. Secondly, looking at Fig. 7.8 it may be observed that the overall magnetic splitting in $\text{Fe}(\text{CF}_3\text{SO}_3)_2$ is $\sim 15\%$ greater than in the case of $\text{Fe}(\text{p-CH}_3\text{C}_6\text{H}_4\text{SO}_3)_2$. This will be reflected in a higher value for A_{\parallel} . One can also say that $A_{\parallel} < 0$ and $A_{\perp} > 0$.

At the present time it is not fully understood why these spectra cannot be analysed using the spin Hamiltonian model. However, the model implicitly assumes no orbital angular momentum and this may not be the case here.

FIG. 7.8 COMPARISON OF MOSSBAUER SPECTRA OF $\text{Fe}(\text{CF}_3\text{SO}_3)_2$ AND $\text{Fe}(\text{p-CH}_3\text{C}_6\text{H}_4\text{SO}_3)_2$ AT 4.2K IN APPLIED MAGNETIC FIELDS OF 1.13 AND 5.63T



7.4 MAGNETICALLY-PERTURBED ^{57}Fe MOSSBAUER SPECTRA OF $\alpha\text{-Fe}(\text{CH}_3\text{SO}_3)_2$

^{57}Fe Mossbauer spectra have been recorded in applied magnetic fields of up to 5.6T at a temperature of 4.2K (101). At 4.2K in the absence of an applied magnetic field a symmetric quadrupole doublet is observed. This observation is typical of high-spin iron(II) acting as a fast relaxing paramagnet and is comparable to the previously discussed case of $\text{Fe}(\text{p-CH}_3\text{C}_6\text{H}_4\text{SO}_3)_2$ (section 7.2).

At 4.2K the application of a magnetic field of 1.1T serves only to broaden the spectral lines. However, in applied magnetic fields of 4.50 and 5.63T a doublet-triplet pattern is produced (Fig. 7.10). The triplet is at higher energy relative to the doublet, indicating that V_{zz} , the principle component of the E.F.G. tensor, is negative. This method of determining the sign of V_{zz} for a polycrystalline sample has been discussed previously (102,103) and in section 7.2.1. Thus the ground state in this isomer is the $|z^2\rangle$ orbital and the distortion from octahedral symmetry corresponds to a compression along the trigonal FeO_6 axis. These results are similar to those observed in the case of $\text{Fe}(\text{H}_2\text{O})_6 \text{SiF}_6$, where the iron cation is surrounded by a trigonally compressed octahedron of water molecules (104).

Attempts were made to analyse the observed spectra assuming isotropic magnetic interactions. However, the ^5D free-ion term for high-spin iron(II) results in highly anisotropic magnetic properties (105) and as can be seen from Fig. 7.9 fits

FIG. 7.9 COMPARISON OF COMPUTED AND EXPERIMENTAL SPECTRA
FOR $\alpha\text{-Fe}(\text{CH}_3\text{SO}_3)_2$ RECORDED AT 4.50T

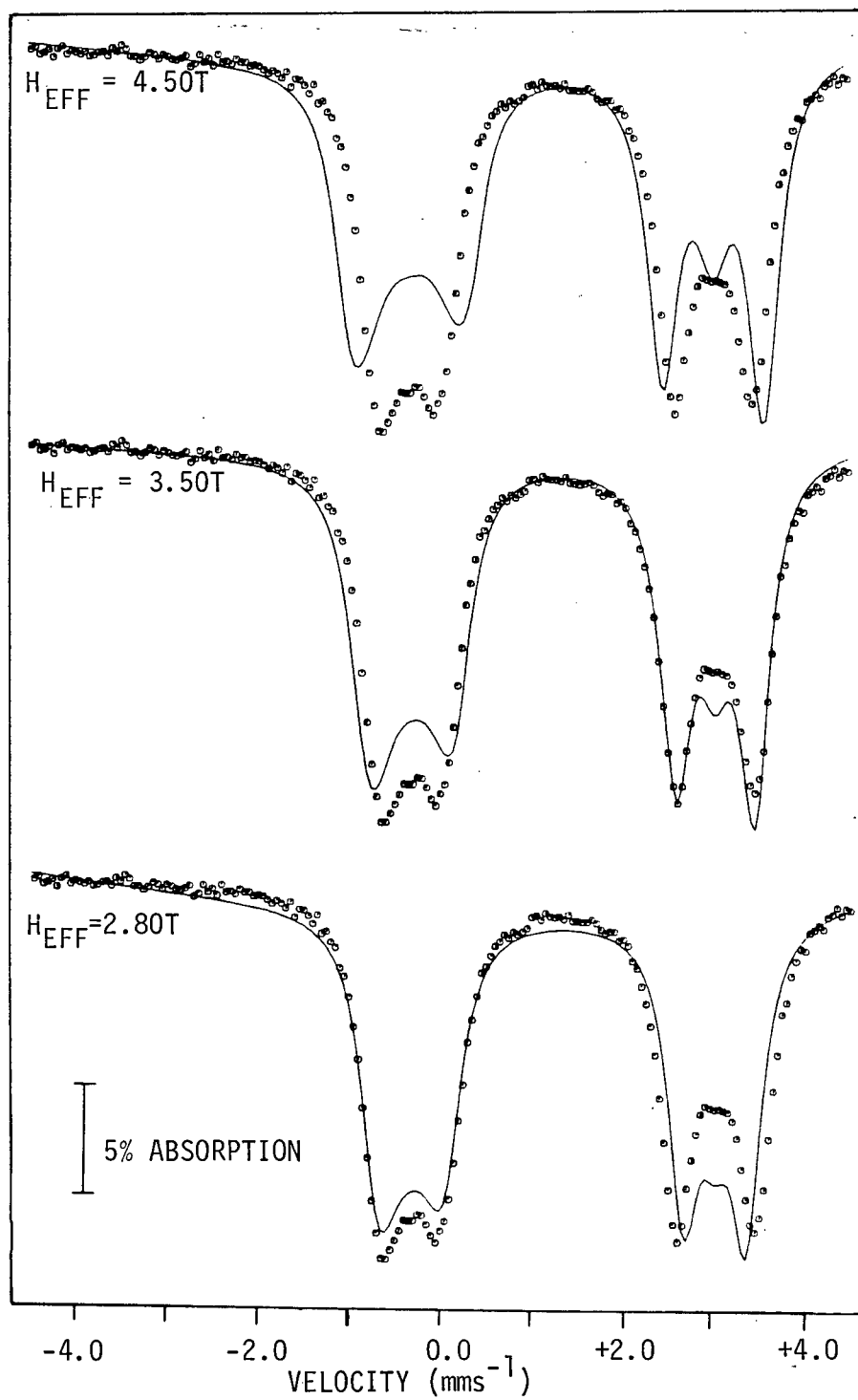
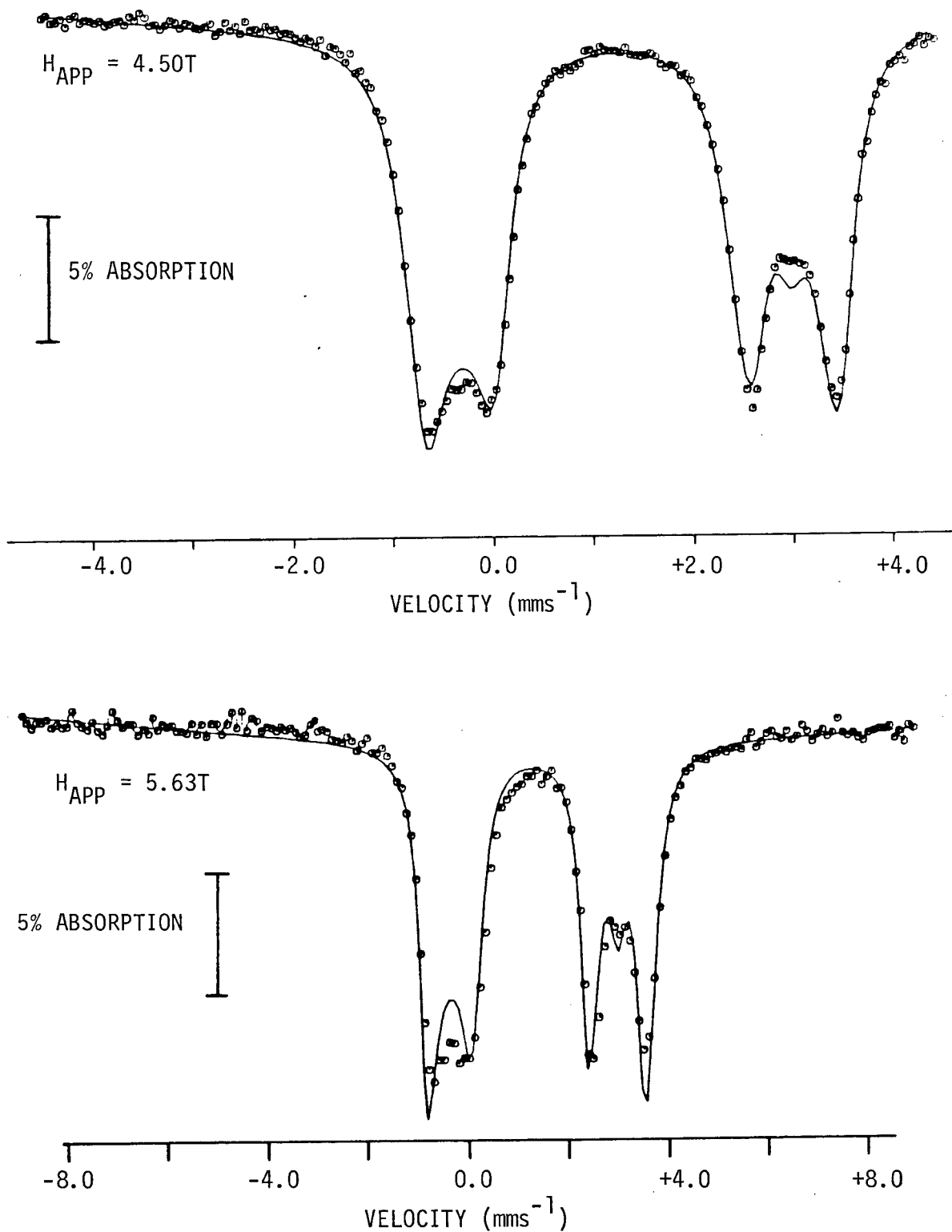


FIG. 7.10 ⁵⁷MOSSBAUER OF $\alpha\text{-Fe}(\text{CH}_3\text{SO}_3)_2$ AT 4.2K IN APPLIED MAGNETIC FIELDS OF 4.50 AND 5.63T.

Computed Spectra generated by the parameters given in Table 7.1



of computed and experimental spectra are poor using this model. From the top spectrum in Fig. 7.9 it may be seen that the magnetic splitting is less than that assuming $H_{\text{EFF}} = H_{\text{APP}}$. The two lower spectra indicate that the effective field is anisotropic; the width of the triplet may be reproduced assuming an effective field of 3.50T and that of the doublet assuming an effective field of 2.80T.

A more successful treatment of the data has used the phenomenological model of Varret (34) which enables the anisotropy of the hyperfine field to be parameterised in the case of weak magnetisation.

The parameters derived from the analysis of the spectra of $\alpha\text{-Fe}(\text{CH}_3\text{SO}_3)_2$ in applied magnetic fields of 4.50 and 5.63T are given in Table 7.2. Experimental and computed spectra (solid lines) are shown in Fig. 7.10.

A few comments about the parameters in Table 7.2 are relevant. Reasonable fits of experimental and computed spectra may be obtained by assuming a zero value for the asymmetry parameter, η and identical values of H_{IX} and H_{IY} , the internal magnetic fields in the X and Y directions. However, a better agreement may be obtained using a finite value of $\eta \approx 0.3$ and $H_{\text{IX}} \neq H_{\text{IY}}$. This value of η suggests a rhombic distortion in the α -species which is consistent with the infrared spectral data where the anion was shown to have C_s symmetry.

TABLE 7.2

PARAMETERS OBTAINED FROM THE VARRET MODEL

FOR $\alpha\text{-Fe}(\text{CH}_3\text{SO}_3)_2$ AND $\text{Fe}(\text{H}_2\text{O})_6 \text{SiF}_6$

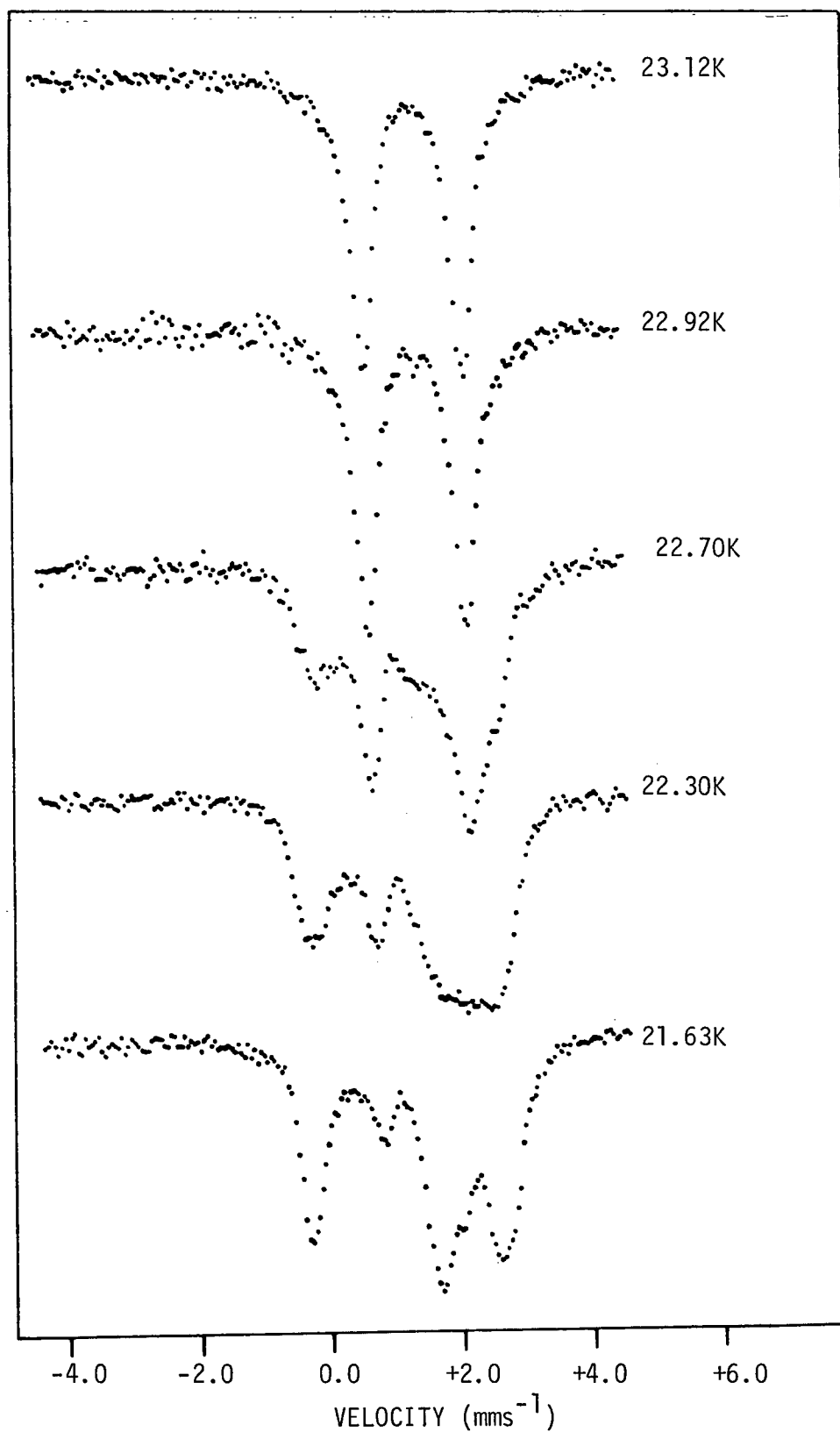
COMPOUND	TEMP (K)	H _{APP} (T)	Γ (mm s ⁻¹)	ΔE_Q (mm s ⁻¹)	η	HIX (T)	HIY (T)	HIZ (T)
$\alpha\text{-Fe}(\text{CH}_3\text{SO}_3)_2$	4.2	4.50	0.40	-3.31	0.30	-1.00	-0.60	-2.00
$\alpha\text{-Fe}(\text{CH}_3\text{SO}_3)_2$	4.2	5.63	0.40	-3.31	0.35	-1.00	-0.60	-2.50
$\text{Fe}(\text{H}_2\text{O})_6 \text{SiF}_6$	3.00	7.5	0.46	-3.35	0.00	-0.60	-0.60	3.30
$\text{Fe}(\text{H}_2\text{O})_6 \text{SiF}_6$	4.2	2.0	0.25	-3.52	0.35	-10.7	-12.3	-7.00

Varret's results for $\text{Fe}(\text{H}_2\text{O})_6 \text{SiF}_6$ (34) indicate that as the temperature was decreased from room temperature to 4.2K the anisotropy of the internal magnetic hyperfine field reversed. This may be due to the large increase in magnetic susceptibility as the temperature is decreased and the highly anisotropic nature of the magnetic interactions. Some parameters obtained by Varret are presented in Table 7.2 along with those for $\alpha\text{-Fe}(\text{CH}_3\text{SO}_3)_2$. From this table it is observed that the values for $\alpha\text{-Fe}(\text{CH}_3\text{SO}_3)_2$ correspond a lot more closely to the high temperature values obtained for $\text{Fe}(\text{H}_2\text{O})_6 \text{SiF}_6$. At high temperatures the magnetic susceptibility of $\text{Fe}(\text{H}_2\text{O})_6 \text{SiF}_6$ is relatively low and even though in the case of $\alpha\text{-Fe}(\text{CH}_3\text{SO}_3)_2$ at low temperatures a high magnetic susceptibility is expected, a proposal of antiferromagnetism in this compound would serve as an effective mechanism for decreasing the susceptibility.

7.5. "MOSSBAUER SPECTRA OF $\beta\text{-Fe}(\text{CH}_3\text{SO}_3)_2$ BELOW 25K

Unlike the Mossbauer spectrum of the α -isomer which remains a quadrupole doublet down to 4.2K, the β -isomer shows a complex spectrum on cooling below ~25K (101). Over a very narrow range of temperature the two line spectrum splits into a complex magnetic hyperfine pattern (see Fig. 7.11). This indicates magnetic ordering of the sample and the observed spectra below the transition temperature are the result of the combined effects of both quadrupole and magnetic interactions. A few tenths of a

FIG. 7.11 ^{57}Fe MOSSBAUER SPECTRA OF $\beta\text{-Fe}(\text{CH}_3\text{SO}_3)_2$ IN THE PROXIMITY
OF THE PHASE TRANSITION TEMPERATURE

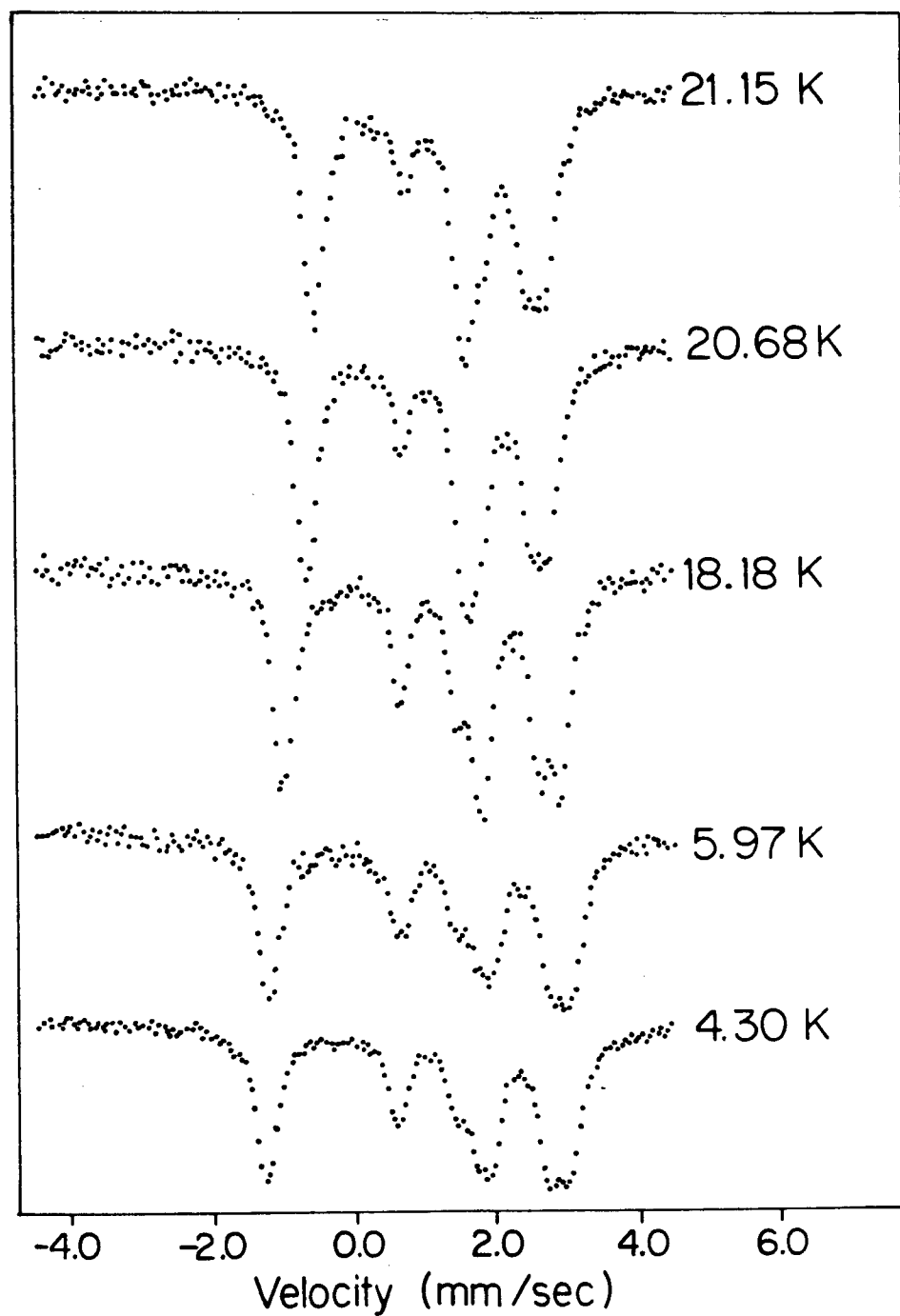


Kelvin degree above the phase transition (e.g. at 22.92K) the spectrum is a sharp quadrupole doublet and as the temperature is lowered (e.g. to 22.70K) one observes the low energy line splitting into an apparent triplet and the high energy line into a doublet (see Fig. 7.11). This splitting of the two lines into a triplet and a doublet is very similar to that observed upon the application of a magnetic field to determine the sign of V_{zz} . At 22.70K this triplet-doublet pattern is observed because at this temperature H_{INT} is small so the magnetic interaction appears as a perturbation of the quadrupole interaction. At lower temperatures where H_{INT} is larger, this situation is reversed and the quadrupole interaction acts as a perturbation on the magnetic interaction. At 22.70K the triplet at low velocity indicates a positive V_{zz} .

The internal magnetic field in $\beta\text{-Fe}(\text{CH}_3\text{SO}_3)_2$ increases with decreasing temperature, and by 18.2K the internal field has reached ~90% of its saturation value of ~14.0T at 4.2K (see Fig. 7.12). Application of a magnetic field of 1.1T at 4.2K only serves to broaden the spectral lines, showing that the observed transition is from a paramagnetic to an antiferromagnetic phase (102,103). This condition results because the applied field simply adds vectorally to a random distribution of internal hyperfine field directions in an anisotropic powder.

The transition is accompanied by a slight hysteresis; upon warming the sample through the transition region, final

FIG. 7.12 MOSSBAUER SPECTRA OF β -Fe(CH₃SO₃)₂ BELOW 21.15 K



collapse of the hyperfine split spectrum to a doublet is not observed below 24.4K.

From the illustrated spectrum at 22.70K (see Fig. 7.11), where the internal field is small, the splitting of the triplet appears first on lowering the temperature; this indicates that the major axis of the internal hyperfine field is perpendicular to the z-axis of the E.F.G., which in this case is also the trigonal z-axis of the FeO_6 chromophore. This suggests that the xy plane is the easy plane of magnetisation and that magnetic ordering takes place within this plane.

CHAPTER 8STUDIES ON IRON(III) SULFONATES8.1. INTRODUCTION

An earlier report suggested the presence of magnetic exchange in the iron(III) sulfonate compound, $\text{Fe}(\text{FSO}_3)_3$ (22). This observation, along with the evidence for magnetic exchange in both forms of iron(II) methanesulfonate, prompted an investigation of several iron(III) sulfonates, $\text{Fe}(\text{CF}_3\text{SO}_3)_3$, $\text{Fe}(\text{CH}_3\text{SO}_3)_3$ and $\text{Fe}(\text{p-CH}_3\text{C}_6\text{H}_4\text{SO}_3)_3$. These three compounds have been synthesised as a part of this study and have been investigated by infrared spectroscopy. Magnetic susceptibility measurements have been recorded between 80 and 310K using a Gouy balance and the field dependence of the magnetic susceptibility was measured at three different magnetic field strengths using a Faraday magnetic balance. Mossbauer spectra have been recorded at two temperatures only (80 and 293K). These preliminary results are now discussed.

8.2. INFRARED SPECTRA OF IRON(III) SULFONATES

Infrared spectral data are given in Table 8.1; assignments are based upon C_{3v} anion symmetry. Significant splitting of the formally doubly degenerate ν_4 and ν_5 modes is observed, consistent with reduction in anion symmetry below C_{3v} . This is of course expected for the iron(III) sulfonates since the stoichiometry of

TABLE 8.1 INFRARED SPECTRAL DATA (cm^{-1}) FOR IRON(III)
SULFONATE COMPOUNDS

C_{3v} ASSIGNMENT FOR ANION	$\text{Fe}(\text{CF}_3\text{SO}_3)_3$	$\text{Fe}(\text{CH}_3\text{SO}_3)_3$	$\text{Fe}(\text{p-CH}_3\text{C}_6\text{H}_4\text{SO}_3)_3$
$\nu_4(\text{E}) \text{SO}_3$ as. str	1230 s 1078 s	1279 s 1050 s.br	1280 s 1030 s
$\nu_1(\text{A}_1) \text{SO}_3$ sym.str.	1014 s	980 sh	1000 s
$\nu_2(\text{A}_1) \text{S-C}$ str.		780 m 760 w	675 m
$\nu_5(\text{E}) \text{SO}_3$ as.def.	635 m 600 w	565 m.sh 530 m	553 s 540 sh
$\nu_3(\text{A}_1) \text{SO}_3$ sym. def.	515 w 505 m	498 m	481 w
$\nu_6(\text{E}) \text{S-C}$ def. and internal vibrations of CF_3 , CH_3 and $\text{p-CH}_3\text{C}_6\text{H}_4$	$\left\{ \begin{array}{l} 1370 \text{ m} \\ 1150 \text{ v.w.} \\ 780 \text{ w} \\ 570 \text{ w} \\ 428 \text{ m} \\ 355 \text{ w} \\ 328 \text{ w} \end{array} \right.$	1340 w.sh 410 m.br. 355 m	1375 w.sh 1112 m.sh 810 s 700 w 420 m.br

$\text{Fe}(\text{XSO}_3)_3$ requires that for an octahedral environment around the iron(III) cation each sulfonate ligand must utilise only two oxygen atoms to coordinate to iron, the third oxygen remaining non-bonding, essentially as $\text{S}=\text{O}$, which accounts for the high frequency of the ν_4 vibration.

A doubling of the ν_2 (A_1) vibration is observed for the $\text{Fe}(\text{CH}_3\text{SO}_3)_3$ compound and this may be caused by non-equivalent anion sites. A doubling of the ν_3 (A_1) vibration is also observed for $\text{Fe}(\text{CF}_3\text{SO}_3)_3$ and may be explained by a similar proposal. There may in fact be structural isomers present in these compounds but this possibility has not yet been explored.

In general the infrared spectra of these iron(III) compounds contain broader, less highly resolved absorptions as compared to those in the corresponding iron(II) compounds.

8.3 MAGNETIC SUSCEPTIBILITIES OF IRON(III) SULFONATES

The magnetic susceptibility results are reported in Tables 8.2 - 8.4 and Fig. 8.1 illustrates the temperature dependence of the magnetic moments for these compounds.

The magnitude of the magnetic moment values indicates that all three compounds are high-spin and thus have a spherically symmetric half-filled d^5 electron configuration. This corresponds to a ${}^6A_{1g}$ ground term for which there should be no reduction of the moment below the spin-only value by spin-orbit coupling with higher ligand field terms. For high-spin iron(III) compounds one expects

TABLE 8.2 MAGNETIC SUSCEPTIBILITY DATA FOR $\text{Fe}(\text{CF}_3\text{SO}_3)_3$

TEMP (K)	$10^6 \chi_A (\text{cm}^3 \text{mol}^{-1})$	$\mu_{\text{EFF}} (\text{B.M.})$
306	13830	5.82
279	14740	5.73
253	16340	5.75
228	17860	5.71
203	19840	5.67
179	22310	5.65
154	25360	5.59
130	29720	5.56
105	35140	5.43
80	42580	5.22

FARADAY RESULTS AT 294K

$\frac{HdH}{dx} (\text{T}^2 \text{cm}^{-1})$	$10^6 \chi_A (\text{cm}^3 \text{mol}^{-1})$	$\mu_{\text{EFF}} (\text{B.M.})$
253	14210	5.78
526	14190	5.77
869	14220	5.78

Diamagnetic corrections $-148 \times 10^{-6} \text{cm}^3 \text{mol}^{-1}$

TABLE 8.3 MAGNETIC SUSCEPTIBILITY DATA FOR $\text{Fe}(\text{CH}_3\text{SO}_3)_3$

TEMP(K)	$10^6 \chi_A (\text{cm}^3 \text{mol}^{-1})$	$\mu_{\text{EFF}} (\text{B.M.})$
303	12530	5.51
280	13670	5.53
255	14950	5.52
232	16400	5.52
208	18190	5.50
182	20400	5.45
149	24450	5.39
124	28470	5.31
101	34010	5.24
84	38570	5.09

FARADAY RESULTS AT 294K

$\frac{HdH}{dx} (\text{T}^2 \text{cm}^{-1})$	$10^6 \chi_A (\text{cm}^3 \text{mol}^{-1})$	$\mu_{\text{EFF}} (\text{B.M.})$
253	12940	5.52
526	12950	5.52
869	13030	5.53

Diamagnetic corrections $-115 \times 10^{-6} \text{ cm}^3 \text{mol}^{-1}$

TABLE 8.4 MAGNETIC SUSCEPTIBILITY DATA FOR $\text{Fe}(\text{p-CH}_3\text{C}_6\text{H}_4\text{SO}_3)_3$

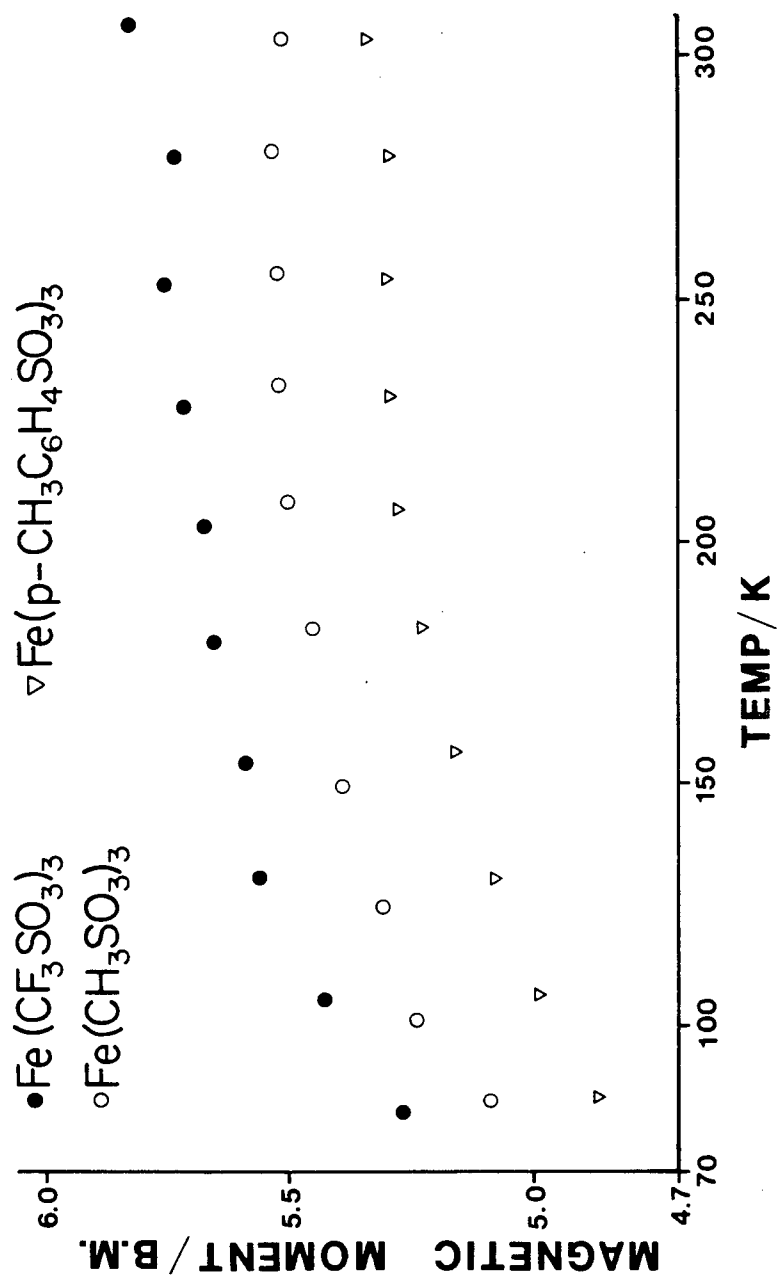
TEMP (K)	$10^6 \chi_A (\text{cm}^3 \text{mol}^{-1})$	$\mu_{\text{EFF}} (\text{B.M.})$
304	11740	5.34
279	12550	5.29
254	13830	5.30
230	15190	5.29
207	16870	5.28
182	18860	5.23
156	21390	5.16
130	24810	5.08
106	29420	4.99
85	34930	4.87

FARADAY RESULTS AT 294K

$\frac{HdH}{dx} (\text{T}^2 \text{cm}^{-1})$	$10^6 \chi_A (\text{cm}^3 \text{mol}^{-1})$	$\mu_{\text{EFF}} (\text{B.M.})$
253	12320	5.30
526	12370	5.31
869	12410	5.32

Diamagnetic corrections - $377 \times 10^{-6} \text{ cm}^3 \text{mol}^{-1}$

FIG 8.1 TEMPERATURE DEPENDENCE OF MAGNETIC MOMENT FOR
 $\text{Fe}(\text{XSO}_3)_3$ COMPOUNDS



a "spin-only" magnetic moment of 5.92 B.M. which should be independent of temperature. However, as can be seen from the experimental data presented here, this is not the case. At room temperature the magnetic moments of the three iron(III) sulfonates are reduced below the "spin-only" value. The absolute magnitude of the magnetic moment decreases in the order $\text{Fe}(\text{CF}_3\text{SO}_3)_3 > \text{Fe}(\text{CH}_3\text{SO}_3)_3 > \text{Fe}(\text{p-CH}_3\text{C}_6\text{H}_4\text{SO}_3)_3$ over the temperature range studied. This decrease in magnetic moment may reflect the order of increasing metal-anion covalency. Also the moments show a pronounced temperature dependence; the moments decreasing monotonically as the temperature decreases.

There are several mechanisms by which the magnetic moment may be reduced below the "spin-only" value and show such a temperature dependence.

(i) A spin crossover situation, in which a high-spin ($t_{2g}^3 e_g^2$) electron configuration goes to a low-spin (t_{2g}^5) electron configuration if the ligand field and electron pairing energies are approximately equal.

(ii) An antiferromagnetic exchange interaction between adjacent iron(III) centres through bridging sulfonate anions.

The presence of greater unpaired electron spin density in a d^5 as opposed to a d^6 electron configuration, and greater effective nuclear charge in iron(III) compared to iron(II), make it more plausible for exchange to take place between iron(III) rather than

iron(II) centres.

Hence case (ii) appears the more likely cause of the low magnetic moments.

All three compounds studied here have magnetic moments which are independent of magnetic field strength. This was not the case for $\text{Fe}(\text{FSO}_3)_3$ where a field dependence is observed and ferromagnetism was proposed (22).

At the present time a detailed analysis of the magnetic moment data for these compounds has not been performed. Preliminary studies using a model proposed by Earnshaw, Figgis and Lewis (106) proved unsuccessful. This model evaluates the magnetic moment as a function of kT/J , where J is the exchange integral, for a linear chain of interacting spins of $S = 5/2$. However the possible structure of iron(III) sulfonates contains bidentate bridging anions, each anion bridging to two different iron(III) cations in a polymeric lattice arrangement, and magnetic exchange may take place in more than one direction through the polymer; a more sophisticated model may have to be applied to analyse the magnetic moment data.

8.4. ⁵⁵MOSSBAUER SPECTROSCOPY OF IRON(III) SULFONATES

Limited ⁵⁵Mossbauer data have been obtained for the iron(III) sulfonate compounds studied and the results are presented in Table 8.5.

TABLE 8.5 ^{57}Fe MOSSBAUER EFFECT DATA FOR IRON(III) SULFONATES

COMPOUND	TEMP (K)	δ (mm s ⁻¹)	ΔE_Q (mm s ⁻¹)	Γ_1 (mm s ⁻¹)	Γ_2 (mm s ⁻¹)
Fe(CF ₃ SO ₃) ₃	293	0.55	0.25	0.78	0.22
	80	0.60	0.33	0.52	0.42
Fe(CH ₃ SO ₃) ₃	293	0.48	0.34	0.49	0.41
	80	0.59	0.36	0.50	0.46
Fe(p-CH ₃ C ₆ H ₄ SO ₃) ₃	293	0.49	0.37	0.57	0.44
	80	0.60	0.39	0.59	0.49

Isomer shift values quoted relative to the centroid of an iron foil spectrum.

All three compounds show similar Mössbauer spectra with respect to isomer shift and quadrupole splitting values. A typical spectrum, that of $\text{Fe}(\text{CH}_3\text{SO}_3)_3$ at 80K, is shown in Fig. 8.2.

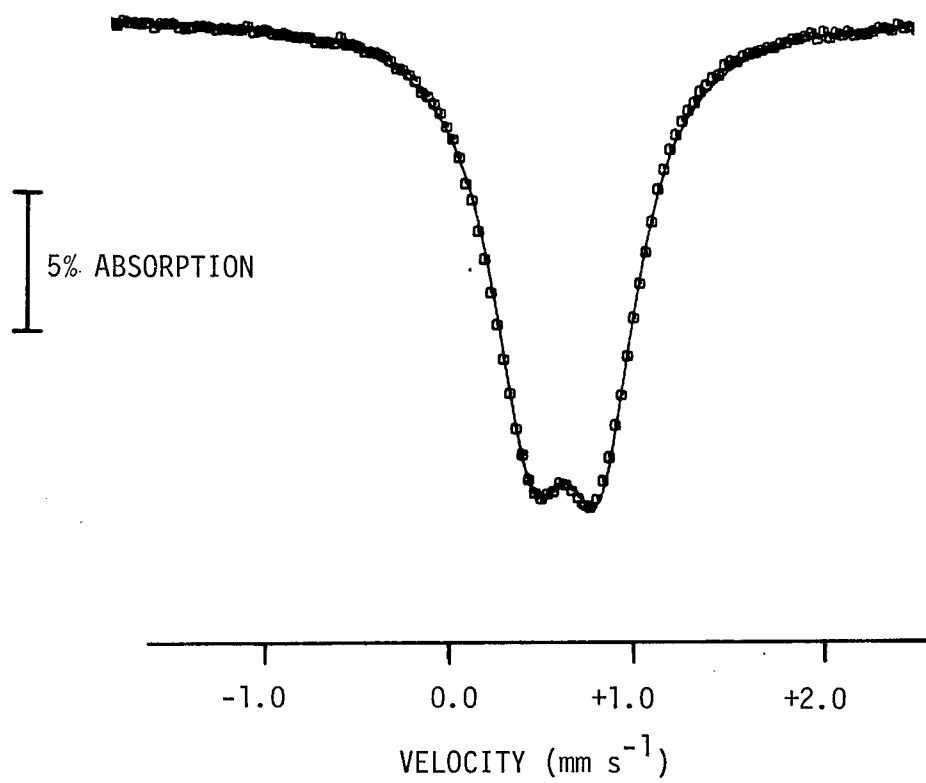
8.4.1. Isomer shift values

The usual range of isomer shift values for high-spin iron(III) is $0.1\text{--}0.6 \text{ mm s}^{-1}$ (71). The values obtained for the iron(III) sulfonates (Table 8.5) all tend to the high side of this range indicating the highly ionic character of these sulfonate compounds. The compounds studied all show comparable values of isomer shift which indicates similar s-electron density in these three compounds and as with the iron(II) sulfonates no correlation can be drawn between isomer shift and anion basicity. The similar isomer shift values indicate that a change in the sulfonate group, with its varying electron withdrawing power, has little effect on the s-electron density at the iron nucleus.

As expected, comparison of isomer shift values of the iron(II) and iron(III) sulfonates shows the iron(II) compounds to exhibit considerably larger values. This is as expected for a d^6 as opposed to a d^5 electron configuration.

The isomer shift values all show a small temperature dependence. This is due to a second-order Doppler effect which is not chemically significant and will not be considered further.

FIG. 8.2 ⁵⁷MOSSBAUER SPECTRUM OF $\text{Fe}(\text{CH}_3\text{SO}_3)_3$ AT 80K



8.4.2. Quadrupole splitting values

No quadrupole splitting is expected for high-spin iron(III) in cubic ligand field environments but as can be seen from Table 8.5 all three compounds studied exhibit a small quadrupole splitting in the range $0.25\text{--}0.39\text{ mm s}^{-1}$. Any valence contribution to the E.F.G. (i.e. unequal electron distributions in either bonding or non-bonding orbitals) is difficult to imagine in the case of a $t_{2g}^3 e_g^2$ electron configuration. A more plausible explanation of this small splitting is a lattice contribution from a non-cubic distribution of lattice charges around the iron(III) cation.

The quadrupole splitting shows only a small temperature dependence presumably because no low-lying thermally accessible levels are present.

It was mentioned in section 8.3 that the possibility of a spin crossover phenomenon was unlikely. This is because only one pair of lines is observed in the Mossbauer spectrum. In a spin crossover situation two pairs of lines would be expected unless the relaxation rate between the two spin states is very rapid, then only one pair of lines would be observed; but this is often accompanied by line broadening and a strong temperature dependence of ΔE_Q .

The line width values given in Table 8.5 are large and Γ_1 is always greater than Γ_2 . This may indicate magnetic exchange broadening (107). The values for $\text{Fe}(\text{CF}_3\text{SO}_3)_3$ at 293K are possibly

spurious and caused by the small quadrupole interaction seen in this compound.

The ^{57}Fe Mossbauer parameters obtained for these compounds are similar to those of some iron(III) carboxylate compounds in which antiferromagnetic coupling was present (108). More detailed investigation, especially at low temperature and in applied magnetic fields should help in examining the phenomenon of magnetic exchange in these compounds.

8.5. CONCLUSIONS

Magnetic susceptibility results clearly show that magnetic exchange in iron sulfonate polymers is possible, particularly where the metal is in the +3 oxidation state. This exchange takes place in spite of the fact that the Fe-O bonds are highly ionic and exchange takes place over three atoms in the bridging ligand. The compounds contain octahedral high spin iron(III) centres with bidentate bridging sulfonate anions.

CHAPTER 9

CONCLUSIONS AND SUGGESTIONS FOR FURTHER STUDY

The work described in this thesis has used several experimental techniques to characterise various iron sulfonate polymers. This chapter discusses some conclusions to be made from this work and the directions in which further study may take.

9.1. CONCLUSIONS

These studies indicate the following general structural model for iron(II) sulfonates. Planes of iron atoms are sandwiched by planes of sulfonate anions. The anions are acting as terdentate ligands each bridging to three different metal centres, and each metal ion is surrounded by oxygen atoms from six different anions. (see Fig. 1.1.) The FeO_6 chromophores are not perfectly octahedral and the distortion which is present may be defined as follows. A compression of the XSO_3^- anion along its C_3 axis will increase the O-S-O bond angle and will result in a trigonal elongation of the FeO_6 octahedra along the C_3 axis perpendicular to the plane of iron atoms. This is the form of distortion found in $\text{Fe}(\text{CF}_3\text{SO}_3)_2$, $\beta\text{-Fe}(\text{CH}_3\text{SO}_3)_2$ and $\text{Fe}(\text{p-CH}_3\text{C}_6\text{H}_4\text{SO}_3)_2$ and the previously reported $\text{Fe}(\text{FSO}_3)_2$.

The α -form of $\text{Fe}(\text{CH}_3\text{SO}_3)_2$ on the other hand, has a situation in which, relative to $\beta\text{-Fe}(\text{CH}_3\text{SO}_3)_2$, the CH_3SO_3^- anions

are elongated along their C_3 axes resulting in a trigonal compression of FeO_6 octahedra.

There is a lack of evidence for any structural isomerism in $Fe(FSO_3)_2$, $Fe(CF_3SO_3)_2$ and $Fe(p-CH_3C_6H_4SO_3)_2$. The absence of any α -forms of $Fe(FSO_3)_2$ and $Fe(CF_3SO_3)_2$ may be rationalised on the basis of electronegativity effects. As the electronegativity of X increases the extent of S-O double bonding in $XS O_3^-$ should increase, favouring larger O-S-O bond angles and therefore trigonally elongated FeO_6 octahedra, i.e. the β -form. For this reason it may be difficult or impossible to isolate divalent metal fluorosulfonates and trifluoromethanesulfonates in the α -form.

The existence of α -forms of $Fe(CH_3SO_3)_2$ and possibly $Co(CH_3SO_3)_2$ and $Zn(CH_3SO_3)_2$ suggests it may be possible to obtain such modifications of other $M(XSO_3)_2$ compounds containing X groups of similar or lower electronegativity to CH_3 . However, this was not the case where X is $p-CH_3C_6H_4$ and this may be due to steric factors.

It is interesting to compare the work on iron(II) sulfonates with the cobalt(II) and copper(II) analogues. In both Fe(II) and Co(II) where the anion is FSO_3^- , $CF_3SO_3^-$ and $p-CH_3C_6H_4SO_3^-$, the anions retain C_{3v} symmetry. It is possible that these compounds have similar structures although the evidence for a trigonal distortion in the cobalt(II) analogues only comes from magnetic moment data recorded over a limited temperature range (80-300K). $Co(CH_3SO_3)_2$ has an almost identical infrared spectrum

to $\alpha\text{-Fe}(\text{CH}_3\text{SO}_3)_2$. Hence, the anions are distorted from C_{3v} symmetry and it was suggested that this arose from a tetragonal distortion of the CoO_6 chromophore. As can be seen from the present work on $\text{Fe}(\text{CH}_3\text{SO}_3)_2$ this need not be the case and indeed it appears as likely that $\text{Co}(\text{CH}_3\text{SO}_3)_2$ contains a trigonally distorted CoO_6 chromophore.

Copper(II) sulfonates have been studied before(14) but because of the high distortion present in these compounds arising from a d^9 electron configuration any comparison with iron(II) sulfonates is difficult. It was previously proposed that copper(II) sulfonates contained tetragonally distorted CuO_6 octahedra. In view of the present work the distortion may be a trigonal compression or elongation or both which may account for the complex nature of their infrared spectra.

9.2. SUGGESTIONS FOR FURTHER WORK

The mechanism for magnetic exchange is not yet fully understood and the antiferromagnetism observed in both forms of iron(II) methanesulfonate is somewhat surprising. This is not only because of the number of bridging atoms through which an exchange would have to be transmitted but also because of the highly ionic nature of these compounds. A fuller understanding of the mechanism could be obtained by performing the following experiments:

- (i) The imminent arrival of a vibrating sample magnetometer in this department will enable magnetic susceptibilities

to be measured down to a temperature of 4.2K. It will be of interest to observe the temperature dependence of the magnetic moment in the vicinity of the magnetic phase transition observed in $\beta\text{-Fe}(\text{CH}_3\text{SO}_3)_2$. Low temperature susceptibility measurements on the other iron(II) sulfonates would enable better crystal-field fits to be obtained.

(ii) Preparation of a range of mixed compounds of general formula $\beta\text{-Fe}_x\text{Zn}_{1-x}(\text{CH}_3\text{SO}_3)_2$ will allow spin dilution experiments to be performed. The effect of this dilution may be monitored by Mössbauer spectroscopy and low-temperature magnetic susceptibility measurements. The resulting effect on the temperature of the magnetic phase transition may then be analysed.

(iii) Results presented in Chapter 7 for $\alpha\text{-Fe}(\text{CH}_3\text{SO}_3)_2$ suggest that at 4.2K in an applied magnetic field of 5.63T the saturation value of the internal hyperfine field has not been attained. In future, temperatures as low as ~1K are anticipated by extensive pumping of the liquid helium bath. Under these conditions the internal magnetic field of $\alpha\text{-Fe}(\text{CH}_3\text{SO}_3)_2$ may become saturated.

In the case of $\text{Fe}(\text{p-CH}_3\text{C}_6\text{H}_4\text{SO}_3)_2$ a more detailed investigation in applied magnetic fields between 1.13 and 3.38T at 2.4 and 4.2K would enable one to define the region in which the magnetic hyperfine field became saturated.

A re-examination of $\text{Fe}(\text{FSO}_3)_2$ is desirable in view of the unsatisfactory nature of the fit of computed to experimental spectra (15).

Results were only obtained in one magnetic field, and this work should be extended so detailed comparisons may be made between the $\text{Fe}(\text{XSO}_3)_2$ compounds.

For the iron(III) sulfonates more detailed information is still to be obtained, e.g. (i) low-temperature (<80K) magnetic susceptibility measurements, (ii) ^{57}Fe Mossbauer spectra to be recorded at temperatures lower than 80K in the presence and absence of an applied magnetic field. These measurements would again enable more information to be deduced about the nature of magnetic exchange interactions in these compounds.

$\text{Fe}(\text{FSO}_3)_3$ should also be re-examined and its ^{57}Fe Mossbauer spectrum recorded over the temperature range 4.2K to room temperature. Unlike $\text{Fe}(\text{XSO}_3)_3$ where X is CF_3 , CH_3 and $p\text{-CH}_3\text{C}_6\text{H}_4$, the $\text{Fe}(\text{FSO}_3)_3$ compound exhibits a field dependent magnetic susceptibility indicative of ferromagnetic exchange (22). In view of the absence of any field dependence where X is CF_3 , CH_3 , and $p\text{-CH}_3\text{C}_6\text{H}_4$ this study should be repeated.

The possibility of isomerism in iron(III) sulfonates has not yet been pursued and these compounds should be treated with D.M.P. and the effects examined.

Other iron coordination polymers should be examined both for structural isomerism and magnetic exchange interactions. Much investigation (109,110) is taking place using the weakly basic phosphinate anions, R_2PO_2^- , where R is an alkyl or aryl group. These anions

exhibit various modes of coordination, and preparation and characterisation of a series of $\text{Fe}(\text{R}_2\text{PO}_2)_2$ compounds may prove interesting.

Previously (111,112), coordinating abilities of weakly basic anions, A^- , have been examined by the characterisation of tetrakis- and bispyridine metal(II) compounds of the general formula $\text{M}(\text{py})_4\text{A}_2$ and $\text{M}(\text{py})_2\text{A}_2$, respectively. The possibility exists for the preparation and characterisation of two series of compounds, $\text{Fe}(\text{py})_4(\text{XSO}_3)_2$ and $\text{Fe}(\text{py})_2(\text{XSO}_3)_2$. The coordinating ability of the anions may be studied by the techniques described in this thesis and, in addition, the possibility of single crystal X-ray diffraction measurements exists for these materials. Again magnetic exchange may be observed, especially in the bispyridine complexes where bidentate bridging XSO_3^- anions may be present. Using a variety of substituted pyridines the effects of varying base strengths on the properties of these iron sulfonate complexes may also be studied. The use of the base pyrazine may also result in extended polymeric lattices (bridging occurring through pyrazine as well as the sulfonate ligand) exhibiting strong magnetic exchange between iron centres. Use of very weakly coordinating anions, e.g. PF_6^- and AsF_6^- , may enable the $\text{Fe}(\text{py})_6^{2+}$ cation to be isolated and the resulting FeN_6 octahedra to be compared to the FeO_6 octahedra studied here.

REFERENCES

1. D.H. Brown, R.H. Nuttall, J. McAvoy, D.W.A. Sharp,
J. Chem. Soc., (A), 892 (1966).
2. F.A. Jurnak, D.R. Greig, K.N. Raymond, Inorg. Chem.,
14, 2585 (1975).
3. M.R. Churchill, A.H. Reis, J.C.S. Dalton, 1570 (1973).
4. E. Lenz, R.K. Murmann, Inorg. Chem., 7, 1880 (1968).
5. S.H. Hunter, R.S. Nyholm, G.A. Rodley, Inorg. Chim. Acta.,
3, 631 (1969).
6. H.G. Mayfield, W.E. Bull, Inorg. Chim. Acta., 3, 676, 1969.
7. R.M. Morrison, R.C. Thompson, J. Trotter, Can. J. Chem., 58,
238 (1980).
8. H.G. Mayfield, W.E. Bull, J. Chem. Soc., (A), 2279 (1971).
9. R.M. Morrison, Ph.D. Thesis, University of British Columbia (1980).
10. S.A. Bell, J.C. Lancaster, W.R. McWhinnie, Inorg. Nucl. Chem. Lett.,
7, 405 (1971).
11. R.M. Morrison, R.C. Thompson, Can. J. Chem., 56, 985 (1978).
12. R.C. Thompson, C.S. Alleyne, Can. J. Chem., 52, 3218 (1974).
13. R.C. Thompson, C.S. Alleyne, Can. J. Chem., 49, 511 (1971).
14. A.L. Arduini, M. Garnett, R.C. Thompson, T.C. Wong, Can. J. Chem.,
53, 3812 (1975).
15. J.R. Sams, R.C. Thompson, T.B. Tsin, Can. J. Chem., 55, 115 (1977).
16. C.S. Alleyne, K. O'Sullivan Mailer, R.C. Thompson, Can. J. Chem.,
52, 336 (1974).
17. F. Charbonnier, R. Faure, H. Loiseleur, Acta Cryst., B33,
1478 (1977).
18. F. Charbonnier, R. Faure, H. Loiseleur, Acta Cryst., B33,
2824 (1977).
19. F. Charbonnier, R. Faure, H. Loiseleur, Acta Cryst., B31,
2693 (1975).

20. F. Charbonnier, R. Faure, H. Loiseleur, *Acta Cryst.*, B34, 1504 (1978).
21. K. Ono, A. Ito, *J. Phys. Soc. Japan*, 19, 899 (1964).
22. J. Goubeau, J.B. Milne, *Can. J. Chem.*, 45, 2321 (1967).
23. G.J. Long, G. Longworth, P. Battle, A.K. Cheetham, R.V. Thundathil, D. Beveridge, *Inorg. Chem.*, 18, 624 (1979).
24. S.F.A. Kettle, "Coordination Compounds", (Studies in Modern Chemistry, T.C. Waddington, ed.), T. Nelson and Sons Ltd., London 1.33 (1969).
25. P. Kovacic, N.O. Brace, *Inorg. Syn.*, 6, 172 (1960).
26. M. Garnett, B.Sc. Thesis, University of British Columbia (1972).
27. G. Charlot, D. Bézier, "Quantitative Inorganic Analysis", Methuen and Co., London p. 447 (1957).
28. H.C. Clark, R.J.O'Brien, *Can. J. Chem.*, 39, 1030 (1961).
29. B.N. Figgis, R.S. Nyholm, *J. Chem. Soc.* 4190 (1958).
30. E. König, "Landolt - Börnstein Numerical Data and Functional Relationships in Science and Technology," New Series II/2, (K.H. Hellwege, A.M. Hellwege, ed.), Springer-Verlag, Berlin (1966).
31. A. Earnshaw, "Introduction to Magnetochemistry," Academic Press, New York (1968).
32. F.E. Mabbs, D.J. Machin, "Magnetism and Transition Metal Complexes," Chapman and Hall, London (1973).
33. G. Lang, *J. Chem. Soc.*, (A), 3245 (1971).
34. F. Varret, *J. Phys. Chem. Solids*, 37, 265, (1976).
35. P.A. Yeats, B.F.E. Ford, J.R. Sams, F. Aubke, *Chem. Comm.*, 791 (1969).
36. F.H. Allen, J.A. Lerbscher, J. Trotter, *J. Chem. Soc.*, (A), 2507 (1971).
37. R.J. Capwell, K.H. Rhee, K.S. Seshadri, *Spectrochim. Acta*, 24A, 955 (1968).

38. M.G. Miles, G. Doyle, R.P. Cooney, R.S. Tobias, *Spectrochim. Acta*, 25A, 1515 (1969).
39. H. Bürger, H. Burczyk, A. Blaschete, *Monat. für Chemie*, 101, 102 (1970).
40. F.A. Schröder, B. Ganswein, G. Brauer, *Z. Anorg. Allg. Chem.*, 391, 295 (1972).
41. P.A. Yeats, J.R. Sams, F. Aubke, *Inorg. Chem.* 10, 1877 (1971).
42. J.R. Dalziel, R.D. Klett, P.A. Yeats, F. Aubke, *Can. J. Chem.*, 52, 231 (1974).
43. A.R. Byington, W.E. Bull, *Inorg. Chim. Acta*, 21, 239 (1977).
44. J.R. Sams, F. Aubke, *Inorg. Chem.*, 16, 1414 (1977).
45. R.J. Gillespie, E.A. Robinson, *Can. J. Chem.*, 40, 644 (1962).
46. S.M. Chackalackal, F.E. Stafford, *J. Am. Chem. Soc.*, 88, 4815 (1966).
47. I. Dézsi, L. Keszthelyi, *Solid State Comm.*, 4, 511 (1966).
48. J.M.D. Coey, I. Dézsi, P.M. Thomas, P.J. Ouseph, *Phys. Lett.*, 41A, 125 (1972).
49. F.A. Cotton, M.D. Meyers, *J. Am. Chem. Soc.*, 82, 5023 (1960).
50. H. Montgomery, R.J. Chastain, J.J. Natt, A.M. Witkouska, E.C. Lingafelter, *Acta Cryst.*, 22, 775 (1967).
51. T.M. Dunn, *Trans. Faraday Soc.*, 57, 1444 (1961).
52. H.A. Jahn, E. Teller, *Proc. Roy. Soc.*, A161, 220 (1937).
53. T.M. Dunn, "Modern Coordination Chemistry", (J. Lewis, R.G. Wilkins, eds.), New York (1960). B.N. Figgis "Introduction to Ligand Fields", Interscience, New York (1966).
54. M. Gerloch, J. Lewis, G.G. Phillips, P.N. Qusted, *J. Chem. Soc.*, (A), 1941 (1970).
55. R.L. Martin, A.H. White, "Transition Metal Chemistry", (R. L. Carlin, ed), M.Dekker Inc., New York, Vol.4, p.113 (1966).
56. R.L. Carlin, A.J. Vanduyneveldt, "Magnetic Properties of Transition Metal Compounds," Springer-Verlag, New York (1977).

57. B.N. Figgis, J. Lewis, F.E. Mabbs, G.A. Webb, J. Chem. Soc., (A), 442 (1967).
58. K. Dwight, J. Appl. Phys., 38, 1505 (1967).
59. B.L. Morris, A. Wold, Rev. Sci. Instr., 39, 1937 (1968).
60. S. Foner, J. Appl. Phys., 38, 1510 (1967).
61. J.H. Van Vleck, "The Theory of Electric and Magnetic Susceptibilities", Oxford University Press (1965).
62. J.S. Griffith, "The Theory of Transition-Metal Ions", Cambridge University Press (1964).
63. M. Gerloch, R.C. Slade, "Ligand Field Parameters", Cambridge University Press (1973).
64. B.N. Figgis, M. Gerloch, J. Lewis, F.E. Mabbs, G.A. Webb, J. Chem. Soc., (A), 2086 (1968).
65. R.W. Jotham, S.F.A. Kettle, J. Chem. Soc. (A), 2816 (1969).
66. R.L. Mossbauer, Z. Physik, 151, 124 (1958).
67. J.O. Artman, A.H. Muir, H. Wiedersich, Phys. Rev., 173, 337, (1968).
68. U. Gonser, R.W. Grant, A.H. Muir, H. Wiedersich, Acta Met., 14, 259 (1966).
69. G.M. Bancroft, R.C. Burns, 5th Mineralogical Assoc. Meeting, Cambridge (1966), Mineral Soc. Special Paper, 36, (1968).
70. J.R. Sams, T.B. Tsin, "The Porphyrins", Vol. IV, Academic Press, New York (1979), p. 425.
71. N.N. Greenwood, T.C. Gibb, "Mossbauer Spectroscopy", Chapman and Hall, London (1971).
72. "Mossbauer Effect Methodology", (I.J. Gruverman ed.), Plenum Press, New York.
73. G.M. Bancroft, R.H. Platt, Adv. Inorg. Chem. Radiochem., 15, 59 (1972).
74. R.C. Axtmann, Y. Hazony, J.W. Hurley, Chem. Phys. Lett., 2, 673 (1968).

75. R.L. Collins, J.C. Travis, "Mössbauer Effect Methodology," (I.J. Gruverman ed.), Vol. 3, Plenum Press, New York (1967), p. 123.
76. G.M. Bancroft, M.J. Mays, B.E. Prater, J. Chem. Soc., (A), 956 (1970).
77. C.J. Ballhausen, "Introduction to Ligand Field Theory" McGraw and Hill, New York (1962).
78. G.K. Wertheim, D.N.E. Buchanan, Phys. Rev., 161, 478 (1967).
79. M. Eibschutz, L. Holmes, H.J. Guggenheim, H.J. Levinstein, J. Appl. Phys. 40, 1312, (1969).
80. G.K. Wertheim, H.J. Guggenheim, H.J. Levinstein, D.N.E. Buchanan, R.C. Sherwood, Phys. Rev., 173 614 (1968).
81. L.R. Walker, G.K. Wertheim, V. Faccarino, Phys. Rev. Lett., 6, 98 (1961).
82. R. Ingalls, Phys. Rev., A133, 787 (1964).
83. T.C. Gibb, J. Chem. Soc., (A), 1439 (1968).
84. J.R. Sams, T.B. Tsin, Inorg. Chem., 14, 1573 (1975).
85. E. König, G. Ritter, H.S. Goodwin, Chem. Phys., 5, 211 (1974).
86. A. Abragam, B. Bleaney, "Electron Paramagnetic Resonance of Transition Ions", Clarendon Press, Oxford (1970).
87. J.N.R. Ruddick, J.R. Sams, J. Chem. Soc. Dalton Trans., 470 (1974).
88. J.R. Sams, J.C. Scott, J. Chem. Soc. Dalton Trans., 2265 (1974).
89. J.R. Sams, T.B. Tsin, Chem. Phys., 15, 209 (1976).
90. T.J. Bergendahl, J.S. Wood, Inorg. Chem., 14, 338 (1975).
91. R.H. Herber, S. Chandra, J. Chem. Phys., 52, 6045 (1970).
92. B.W. Fitzsimmons, C.E. Johnson, Chem. Phys. Lett., 6, 267 (1970).
93. M. Blume, Phys. Rev. Lett., 18, 305 (1967).

94. M. Coz, B.W. Fitzsimmons, A.W. Smith, L.F. Larkworthy,
K.A. Rogers, Chem. Comm., 183 (1969).
95. V.I. Gol'danskii, E.F. Makarov, V.V. Khrapov, Phys. Lett.,
3, 344 (1963).
96. P.A. Flinn, S.L. Ruby, W.L. Kehl, Science, 143, 1434 (1964).
97. H.H. Wickham, G.K. Wertheim, "Chemical Applications of
Mossbauer Spectroscopy", Academic Press, New York
(1968).
98. M.G. Clark, G.M. Bancroft, A.J. Stone, J. Chem. Phys.,
47, 4250 (1967).
99. M.G. Clark, J. Chem. Phys., 48, 3246 (1968).
100. R. Zimmermann, H. Spiering, G. Ritter, Chem. Phys., 4
133 (1974).
101. J.S. Haynes, J.R. Sams, R.C. Thompson, Chem. Phys. Lett.,
accepted for Publication.
102. W.M. Reiff, Coord. Chem. Rev., 10, 37 (1973).
103. R.L. Collins, J. Chem. Phys., 42, 1072 (1965).
104. R.W. Grant, A. Wiedersich, A.H. Muir, U. Gonser, W.N. Delglas,
J. Chem. Phys., 45, 1015 (1966).
105. C.E. Johnson, Proc. Phys. Soc., 92, 748 (1967).
106. A. Earnshaw, B.N. Figgis, J. Lewis, J. Chem. Soc., (A),
1656 (1966).
107. M. Blume, Phys. Rev. Lett., 14, 96 (1965).
108. G.J. Long, W.T. Robinson, W.P. Tappmeyer, D.L. Bridges,
J. Chem. Soc. Dalton, 573 (1973).
109. B.P. Block, Inorg. Macromol. Rev., 1, 115 (1970).
110. H.D. Gillman, Inorg. Chem. 13, 1921 (1974).
111. R.C. Thompson, R.M. Morrison, Inorg. Nucl. Chem. Lett.,
12, 937 (1976).
112. B.F. Little, G.J. Long, Inorg. Chem., 17, 3401 (1978).

APPENDIX
ABBREVIATIONS

s	strong
m	medium
w	weak
v.s	very strong
v.w	very weak
br	broad
as	asymmetric
sym	symmetric
def	deformation
sh.	shoulder
D.M.P.	2,2-dimethoxypropane
E.F.G.	electric field gradient
n.m.r.	nuclear magnetic resonance
e.s.r.	electron spin resonance